



The World's Largest Open Access Agricultural & Applied Economics Digital Library

This document is discoverable and free to researchers across the globe due to the work of AgEcon Search.

Help ensure our sustainability.

Give to AgEcon Search

AgEcon Search
<http://ageconsearch.umn.edu>
aesearch@umn.edu

*Papers downloaded from **AgEcon Search** may be used for non-commercial purposes and personal study only. No other use, including posting to another Internet site, is permitted without permission from the copyright owner (not AgEcon Search), or as allowed under the provisions of Fair Use, U.S. Copyright Act, Title 17 U.S.C.*

CA

CONTRIBUTION 202

**EVAPORATION RATES FROM
TEMPERATURE-STRATIFIED SALINE LAKES
USING A ONE-DIMENSIONAL
INTEGRATED EVAPORATION METHODOLOGY**

-Mono Lake as a Case Study-

by

Ben J. Tsuang

and

John A. Dracup



CALIFORNIA WATER RESOURCES CENTER

University of California

Contribution 202

ISSN 0575-4941

March 1991

**EVAPORATION RATES FROM
TEMPERATURE-STRATIFIED SALINE LAKES
USING A ONE-DIMENSIONAL
INTEGRATED EVAPORATION METHODOLOGY
-Mono Lake as a Case Study-**

by

Ben J. Tsuang

and

John A. Dracup

Civil Engineering Department

University of California

Los Angeles, CA 90024-1593



CALIFORNIA WATER RESOURCES CENTER
University of California
Contribution 202
ISSN 0575-4941
March 1991

This publication is furnished as part of the information exchange program in water resources research and is published and distributed by the DIRECTOR'S OFFICE OF THE CALIFORNIA WATER RESOURCES CENTER. The Center sponsors projects in water resources and related research on the several campuses of the University of California with funds provided by the U.S. Department of Interior, U.S. Geological Survey, and from the State of California. The contents of this publication do not necessarily reflect the views and policies of the Department of Interior, nor does mention of trade names or commercial products constitute their endorsement by the United States Government. Copies of this and other reports published by the Center may be obtained from:

WATER RESOURCES CENTER
UNIVERSITY OF CALIFORNIA
RUBIDOUX HALL
4501 GLENWOOD DRIVE
RIVERSIDE, CA 92501
(714) 787-4327

Copies of Center publications may be examined at either the Water Resources Center Northern Regional Office, 1333 Research Park Drive, Davis, CA 95616-8750, (916) 757-8901 or the Water Resources Center Archives, 410 O'Brien Hall, Berkeley Campus, (415) 642-2666

The University of California, in compliance with the Civil Rights Act of 1964, Title IX of the Education Amendments of 1972, and the Rehabilitation Act of 1973, does not discriminate on the basis of race, creed, religion, color, national origin, sex or mental or physical handicap in any of its programs or activities, or with respect to any of its employment policies, practices or procedures. The University of California does not discriminate on the basis of age, ancestry, sexual orientation, marital status, citizenship, medical condition (as defined in section 12926 of the California Government Code), or because individuals are disabled or Vietnam era veterans. Inquiries regarding this policy may be directed to the Personnel Studies and Affirmative Action Manager, Agriculture and Natural Resources, 300 Lakeside Drive, 6th Floor, Oakland, California 94612-3560, (415) 987-0080.

ABSTRACT

A methodology for determining the evaporation rates from temperature-stratified saline lakes has been developed. The technique is called an Integrated Evaporation Methodology (IEM). The initial motivation was to develop a technique which would be more accurate than the widely used evaporation pan method, would utilize meteorological data inputs that are normally available at U.S. National Weather Stations, and only require data which can be measured as inexpensively as possible.

Four functional modules are combined in the IEM model: a modified mass transfer function, a simulated solar radiation function, a simulated surface energy balance function, and a simulated water thermocline function. The IEM incorporates the salinity and the heat transfer effect in the simulation. An one-dimensional thermocline simulation module was developed to simulate seasonal water temperature. The required input data for the IEM model are lake location (latitude and elevation), air temperature, wind speed, humidity, cloud cover, and the lake characteristics of area, depth, and salinity. The model outputs are the lake evaporation rate and the lake water temperature. The continuous measurement of lake water temperature is not required as a model input, but is determined as a model output.

The IEM was validated and applied to Mono Lake. The saline water evaporation rates were simulated. They compared favorably with results from other saline water evaporation studies both in economy and accuracy. Using the 1982 data year as a basis, it was determined that the long-term evaporation rate from Mono Lake is 1.08 m/yr (42.5 in/yr). This value compares favorably with the results from other studies.

KEYWORDS: Evaporation, Energy Budget, Lakes, Mono Lake.

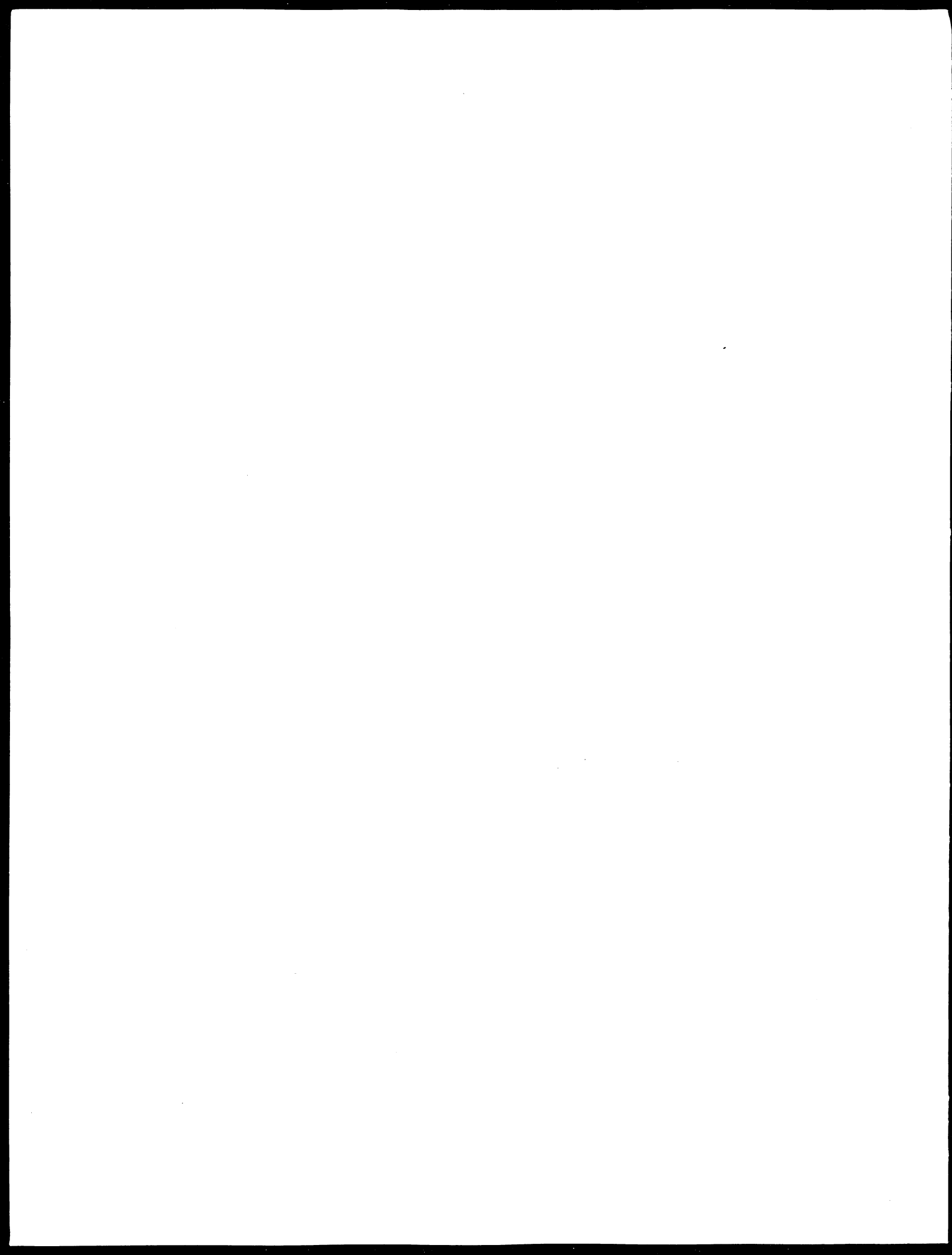


Table of Contents

1. Introduction	1
2. Review of the Literature	7
3. Methodology	9
3.1 Theory	9
3.1.1 Mass Transfer Method Module	11
3.1.2 Net Radiation Module	14
3.1.3 Surface Energy Budget Module	18
3.1.4 Water Thermocline Simulation Module	21
3.1.4.1 Stratified Period - Three Layer Sub-Model	22
3.1.4.2 Turn Over Period - Single Layer Sub-Model	25
3.1.4.3 Summary	26
3.2 Numerical Scheme	27
3.3 Model Calibration	29
4. A Case Study Using Mono Lake, CA.	30
4.1 Introduction	30
4.2 Inputs	33
4.2.1 Meteorological Data in Mono Basin	33
4.2.1.1 Cloud Cover	34
4.2.1.2 Wind Speed	36
4.2.1.2.1 Land-Water Adjustment	36
4.2.1.2.2 Height Adjustment	37
4.2.1.2.3 Total Wind Speed Adjustment	38
4.2.1.2.4 Lee Vining Station & Simis Station	38
4.2.1.3 Humidity	41
4.2.1.4 Air Temperature	42
4.2.2 Lake Properties	43
4.2.3 Parameters Used for the Mono Lake Simulation	46
4.3 Results	47
4.3.1 Water Thermal Structure	50
4.3.2 Evaporation Rate	51
4.3.3 Distribution of Energy	53
5. Model Uncertainties	55
5.1 Uncertainty due to the Change of the Frequency of the Input Meteorological Data	55
5.2 Uncertainty due to Lake Parameters	56
6. Application	57
6.1 Time Lag Effect	57
6.2 Sensitivity to Climatic Variations	59
6.3 Maximum & Minimum Evaporation Rate	60
6.4 Evaporation and Wind Speed	61
6.5 Sensitivity to Salinity	62
6.6 Pan Coefficient	63
6.7 Long-Term Evaporation	64
7. Conclusion	66
8. Future Research	68

Acknowledgments	69
Notation Index	70
Bibliography	73
Appendix	A-1
Program Code	A-1

List of Figures

1. Typical Day-Time Energy Balance Schematic Diagram	F-1
2. Interconnection flow chart of four functional modules	F-2
3. Flow chart of the water thermocline simulation module	F-3
4. Model calibration flow chart	F-4
5. Location and Hydrology Map of Mono Lake, California.	F-5
6. Climatic Measurement Sites, Mono Basin, CA.	F-6
7. Equivalent fractional Cloud Cover, 1982	F-7
8. Monthly wind speed at the Lee Vining Station, 1982	F-8
9. Diurnal wind speed at Lee Vining, 1982	F-9
10. Relative humidity at the Simis Station, 1982	F-10
11. Absolute humidity at the Simis Station, 1982	F-11
12. Daily air temperature at the Lee Vining station, 1982	F-12
13. Diurnal air temperature at Lee Vining, 1982.	F-13
14. Simulated monthly water temperature of Mono Lake, 1982.	F-14
15. Simulated diurnal water temperature of Mono Lake, 1982.	F-15
16. Simulated diurnal water temperature in the top layer.	F-16
17. Simulated diurnal water temperature in the middle layer.	F-17
18. Simulated diurnal water temperature in the bottom layer.	F-18
19. Simulated monthly evaporation rates from Mono Lake.	F-19
20. Simulated diurnal evaporation rates from Mono Lake.	F-20
21. Simulated monthly energy flux of Mono Lake.	F-21
22. Simulated diurnal energy flux of Mono Lake.	F-22
23. Monthly Bowen Ratio at Mono Lake, 1982.	F-23
24. Diurnal Bowen Ratio at Mono Lake, Sep. 22nd, 1982.	F-24
25. Simulated water temperature with daily and hourly data	F-25
26. Simulated evaporation rates with daily and hourly data	F-26
27. Daily evaporation deviation using daily data	F-27
28. Sensitivity of evaporation to heat diffusivity	F-28
29. Sensitivity of evaporation to the thickness of top layer	F-29
30. Time Lag Effect between Incoming & Outgoing Energy	F-30
31. Sensitivity of Evaporation to Climates by Hostetler	F-31
32. Sensitivity of Evaporation to Climates with IEM	F-32
33. Evaporation VS. Cloud Cover	F-33
34. Wind Speed and Inter-annual Water Temperature Variation	F-34
35. Comparison of Salinity Adjustment Ratio	F-35
36. Long-Term Evaporation Rates using Simis Pan Data	F-36
37. Long-Term Evaporation Rates using the Grant Lake Data	F-37

List of Tables

1. The Accuracies of Evaporation Methodologies	5
2. Data Required by Evaporation Methodologies	6
3. Data Available in the Mono Basin	32
4. Mono Basin Monthly Meteorological Data	33
5. Cain Ranch Fractional Cloud Cover Data, 1982	35
6. Over-Water Wind Speeds and Parameters	40
7. Constants for the Year 1982	46
8. Monthly Results using IEM for Mono Lake, 1982	48
9. Diurnal Results using IEM for Mono Lake, Sep. 22nd, 1982	49
10. Evaporation by IEM & Pan	52
11. Simulated Monthly Radiation Fluxes at Mono Lake, 1982	54
12. Evaporation Rate vs. Fractional Cloud Cover	60

1. Introduction

An accurate determination of evaporation rates from bodies of water is important to many disciplines including meteorology, hydrology and water resource engineering. Current methods for determining evaporation rates are often expensive, i.e. the energy budget method (Dunne and Leopold, 1978), or not accurate, e.g. the evaporation pan method (Winter, 1981). The purpose of this study is to develop a numerical methodology, for determining evaporation rates from deep saline water bodies, which overcomes these two problems. The criteria for this numerical methodology is (1) the required data should be easily accessible and economically obtainable, (2) the method should be more accurate than evaporation pan observations, and (3) the resulting evaporation calculation should be practical for engineering applications.

The development of the numerical methodology presented here results from the combination of the mass transfer function, the energy budget method and a water thermocline simulation model. The mass transfer function and the energy budget method are two major, but independent techniques, traditionally used to evaluate evaporation rates. Linking these two methods together reduces the data required and results in a more economical model. The water body temperature is the key linkage between the methods. A water thermocline model was developed to simulate the water temperature, which is normally expensive to obtain from field surveys. The resulting model has been named an Integrated Evaporation Methodology (IEM).

The only meteorological inputs required by the IEM model are air temperature, humidity, wind speed and cloud cover. All of these data are normally available at U.S. weather stations. Furthermore, pan evaporation data can substitute as one of the required meteorological inputs or it can be used to calibrate the model. Incoming short wave radiation and long wave radiation data are optional inputs which eliminate the cloud cover input data requirement. The IEM model simulates both the lake thermal structure and the evaporation rates. Salinity effects are included.

Approaches similar to the IEM method have been developed and validated for determining evaporation rates from fresh water (Hostetler, 1987; Croley, 1989). Hostetler (1987) tested and validated a similar model using U.S. Geological Survey data at the Salton Sea, California, and at Pretty Lake, Indiana. Croley (1989) applied a similar model to the Laurentian Great Lakes.

The rate of evaporation is also affected by the salinity of the water surface (Harbeck, 1955; Calder and Neal, 1984; Salhotra et al., 1985; 1987). It is well known that evaporation from saline water is less than that from fresh water; however, few comprehensive studies of evaporation from saline water bodies have been reported in the literature. The effect of salinity on evaporation is important for water balance computations and other engineering studies such as terminal lakes (e.g. Mono Lake or the Dead Sea) and salt gradient solar ponds. The model was further modified in order to respond to the variation of a salinity effect. The β approach for adjusting salinity effects, as suggested by Salhotra et al. (1985), is integrated in this IEM model, which modified the mass transfer function.

The IEM methodology was validated by applying it to Mono Lake, California, which is a terminal saline lake. Using 1982 meteorological data, (1982 was the only year during which all of the required data inputs were available), the IEM simulated the lake thermal structure and evaporation rate. The simulated evaporation rate from Mono Lake during 1982 was determined to be 1.03 m/yr (40.4 in/yr). This evaporation rate is close to values obtained using the evaporation pan method 39.7 in/yr (Vorster, 1985). The thermal structure derived from the IEM model indicated that the lake stratified from February, 1982, until November, 1982, and that the water surface temperature ranged from 0°C to 23°C. These values have been confirmed by several field studies in other years (1982 data are not available) (Mason 1967; Winkler 1977; Melack 1983; NRC 1987).

The IEM model is believed to be more accurate than the evaporation pan method although this has not been tested. Hostetler (1987) found that the difference between a field-survey energy budget evaporation method and a numerical evaporation method, which combines an energy budget, a mass transfer function and a water thermocline simulation model, is less than 4 %. Furthermore,

Hostetler (1987) indicated that if the mass transfer coefficient of the numerical model is corrected, the difference between the numerical method and the energy budget method is only 1 %. The annual accuracy of an energy budget method is 10% (Winter, 1981). Therefore, the annual accuracy of the numerical model is less than 14%. The widely used Class A pan method is the least accurate. Winter (1981) reviewed historical studies (Kohler, 1954; Kohler, et al., 1955, 1959; Hounam, 1973; Yonts, et al., 1973; Brutsaert and Yeh, 1970; Ficke, 1972, 1977; Keijman and Koopmans, 1973) and concluded that pan coefficients vary from about 0.4 to 2.0 for monthly data, and from 0.5 to 0.9 for annual data. Therefore, if a 0.7 (e.g. Hounam, 1973; Kohler, et al., 1955) pan coefficient is used, the annual error is about 28%. If lake depth and climatic regime are considered in selecting the pan coefficient, the error of the pan method is within 15 % (Kohler, 1954). The estimated accuracies of the IEM and other methodologies are presented in Table 1. An error analysis of the IEM approach indicates improved results over that of the evaporation pan method.

The data required by various evaporation methodologies are listed in Table 2. An important advantage and benefit of the IEM approach is the elimination of the requirement for the measurement of water temperature which is required by both the energy budget method and the mass transfer method. The measurement of water temperature is expensive to perform since it requires a continuous in-water measurement. The accuracy of lake evaporation as determined by the energy budget method or the mass transfer method depends on the precision of water thermal measurements, which in turn is related to the number and the distribution of temperature measuring points. Crow (1973) determined the optimum number of temperature measuring points to be one station per 520 acres (2.1 km^2 or 0.81 mi^2). Using his criteria, 83 sites would be needed for Mono Lake which has an area of 69 mi^2 . Therefore, the cost of the data acquisition is significant for either the energy budget method or the mass transfer method. Using the IEM, interactions between the atmosphere and saline water bodies are studied, including the sensitivity of evaporation to climatic variation, an approximate maximum and minimum evaporation rate, and the sensitivity of evaporation to different salinities.

In summary, the IEM can be shown to be a cost effective and accurate method when applied to a saline water body.

In the following section, a literature review is presented. In section 3, the theoretical basis for the IEM model is developed. In section 4, the model is applied to Mono Lake, California. In section 5, a model uncertainty analysis is performed. In section 6, the characteristics of evaporation and application of IEM are discussed. In section 7, are the conclusions. In section 8, further improvements required in this numerical model are presented.

Table 1. The Accuracies of Evaporation Methodologies

Methodology	Annual Accuracy Estimation	Monthly Accuracy Estimation
Energy Budget ¹	≤10%	13%
Mass Transfer ¹	15%	25%
Evaporation Pan ¹	15-28%	50-180%
Pan Conversion ²	-	-
IEM ³ + R _n	11-14%	25%
IEM ⁴ + E _p	-	-
IEM ⁵ + M _c	13-16%	28%

1: Winter (1981)
 2: The Pan Conversion Method has not been tested. Brutsaert (1982) estimated the accuracy would be better than the evaporation pan method.
 3: IEM with net radiation (R_n) input. The error was estimated from a similar approach by Hostetler (1987). The value is subject to change after an error analysis of IEM is performed.
 4: IEM with evaporation pan data (E_p) input. The method has not been tested. The accuracy should be between the IEM + R_n and the IEM + M_c methods.
 5: IEM with cloud cover (M_c) input. The error was estimated from a similar approach by Hostetler (1987) and Anderson (1954). The value is subject to change after an error analysis of IEM is performed.

Table 2. Data Required by Evaporation Methodologies

Methodology	Ta	Tw	Tp	U	R _a	X	M _c	Ep
Energy Budget	R	R	-	-	R	R	-	-
Mass Transfer	R	R	-	R	-	R	-	-
Evaporation Pan	-	-	-	-	-	-	-	R
Pan Conversion	-	R	R	-	-	R	-	R
IEM ¹	R	-	-	R	O	R	O	O

R ≡ Required

O ≡ Optional

Ta: Atmosphere Temperature

Tw: Lake Water Surface Temperature

Tp: Pan Water Temperature

U: Wind Speed

R_a: Net Solar Radiation

X: Humidity

M_c: Fractional Cloud Cover of the Sky

Ep: Pan Evaporation Rate

*1: IEM requires any one of the R_a, M_c or E_p

2. Review of the Literature

The mass transfer and the energy budget methods are reviewed by Brutsaert (1982) and Henderson-Sellers (1986). These methods require field surveys. New theoretical approaches have emphasized the determination of evaporation rates from meteorological observations and have eliminated the requirement of water body surface temperature. Most theoretical approaches (Kohler et al., 1955, 1967; Priestley et al., 1972; Stewart et al., 1976, 1977; Linacre, 1977; deBruin, 1978) are based on the Penman approach, which assumes that the surface specific humidity is equal to the saturation value at the surface temperature (Brutsaert, 1982). Warnaka (1988) did a comparison among these methods and found that the discrepancies are large. These theoretical studies assume that the heat flow into the subsurface is negligible. Therefore, these methods are only valid for shallow water bodies (Hounam, 1973). A calculation of deep water bodies should consider the subsurface heat flow and a thermal lag effect. Kondo et al., (1979) performed a theoretical calculation of temperature profiles in oceans due to diurnal solar energies. However, he assumes that the evaporation rate is negligible. A thorough development of evaporation from deep saline water bodies will require an integration of Kondo's research with the methods reviewed by Brutsaert (1982).

Hostetler (1987), Croley (1989) and this study use an integrated numerical methodology. This integrated methodology combines a simulated thermal structure of the water body with the traditional mass transfer and energy budget methods. The combination of numerical models of the thermocline simulation (Babajimopoulos et al., 1986; Henderson-Sellers, 1985, 1987; Aldama et al. 1989), evapotranspiration (Milly, 1984a; 1984b; 1987; Abdulkumin et al. 1987; van de Griend, 1989) and recent advances in droplet vaporization and combustion (Persaud, 1977; Briscoe, 1980; Law, 1982; Faeth, 1983; Sirignano, 1983, and Williams, 1985) led to the development of the integrated numerical methods.

The methodology used to simulate water body temperature is the major difference between this study and that of Hostetler (1987) and Croley (1989). This IEM study uses a lumped one-dimensional 3-layer model. Hostetler (1987) adopted an eddy diffusion model. Croley (1989) adopted a deterministic formula to calculate water surface temperature. The thermal structure of a lake can be simulated by any of four modeling approaches: (1) eddy diffusion models, (2) integrated mixed-layer models, (3) turbulence closure models, and (4) deterministic models (Henderson-Sellers, 1984 and Hostetler, 1987). All of these models simulate lake temperature in response to inputs of the surface energy balance and a set of meteorological variables. The basic difference between these modeling schemes is the method used to simulate the turbulent transfer of energy and heat. In the eddy diffusion models, an assumption is made that the turbulent transport of heat within the water column can adequately be accounted for by wind-driven diffusion of heat into the lake (Kondo, 1979, Henderson-Sellers, 1985; Babajimopoulos et al., 1986; Hostetler, 1987). In the mixed-layer models, the thermal structure of lakes is roughly divided into three layers, the epilimnion, the metalimnion and the hypolimnion layers (Welch, 1935; Hutchinson, 1957; Wetzel, 1983; Goldman et al., 1983). This division simplifies the thermal structure of water body into a mixed-layer model (Haney, 1976; Niiler and Kraus, 1977; Spigel, 1980; Meehl, 1984). Although the eddy diffusion approach, which was incorporated in Hostetler's model (1987), has a higher potential for describing shorter time and space scales (McCormick and Scavia, 1981), the mixed-layer models are simpler and require less computer time. Therefore, a three-layer model which is similar to mixed-layer models is adopted in this IEM approach. Croley's (1989) deterministic formula for calculating water surface temperature requires several years' of observed water temperature to calibrate.

Salinity effects are discussed in detail by Harbeck (1955), Calder et al. (1984) and Salhotra et al. (1985; 1987). The β approach for salinity effects, as suggested by Salhotra et al. (1985), is adopted in the IEM model.

3. Methodology

3.1 Theory

A typical daytime one-dimensional energy balance schematic chart of IEM model for water body is presented in Figure 1, where extraterrestrial solar radiation energy comes from the sun. Some portion of the extraterrestrial solar radiation energy is reflected and absorbed by the clouds and atmosphere. Most of the remaining solar radiation (R_s) is absorbed by the water body. Only a small portion of solar radiation is reflected by the water body. The absorbed solar radiation energy, in addition to long wave radiation energy from the atmosphere (R_{ld}), heat the water. Due to a higher-than-absolute-zero-Kelvin-degree water temperature, water body emits long wave radiation energy to the atmosphere (R_{lu}). The residue (net) of this radiation energy (R_n) was stored in the water body, which changes the water temperature (T_w). The stored energy in the water body eventually will return to the atmosphere in the forms of sensible heat (H) and latent heat (LE). The rate of this return depends on the climatic conditions and surface water temperature.

The IEM model can be divided into four modules: the mass transfer function module, the net solar radiation module, the surface energy balance module and the water thermocline simulation module. The connections among these modules are shown in Figure 2. The water temperature (T_w) and evaporation rates (E) are implicitly determined. The inputs of the model include location (latitude), meteorologic data and lake characteristics. The outputs are evaporation rate, surface water temperature and surface energy components.

The only meteorological inputs required in the IEM are air temperature (T_a), humidity (X), wind velocity (U) and cloud cover (Mc). All of these data are normally available at U.S. National Weather Stations. Furthermore, pan evaporation data can substitute as one of the required meteorological inputs or can be used to calibrate the model. Incoming short wave radiation and long wave radiation data are optional inputs. The lake characteristics required are the lake area (A), the depth (Z) and the salinity (S).

Each of the four IEM modules will now be discussed in detail. The numerical connection of the four modules is presented in section 3.2. The calibration of IEM model is discussed in section 3.3.

3.1.1 Mass Transfer Method Module

The purpose of the mass transfer method module is to calculate the evaporation rate from water bodies. The data required of this module includes external and inter-module inputs. The external inputs for this module are salinity (S), vapor pressure of the air (e_a) and the water body surface area (A). The inter-module input is water surface temperature (T_s), which is derived from the water thermocline simulation module and discussed in section 3.1.3.

Evaporation from water bodies depends on wind speed and the difference of vapor pressure between atmosphere and water surface. The relation was expressed as the mass transfer function. The original form was developed from the work of Dalton (Brutsaert, 1982). The equation was further modified in order to respond to the variation of surface area (Marciano and Harbeck, 1952) and salinity effect (Harbeck, 1955; Calder and Neal, 1984; Salhotra et al., 1985,1987).

The rate of evaporation, per unit area of a saline water surface, E, is computed by the β approach of Salhotra et al.(1985, 1987). The equation can be expressed as:

$$E = Nu_2 [e^*(S, T_s) - e_a] \quad (1a)$$

$$= Nu_2 [\beta(S)e^*(T_s) - \chi e^*(T_a)] \quad (1b)$$

where

- E = saline evaporation rate (L/T),
 N = mass transfer coefficient for a specific lake,
 u_2 = average wind speed measured 2 meters (6.56 ft) above the water surface (L/T),
 S = surface lake salinity (g/kg),
 e^* = saturation vapor pressure above a water surface as a function of salinity (S), water surface temperature (T_s) (mb),
 T_s = water surface temperature ($^{\circ}$ C or $^{\circ}$ K),
 β = activity coefficient of water for a specific salinity,

- T_a = air temperatures ($^{\circ}\text{C}$ or $^{\circ}\text{K}$),
 e_a = vapor pressure of the air (mb),
 χ = relative humidity of the air (%).

The saturated vapor pressure, e^* , in equation (1), is estimated as a function of water surface temperature (Richards, 1971; Brutsaert, 1982).

$$e^*(T_s) = 1013.25 \exp(13.3185t_R - 1.9760_R^2 - 0.6445t_R^3 - 0.1299t_R^4) \quad (2)$$

where

- t_R = $1 - (373.15/T_s)$,
 T_s = water surface temperature ($^{\circ}\text{K}$),

The accuracy of equation (2) is of the order of 10^{-2} percent (Brutsaert, 1982). An advantage of equation (2) is that it yields the variation of saturation vapor pressure with temperature, which follows the same form as the Clausius-Clapeyron Equation (Brutsaert, 1982).

$$\frac{de^*}{dT} = \frac{373.15e^*}{T^2} (13.3185 - 3.952t_R - 1.9335t_R^2 - 0.5196t_R^3) \quad (3)$$

The mass-transfer coefficient, N , in equation (1), can be determined using the empirical relationship (Harbeck, 1962),

$$N = 3.367 \times 10^{-9} A^{-0.05} \quad (4)$$

where

- A = water body surface area (m^2).

The mass-transfer coefficient, N , estimated by Harbeck's formula is subject to some uncertainty (Ficke, 1972; Dunne & Leopold, 1978; Brutsaert, 1982), and is also affected by local conditions such as topography, the point of wind measurement and the stability of climate. Croley (1989) modified this coefficient using an atmospheric boundary layer theory.

The activity coefficient β , in equation (1), depends on the salinity, S (Salhotra et. al., 1985). The coefficient can be determined from figure 1 of Salhotra et. al. (1985). That is,

$$\beta = \beta(S) \quad (5)$$

In summary, the mass transfer method module determines the evaporation rate from a saline water body. The rate is then used as an input to the surface energy budget module which is discussed in section 3.1.3.

3.1.2 Net Radiation Module

The net radiation module calculates the net radiation energy. The required data include external inputs and inter-module inputs. The external inputs for this module are latitude (θ), Julian date (t_j) and hour (t_h) and air temperature (Ta). The inter-module input is the water surface temperature (T_s) obtained from the thermocline simulation module in section 3.1.4.

Net radiation can be expressed as

$$R_n = (1 - \alpha)R_s + R_{ld} - R_{lu} \quad (6)$$

where

R_n = net radiative flux density at the upper surface of the layer (w/m^2),

R_s = solar radiation energy flux on the water surface (w/m^2),

α = albedo of the water surface,

R_{ld} = downward long-wave atmospheric radiation (w/m^2),

R_{lu} = upward long-wave radiation (w/m^2).

Because the lake surface reflects light, a certain portion of incoming shortwave radiation is reflected back into the atmosphere.

The albedo of a water surface depends on the spectral composition of the radiation, cloud cover, time of year, and roughness of the lake surface, varying from 0.04 to 0.08. In this study, an average albedo, 0.06, is used.

The intensity of solar radiation depends primarily on cloud cover and earth-sun geometry, which can be expressed as (Brutsaert, 1982)

$$R_s = R_{se}(0.75 - 0.5m_c) \quad (7)$$

where

R_{se} = extraterrestrial radiation (w/m^2)-that is, the solar radiation which would reach a horizontal surface in the absence of the atmosphere,

m_c = fractional cloud cover,

The extraterrestrial radiation depends on location, Julian date (t_j) and local time (t_h). It can be calculated as (Oke, 1987)

$$\begin{cases} R_{se} = E_{b0} \cos(z), & \text{during the day} \\ = E_{b0}(\cos \phi \cos \theta \cos \delta + \sin \theta \sin \delta) \\ R_{se} = 0, & \text{during the night} \end{cases} \quad (8)$$

where

E_{b0} = solar constant, w/m^2 ,

z = solar zenith angle,

ϕ = hour angle, 0° at noon,

θ = latitude,

δ = Earth's declination, $\pm 23.4^\circ$ at the summer and winter solstice,
respectively; 0° at the spring and autumn equinox,

Accurate information of θ and δ is published in almanacs. For a first approximation it may be calculated from

$$\delta = -23.4 \cos[360(t_j + 10)/365] \quad (9)$$

$$\phi = 15(12 - t_h) \quad (10)$$

where

t_j = the Julian date (number of the year) in the year,

t_h = the local apparent solar time (using a 24-hour clock).

Recently, the solar constant was measured as 1367 w/m^2 (Oke, 1987; Lean, 1989). However, this study used 1395 w/m^2 ($2.0 \text{ cal min}^{-1} \text{cm}^{-2}$) as a model input since that value was adopted in the above empirical formula (Brutsaert, 1982).

Atmospheric longwave radiation was estimated empirically. Most of the empirical formula assume that atmospheric longwave radiation follows the Stephan-Boltzman law, and can be written as (Brutsaert, 1982; Henderson-Sellers, 1986)

$$R_{ld} = R_{ldc}(1 + am_c^b) \quad (11a)$$

$$= \varepsilon_{ac} \sigma T_a^4 (1 + am_c^b) \quad (11b)$$

where

R_{ldc} = atmospheric radiation under clear skies (w/m^2),

a,b = constants, a = 0.22, b = 2 (Brutsaert, 1982),

σ = Stephan-Boltzman constant, $5.6697 \times 10^{-8} \text{ w m}^{-2} \text{ K}^{-4}$,

ε_{ac} = emissivity of the atmosphere.

Estimating the atmospheric emissivity in equation (11) is difficult since it is a function of the prevailing atmospheric composition (especially tri-molecular compounds such as CO_2 and H_2O). Likewise, the effective temperature of the atmosphere, T_a , is also difficult to obtain.

There are numerous empirical equations available for estimating atmospheric emissivity as a function of air temperature or of air vapor pressure, or some combination thereof (Brutsaert, 1982; Oke, 1987). An empirical equation for emissivity is given by Satterlund (1979), which is in better agreement with the data presented for below freezing temperature (Brutsaert, 1982)

$$\varepsilon_{ac} = 1.08 \left[1 - \exp \left(-e_a^{T_a/2016} \right) \right] \quad (12)$$

where

e_a = vapor pressure in the air (mb),

T_a = air temperatures ($^{\circ}\text{K}$).

Longwave radiation emitted from a lake surface is also determined by the Stephan-Boltzman law

$$R_u = \varepsilon_s \sigma T_s^4 \quad (13)$$

where

ε_s = emissivity of the water surface, 0.97 (Brutsaert, 1982),

T_s = water surface temperature (°K).

In this module, the net radiation energy was thus calculated and will be used as an input in the surface energy budget module in section 3.1.3.

3.1.3 Surface Energy Budget Module

The purpose of the surface energy budget module is to determine the specific energy flux into the water body (G_s) and requires inter-module inputs. The inter-module inputs are the net radiation and the evaporation rate from the net solar radiation module and the mass transfer method module, respectively.

The specific energy flux into the water body can be calculated from the residue of the energy balance in surface water, and can be expressed as (Brutsaert, 1982)

$$G_s = R_n - H - LE - L_p F_p - A_h - \frac{\partial W}{\partial t} \quad (14)$$

where

- G_s = specific energy flux into the water body (w/m^2),
- R_n = net radiation flux density at the air-water interface (w/m^2),
- H = sensible heat (w/m^2),
- L = latent heat of vaporization (j/m^3),
- E = saline evaporation rate (L/T),
- L_p = thermal conversion factor for fixation of carbon dioxide (j/m^3),
- F_p = specific flux of CO_2 (L/T),
- A_h = energy advection into the layer expressed as specific flux (w/m^2),
- $\frac{\partial W}{\partial t}$ = rate of energy storage per unit area in the layer (w/m^2).

Since the thickness of surface layer for the calculation of surface energy balance is infinitely small, $\frac{\partial W}{\partial t}$ term can be negligible. Therefore, specific energy flux into the water body can be calculated as

$$G_s = R_n - H - LE - L_p F_p - A_h \quad (15)$$

Since a Bowen ratio is defined as (Brutsaert, 1982)

$$B_o = \frac{H}{LE} \quad (16)$$

where

$$B_o = \text{Bowen ratio.}$$

Equation (15) can be rewritten as

$$G_s = R_s - LE(1 + B_o) - L_p F_p - A_k \quad (17)$$

Bowen Ratio

The Bowen ratio (B_o) is the ratio between sensible heat and latent heat. The ratio is written as follows (Dunne and Leopold, 1978; Brutsaert, 1982)

$$B_o = \gamma \frac{(T_w - T_a)}{(\beta e^*(T_w) - e_a)} \quad (18)$$

$$\gamma = \frac{C_p}{0.622L_e} P \quad (19)$$

where

γ = psychrometric constant,

T_w, T_a = temperature of the water surface and the atmosphere ($^{\circ}\text{C}$),

β = activity coefficient of saline water (dimensionless),

e^*, e_a = the vapor pressure of the water surface and the atmosphere (mb),

P = atmospheric pressure (mb),

C_p = specific heat of air ($\text{J/kg}/^{\circ}\text{K}$),

L_e = latent heat of the water body (J/kg).

The water vapor pressure of the water surface depends upon the temperature of the water which is difficult to measure. Penman suggests another approach which depends solely on air temperature (Brutsaert, 1982).

$$B_o = \alpha_e^{-1} \left(\frac{\gamma}{\Delta} \right) + (\alpha_e^{-1} - 1) \quad (20a)$$

where

- B_o = Bowen ratio,
- α_e = minimal advection constant,
- γ = psychrometric constant,
- Δ = de^*/dT_a , slope of saturation vapor-pressure versus temperature curve as a function of air temperature.

The optimal value of α_e is estimated to be 1.28 (Brutsaert, 1982). The above equation can be written as

$$B_o = 0.78 \frac{\gamma}{de^*/dT_a} - 0.22 \quad (20b)$$

The exact form of de^*/dT_a is shown in equations (2) and (3).

Since the IEM can simulate surface temperature, the equations (18) and (19) are used to calculate Bowen ratio by an iteration method. A comparison with the Penman approach presented in equation (20) will be discussed in Section 4.3.3.

This module calculates the specific energy flux into the water body which will be used as an input to the water thermocline simulation module in section 3.1.4.

3.1.4 Water Thermocline Simulation Module

The purpose of the water thermocline simulation module is to calculate water surface temperature (T_s). This module requires external and inter-module inputs. The external inputs for this module consist of the thickness of each layer in the water body (z_t, z_m, z_b), the diffusivity coefficient ($\alpha_s, \alpha_m, \alpha_b$), as well as the density and specific heat of the water (ρ, C_w). The inter-module input is the energy flux (G_s) calculated from the surface energy budget module. The outputs of this module are water body temperatures (T_t, T_m and T_b).

The theoretical water temperature is determined from (Henderson-Sellers, 1985; Babaji-mopoulos, 1986)

$$A(z) \frac{\partial T_w}{\partial t} = \frac{\partial}{\partial z} \left(A(z) (\alpha_m + \alpha_e(z, t)) \frac{\partial T_w}{\partial z} \right) + \frac{1}{\rho C_w} \left(\frac{\partial}{\partial z} \right) A(z) q(z) \quad (21)$$

where

A = horizontal lake area at depth z (L^2),

$\partial T_w / \partial t$ = the rate of change of the water temperature ($^{\circ}C / T$ or $^{\circ}K / T$),

α_m = molecular heat diffusivity (L^2/T),

α_e = eddy heat diffusivity coefficients (L^2/T),

$\partial T_w / \partial z$ = the gradient of the water temperature ($^{\circ}C/L$ or $^{\circ}K/L$),

ρ = water density (M/L^3),

C_w = specific heat (J/kg),

$q(z)$ = net penetrating radiation absorbed at depth, z , of the water body (w/m^2).

The eddy heat diffusivity coefficient of water is not constant (Henderson-Sellers, 1985) varying with time and depth. In addition, the area of a water body varies with the depth. Due to these factors, the above equation is a nonlinear partial differential equation. In order to overcome this problem, and taking into account that water temperature is not our major interest, a lumped one-dimensional thermocline model is used to simulate the thermal structure of the water.

Physically, the thermal structure of lakes can be broken into three layers: the top layer is the epilimnion, the middle layer is the metalimnion (thermocline) and the bottom layer is the hypolimnion (Welch, 1935; Hutchinson, 1957; Wetzel, 1983; Goldman et al., 1983, Henderson-Sellers, 1984). Since the thickness of metalimnion is very small, water temperatures at the epilimnion and the hypolimnion layers can represent the thermal structure of the entire water column. The temperature gradients of the hypolimnion and the epilimnion layers are negligible. As a result, homogeneous temperatures can be assumed for the both layers. However, for seasonal simulation, the depth of thermocline increases during a stratified period.

Two sub-models are used for the calculation of the thermal structure of lakes and reservoirs. The first consists of three layers used when the lake is stratified. The second consists of a single layer used during turn-over periods. The determination of which sub-model should be used during a certain time frame is shown in Figure 3. Initially, water temperature is calculated using the three layer sub-model. A turn-over occurs if the result of this sub-model shows that water density, a function of water temperature and salinity, is lower at a deeper layer than that at an upper layer. Hence, the single layer sub-model can be used to simulate the water temperature. Lakes are usually stratified during the summer and winter with turn-overs occurring during the fall and spring.

3.1.4.1 Stratified Period - Three Layer Sub-Model

While the lake is stratified, the following three layer model should be applied to calculate the thermal structure of the water bodies.

The Top Layer (the Epilimnion Layer):

The water temperature in the top layer is determined by a heat transfer equation. The determined temperature is used to represent water surface temperature. Assuming all the radiation energy is absorbed in the top layer, then, the conservation of energy budget in this layer may be written as

$$G_s = G_m + \frac{\partial W}{\partial t} \quad (22a)$$

$$= G_m + \rho C_w \left(\frac{\partial T_t}{\partial t} \right) Z_t \quad (22b)$$

$$= \rho C_w \left[\alpha_m \left(\frac{\partial T_m}{\partial z} \right) + \left(\frac{\partial T_t}{\partial t} \right) Z_t \right] \quad (22c)$$

Using a forward finite difference scheme, the equation is rewritten as

$$G_s \sim \rho C_w \left[\alpha_m \left(\frac{T_t - T_m}{\frac{1}{2}(z_t + z_m)} \right) + \left(\frac{T_t' - T_t}{\Delta t} \right) Z_t \right] \quad (22d)$$

where

G_s = specific energy flux from water surface into water body (w/m^2),

G_m = specific energy flux leaving the top layer and going to the middle layer (w/m^2),

$\partial W / \partial t$ = rate of energy storage per unit area in the layer (w/m^2),

ρ = density of the water (kg/m^3),

C_w = specific heat of the water (j/kg),

α_m = heat diffusivity in the layer between the top and the middle layers (m^2/s),

T_t, T_m = temperature in the top and the middle layers, respectively ($^{\circ}\text{C}$ or $^{\circ}\text{K}$),

Z_t, Z_m = thickness of the top and middle layers, respectively (m),

T_t' = temperature in the top layer after time lag Δt ($^{\circ}\text{C}$ or $^{\circ}\text{K}$),

Δt = time interval (hours).

Since T_t' is the unknown of the above equation, we can rewrite the equation as

$$T'_t = \left(\frac{G_s}{\rho C_w} - \alpha_{tm} \frac{T_t - T_m}{\frac{1}{2}(z_t + z_m)} \right) \frac{\Delta t}{z_t} + T_t \quad (23)$$

Likewise:

The Middle Layer (the Metalimnion layer):

$$T'_m = \left(\alpha_{mb} \frac{T_t - T_m}{\frac{1}{2}(z_t + z_m)} - \alpha_{mb} \frac{T_m - T_b}{\frac{1}{2}(z_m + z_b)} \right) \frac{\Delta t}{z_m} + T_m \quad (24)$$

where

T'_m = temperature in the metalimnion layer after time lag Δt ($^{\circ}\text{C}$ or $^{\circ}\text{K}$),

α_{mb} = heat diffusivity in the layer between the middle and the bottom layers (m^2/s),

T_b = temperature in the bottom layer ($^{\circ}\text{C}$ or $^{\circ}\text{K}$),

Z_b = thickness of the bottom layer (m).

The Bottom Layer (the Hypolimnion layer):

$$T'_b = \left(\alpha_{mb} \frac{T_m - T_b}{\frac{1}{2}(z_m + z_b)} - \frac{G_{bed}}{\rho C_w} \frac{\Delta t}{z_b} \right) + T_b \quad (25a)$$

where

T'_b = temperature in the bottom layer after time lag Δt ($^{\circ}\text{C}$ or $^{\circ}\text{K}$),

G_{bed} = specific energy flux leaving the layer at the bottom layer and going into the lake bed (w/m^2).

Since the temperature gradient of the hypolimnion layer is very small we can assume $G_{bed} = 0$. Hence, the equation can be expressed as

$$T'_b = \left(\alpha_{mb} \frac{T_m - T_b}{\frac{1}{2}(z_m + z_b)} \right) \frac{\Delta t}{z_b} + T_b \quad (25b)$$

Heat Diffusivity:

The heat diffusivity used between the layers in the three layer model is determined from the following:

$$\frac{1}{\alpha_{tm}} = \left(\frac{1}{\alpha_t} + \frac{1}{\alpha_m} \right) / 2 \quad (26a)$$

$$\frac{1}{\alpha_{mb}} = \left(\frac{1}{\alpha_m} + \frac{1}{\alpha_b} \right) / 2 \quad (26b)$$

where

α_{tm} = heat diffusivity in the layer between the top and the middle layers
 (L^2/T) ,

α_{mb} = heat diffusivity in the layer between the middle and the bottom layers
 (L^2/T) ,

α_t = heat diffusivity in the top layer, i.e., in the epilimnion layer
 (L^2/T) ,

α_m = heat diffusivity in the middle layer, which is assumed to be the harmonic average of the heat diffusivity in the epilimnion and the hypolimnion layer (L^2/T) ,

α_b = heat diffusivity in the bottom layer, i.e., in the hypolimnion layer (L^2/T) .

3.1.4.2 Turn Over Period - Single Layer Sub-Model

There are two situations in which a single layer model is valid. One occurs when the depth of the water body is shallow, such as is seen in an evaporation pan or in lakes with a

depth of less than 2-3 m. A second situation occurs when the density in the deeper layer is lower than in the upper layer. With either situation, we can assume the water temperature is the same at a given depth. Therefore, the energy equation of these situations can be expressed as (assume $G_{bed} = 0$)

$$G_s = \frac{\partial W}{\partial t}$$

$$= \rho C_w \frac{\partial T_w}{\partial t} Z \quad (27)$$

where

T_w = water temperature, °C or °K,

Z = average depth of a water body, m,

Using a forward finite difference scheme, the equation can be rewritten as

$$T'_w = \frac{G_s \Delta t}{\rho C_w Z} + T_w \quad (28)$$

where

T'_w = water temperature after time lag Δt .

3.1.4.3 Summary

These two sub-models simulate water body temperatures. Although these algorithms are relatively simple, the calculated water surface temperature is found to be accurate enough to simulate evaporation. This temperature is used as an input in both the mass transfer method module and the net radiation module.

3.2 Numerical Scheme

In the connection of the four modules, two numerical difficulties must be discussed:

1) Nonlinearity of Inter-Module Implicit Term (Water Surface Temperature):

Water surface temperature is not only the output of the thermocline simulation module but it also affects the value of the inputs. The water surface temperature input to the thermocline simulation is affected by the calculated water surface temperature through the mass transfer module and the net solar radiation module. That is, the determination of the water surface temperature forms a closed loop as shown in Figure 2. Since longwave upward radiation is not sensitive to the diurnal change of water surface temperature, the water surface temperature of the previous time step (1 hour) is used for the input of the net solar radiation module. To solve the nonlinearity among the loop, an iterated method was used. To begin with, the previous water surface temperature is first used as an input of the mass transfer method module, then, a water surface temperature from the thermocline simulation module is calculated. Secondly, the newly obtained water surface temperature is used for starting the loop within these four modules and water surface temperature is calculated again. The second step is repeated until the difference between the new and the old water surface temperatures are within a reasonable range. After three such iterations the solution becomes stable.

2) Stability Criterion of the Thermocline Simulation Module:

Since the algorithm developed in the thermocline simulation module is derived from a form of the explicit finite difference technique, it has to meet the constraints of the explicit finite difference scheme. The stability of the finite difference scheme is subject to (e.g. Sod, 1985)

$$\Delta t \leq \Delta z^2 / 2\alpha \quad (29)$$

where

Δt = time step of the scheme (s),

Δz = grid size of the scheme (m),

α = the diffusivity coefficient of the parabolic partial differential equation
(m^2/s).

Solutions are based on a specified temporal and spatial solution grid with mesh size Δt by Δz . A grid size of 1 hour by a thickness of each layer is used in the present solution.

3.3 Model Calibration

The inter-annual water temperature is simulated to calibrate the over-water wind speed and a mass transfer coefficient, terms that contain large uncertainty.

The mass-transfer coefficient, N , estimated by Harbeck's formula is subject to uncertainty (Ficke, 1972; Dunne & Leopold, 1978; Brutsaert, 1982; Croley, 1989) and is also affected by local conditions such as topography, the point of the wind speed measurement and the stability of the climate. Croley (1989) modified this coefficient using atmospheric boundary layer theory. The estimation of over-water wind speed is also subject to a large error, shown in the following case study. Since the mass transfer coefficient and the over-water wind speed can be treated as one term: Nu_2 in the mass transfer equation (1), we only have to calibrate the value of Nu_2 .

Croley (1989) calibrated the uncertainty of a numerical model by a comparison between the simulated and the observed water temperature. Since water temperature data are generally not available, this study tested the difference of the simulated inter-annual water temperature by changing the value of Nu_2 . The test assumes that the variation of a simulated inter-annual water temperature should be within a reasonable range. Using this criterion, the study obtained the value of Nu_2 to keep the variation of a simulated inter-annual water temperature within a reasonable range. The flowchart which adjusts this value is represented in Figure 4.

4. A Case Study Using Mono Lake, CA.

4.1 Introduction

Mono Lake (Figure 5) is a terminal saline lake located in east-central California. Its latitude is 38°N and the longitude is 119°W. Currently, the lake covers approximately 69 square miles (44,000 acres) and its surface is at elevation 1945 m (6380 feet). The average depth is calculated to be 21 m (69 feet) (LADWP, 1987). The salinity of the lake, at an average of 83.4 g/kg total dissolved solids (TDS), is about two and one-half times that of the Pacific Ocean (LADWP, 1986; 1987).

Evaporation estimates and data have been collected in the Mono Basin since 1934 (LADWP, 1987; Vorster, 1985). These evaporation values, as reported in 21 different studies, have varied from 23.1 to 78.8 inches per year (Vorster, 1985). The energy budget method was conducted in historic evaporation studies (Black, 1958; Mason, 1967 and Winkler, 1977). Black (1958) determined that the evaporation rate was 51 in/yr, Mason (1967) 79 in/yr, and Otuski (in Winkler, 1977) 67 in/yr. Although the energy budget method is considered to be the most accurate method to determine evaporation rates, Mason (1967) and Otuski (in Winkler, 1977) over-estimated the amount of evaporation, because their measurement of solar radiation energies exceeded the theoretical value. Mason (1967) measured the solar radiation energy to be 777 cal/cm²/day in July, and Otuski (in Winkler, 1977) measured it to be 900 cal/cm²/day. However, the theoretical maximum value is 721 cal/cm²/day under clear sky condition according to the equation (7). A critique of the other studies was presented by Vorster (1985). The currently available water balance models of Mono Lake use pan evaporation values as a basis for their evaporation calculations (Vorster, 1985; LADWP, 1987). Winter (1981) reviewed several evaporation methodologies used in lake water balance studies and found that the error of the pan evaporation method is 15-28%. The large uncertainty of pan evaporation calculations points to the need for a more accurate estimation technique.

A summary of the data available in the Mono Basin for the determination of evaporation is presented in Table 3. Historically, there have been four evaporation stations in the Mono Basin (Figure 6), located at Lee Vining, Simis, Cain Ranch and Mono Lake. However, the Mono Lake and the Simis stations were abandoned in 1959 and in 1983, respectively. The Lee Vining station is located east of Mono Lake, the Simis station at the north, and the Cain Ranch station is 5 miles south-east of the lake. All of these stations, except the one at Mono Lake, are on-shore. The salinity of the lake further complicates the evaporation estimation.

Due to data deficiencies for the application of the energy budget method and the mass transfer method, the proposed integrated evaporation methodology (IEM) has been tested using data only from 1982, which is the one year when all of the required data were available. In section 4.2, the meteorological data of 1982, lake information and other miscellaneous parameters required for the inputs of IEM are discussed. Section 4.3 presents the simulating results of 1982 using IEM.

Table 3. Data Available in the Mono Basin

Station Name	Ta	Tw	Tp	U	R_n	X	M_c	Ep	Operation Period (YR)
Cain Ranch	Y	N	N	Y	N	N	Y	Y	'32-'89
Simis Station	Y	N	N	Y	N	N	N	Y	'80-'83
Lee Vining	Y	N	N	Y	N	N	N	N	'82-'89
Mono Lake ¹	N	Y	Y	N	N	Y	N	Y	'49-'59

Ta: Atmosphere Temperature
 Tw: Lake Water Surface Temperature
 Tp: Evaporation Pan Water Temperature
 U: Wind Speed
 R_n : Net Radiation
 X: Humidity
 M_c : Fractional Cloud Cover of the Sky
 Ep: Pan Evaporation Rate

¹: Weekly Floating Pan Data

4.2 Inputs

4.2.1 Meteorological Data in Mono Basin

The monthly average meteorological data of Mono Basin in 1982 are listed in Table 4.

They will be discussed in detail in the followings.

Table 4. Mono Basin Monthly Meteorological Data, 1982

Month	Cloud Cover (Cain Ranch)	Air Temperature (Lee Vining) (C)	Absolute Humidity (Simis) (mb)	Wind Speed (Lee Vining) (M/S)
January	0.57	-7.73	3.60	1.34
February	0.30	-7.73	3.52	1.30
March	0.30	-0.56	3.01	1.75
April	0.23	-0.56	3.55	1.86
May	0.17	10.46	4.93	1.61
June	0.16	11.92	6.23	1.55
July	0.16	16.39	7.87	1.40
August	0.19	17.04	9.41	1.24
September	0.37	11.74	6.35	1.48
October	0.33	5.65	5.05	1.20
November	0.45	-1.44	3.75	1.11
December	0.61	-3.59	4.25	1.46
Annual Average	0.27	4.30	5.13	1.44

4.2.1.1 Cloud Cover

Cloud cover information is not currently available in the Mono Basin. However, this data can be obtained by using two potential approaches. One involves using the "daily characteristics" data which are categorized at the Cain Ranch station, and the other uses the evaporation pan data measured at the Simis station.

Solar radiation is the most sensitive parameter for evaporation (see Section 6.2). The fraction of cloud cover can affect evaporation rates from the range of 0.57 m/yr to 1.22 m/yr at Mono Lake (see Section 6.3), corresponding to a full cloud cover or a clear sky condition, making a careful determination of the cloud cover necessary. The Cain Ranch station categorizes a day as being either clear sky, partly cloudy, cloudy, snowing, raining or foggy. From these data, an equivalent weight of fractional cloud cover (W_{Mc}) for each category was assumed. The percentage weights are 0%, 40%, 100%, 60%, 100%, 60% for clear skies, partly cloudy, cloudy, snow, fog and rain, respectively. The calculation of equivalent fractional cloud cover for each month is presented in Table 5. In 1982, the cloud cover for the summer is about 20%, and about 50% during winter (see Figure 7). The annual average cloud cover for 1982 is 27%. If the weights for each category are changed, the annual average of equivalent cloud cover varies within a range of 25% to 35%. This range can be used as the uncertainty of this approximation. Since the evaporation pan and the lake are in the same basin, the evaporation pan shares the same cloud cover and the same solar radiation energy as the lake. Therefore, we can use the evaporation pan data to restore the missing cloud cover information. However, this concept has not yet been tested.

**Table 5. Fractional Cloud Cover Information
1982 Cain Ranch Station
from LADWP**

	W _{mc} (%)	J (d)	F (d)	M (d)	A (d)	M (d)	J (d)	J (d)	A (d)	S (d)	O (d)	N (d)	D (d)
C	0	10	11	16	18	23	21	20	23	13	18	11	6
PT CL	40	2	13	6	7	4	7	10	2	7	4	7	7
CL	100	3	2	4	3	3	2	1	4	6	8	10	7
SN	60	5	2	5	1	1	0			2		1	3
FOG	100	11	0	0	0	0	0					1	6
RN	60	0	0	0	0	0	0		2	2	1		
Others											1		
Effective Days		31	28	31	30	31	30	31	31	30	31	30	29
<i>M_c</i>		0.57	0.30	0.30	0.23	0.17	0.16	0.16	0.19	0.37	0.33	0.45	0.61
<i>R_{se}</i> (cal/d/cm ²)		380	510	690	810	935	945	935	880	750	580	400	340
<i>M_c</i> × <i>R_{se}</i>		218	153	209	189	157	151	151	170	280	191	179	206

$$\text{Annual } M_c = \sum(M_c \times R_{se}) / \sum R_{se} = 0.27$$

- C: Clear Sky
 PT CL: Partial Cloud Cover
 CL: Cloudy Day
 SN: Snow
 RN: Rain
 W_{mc}: Equivalent Weight of Fractional Cloud Cover
 M_c: Fractional Cloud Cover
 R_{se}: Extraterrestrial Radiation

4.2.1.2 Wind Speed

The seasonal wind speed measured at the Lee Vining station during 1982 is shown in Figure 8. The average wind speed measured 1.44 m/s with the highest wind speed occurring in April and the lowest in November. The diurnal wind speed pattern measured at the Lee Vining station is shown in Figure 9. A diurnal variation is evident. The peak speed occurs during the late afternoon. The wind speed as an input to the IEM should be measured at 2 meters above the water surface. However, all of the wind speeds are measured on shore. Since the surface roughness and elevation of the water and of the land are different, an over-water and a height adjustment of wind speed are required.

4.2.1.2.1 Land-Water Adjustment

Since the roughness above water surface is less than that above land, the over-water wind speed is higher than the wind speed evaluated on the shore. The conversion method is derived from the concept of the conservation of the momentum (Henderson-Sellers, 1984).

$$u_w = u_l \frac{\ln(h/z_{ow}) \ln(\delta/z_{ol})}{\ln((h-d)/z_{ol}) \ln(\delta/z_{ow})} \quad (30)$$

$$\delta = 0.86x^{0.8} z_{ol}^{0.2} \quad (31)$$

where

u_w = wind speed related to the observed land wind speed (u_l) at the same height,

u_l = observed land wind speed,

z_{ow} = water surface roughness,

h = height of the measurement point,

d = zero plane displacement of land,

z_{ol} = land surface roughness,

- δ = the thickness of the boundary layer at a distance, x , downwind,
 x = downwind distance.

4.2.1.2.2 Height Adjustment

A height adjustment for wind speed includes the stability of atmosphere with the Monin-Obukhov length (Brutsaert, 1982; Oke, 1987). The incorporation of this concept requires the measurement of wind speed at either two elevations, or at only one elevation with stability condition. However, the wind speed available in the Mono basin is only measured at one elevation. Hence, this study assumes a neutral stability condition. The height adjustment for wind speed in the neutral stability condition can be written as (Brutsaert, 1982)

$$u_h = \frac{u_*}{k} \ln(h/z_o) \quad (32)$$

where

- u_h = wind speed at height, h ,
 u_* = friction velocity,
 k = the von Karman constant, $k = 0.4$,
 h = height of the wind speed,
 z_o = surface roughness length.

From the above equation (30), the wind speed at two meter height in a neutral condition can be calculated from a wind speed at one level by eliminating the $\frac{u_*}{k}$ term, which can be expressed as

$$u_2 = u_h \frac{\ln(2/z_o)}{\ln(h/z_o)} \quad (33)$$

- u_2 = wind speed at two meter height,

- u_h = wind speed at height, h ,
 z_o = surface roughness length.

4.2.1.2.3 Total Wind Speed Adjustment

Combining equation (30) and (33), the over-water wind speed at two meter height can be calculated from an on-shore wind speed as

$$u_{w2} = u_{lh} \frac{\ln(2/z_{ow}) \ln(\delta/z_{ol})}{\ln((h-d)/z_{ol}) \ln(\delta/z_{ow})} \quad (34)$$

$$\delta = 0.86x^{0.8} z_{ol}^{0.2} \quad (31)$$

- u_{w2} = over-water wind speed at two meter height,
 u_{lh} = observed land wind speed at the height, h ,
 h = height of the wind speed,
 z_{ow} = water surface roughness length,
 d = zero plane displacement,
 z_{ol} = land surface roughness length,
 δ = the thickness of the boundary layer at a distance, x , downwind,
 x = downwind distance.

4.2.1.2.4 Lee Vining Station & Simis Station

The over-water wind speed can be calculated from the data measured at the Lee Vining and the Simis stations using the above adjustment formulas for the wind. The results and the parameters chosen for the calculation are listed in Table 6. Due to fact that the values of land surface roughness at both stations are not available, these values were chosen from the table of Brutsaert (1982). The Lee Vining station is located in the small town of Lee

Vining, CA, located in the junction of a mountain and a lake. The Simis station is surrounded in a grass land with average vegetation height about 1 m. The calculated over-water wind speeds are 2.76 m/s using the data measured at the Lee Vining station where the average wind speed is 1.44 m/s. The calculated over-water wind speed is 2.95 m/s using the data measured at the Simis station where the average wind speed is 1.99 m/s.

The calculated over-water wind speed would vary if the value of surface roughness is changed and the displacement distance is considered. This will be illustrated in the following four examples using the Simis station. Example (1) assumed d of 1.0 m for grass height 1.2 m, the calculated over-water wind speed would be 3.23 m/s. Example (2) if z_{ow} = 0.04 instead of .0004 and d = 1.0 m, the calculated over-water wind speed would be 2.88 m/s. Example (3) assumes the area around the Simis station is grassland with an average height of crop of 0.4 m, grass displacement of 0.32 m and z_{ol} = 0.04 m, the calculated over-water wind speed would be 2.53 m/s; Example (4) same as example (3) but z_{ow} = .004 instead of 0.0004, the calculated over-water wind speed would be 2.27 m/s. As illustrated, the calculated over-water wind speed for the Simis station varies from a high of 3.23 m/s to a low of 2.27 m/s. This shows that the calculated over-water wind speed is subject to a large error.

As discussed in the section 3.3 Model Calibration, an over-water wind speed is calculated by assuming the zero degree deviation of simulated inter-annual water temperature and Harbeck's formula is correct for estimating mass transfer coefficient. The calculation is similar to the sensitivity of wind speed on the simulated water temperature as shown in section 6.4. The wind speed is determined to be 2.84 m/s. This value is close to the 2.76 m/s derived from the Lee Vining station. The only over-water measurement found in the literature is in Otsuki's study (in Winkler, 1977). He obtained a value of 4.2 m/s measured at a small flat island just west of the Paoha Island during the summer of 1977. The height of measurement is 2 meter above the mean water surface. Unfortunately, both the Lee Vining

and the Simis stations were not operating during 1977. But, since the value 4.2 m/s is much larger than any measured over-land wind speed during the summer in other years (e.g. wind speed at the Lee Vining station in the summer, 1982), it can be concluded that over-water wind is larger than over-land wind speed. Therefore, a 2.76 m/s value from the Lee Vining station for the annual mean over-water speed seems reasonable and is used in this study.

Table 6. Over-Water Wind Speeds and Parameters							
Stations	u_{lh} m/s	z_{ol} m	d m	h m	x m	δ m	u_{w2} m/s
Lee Vining	1.44	0.4 ¹	0	4	6123.5	766.5	2.76
Simis	1.99	0.133 ²	0	4	6123.5	615.0	2.95
z_{ow} (m)	0.0004						
u_{lh} :	on-shore observed wind speed						
z_{ol} :	roughness of land						
d :	zero plane displacement						
h :	height of measurement point						
x:	distance between the center of lake and station						
δ :	thickness of the boundary at the center of the lake						
u_{w2} :	over-water wind speed at 2 m elevation						
z_{ow} :	roughness of water surface (Brutsaert, 1982)						

¹: town (Brutsaert, 1982)

²: grass land (Brutsaert, 1982)

4.2.1.3 Humidity

Humidity data in Mono Basin are available at the Cain Ranch station and the Simis station. This study only considers the Simis station data as an input to IEM model since it is the closest station to Mono Lake. The data available at the Simis station were recorded as daily maximum and minimum relative humidity as shown in Figure 10. The relative humidity was changed to absolute humidity, and the average value of maximum and minimum humidity was calculated.

The results of the absolute water vapor pressure measured at the Simis station during 1982 are shown in Figure 11. The values vary from 3 mb to 10 mb. The maximum value occurred during August.

Because the daily maximum relative humidities at the Simis station were almost 100%, the Simis station is very close to the lake, and the station is not always on the upwind direction, there are no adjustments made to account for the fact that water vapor over much of the lake would have been larger than the land values.

4.2.1.4 Air Temperature

The daily air temperature measured at the Lee Vining station during 1982 is shown in Figure 12. The average monthly temperature range varies from -8 °C in the winter to 17 °C in the summer. The hottest month is August and the coldest months are January and February. The diurnal air temperature on September 22nd and the calculated annual mean of diurnal air temperature at the Lee Vining station in 1982 is shown in Figure 13. The annual mean temperature varies from -1.5°C to 11°C. The diurnal air temperature on September 22nd varies from 4°C to 26°C. Both diurnal air temperature patterns peak at about 1 to 2 PM, and are lowest at about 6 AM.

4.2.2 Lake Properties

During 1982, the water surface elevation of Mono Lake was at an elevation of 1943 m (6372 ft) and the lake covered approximately 150 km². The average lake depth was 17.8 m, and the salinity was 92.1 g/kg (LADWP, 1986; 1987). The corresponding activity coefficient, β , was 0.95 (figure 1, Salhotra et al., 1985). The activity coefficient, β , can be expressed as a function of salinity, S , by using the Lagrangian approximation to the figure 1 of Salhotra et al. (1985), assuming the composition of the saline water in Mono Lake is NaCl,

$$\begin{aligned}\beta(S) = & \frac{(S - 0.05)(S - 0.1)(S - 0.2)}{-0.001} + \frac{0.975S(S - 0.1)(S - 0.2)}{3.75 \times 10^{-4}} \\ & + \frac{0.940S(S - 0.05)(S - 0.2)}{-5 \times 10^{-4}} + \frac{0.840S(S - 0.05)(S - 0.1)}{3.0 \times 10^{-3}}\end{aligned}\quad (36)$$

To complete the thermocline simulation module, it is necessary to specify initial values. The initial conditions are required to describe the existing lake temperature profile. If modeling begins while a lake is isothermal, the initial conditions can be written $T(0, z) = T_0$, for all z . However, any nonisothermal temperature structure could be specified. January 1st, 0:00, is set to be time 0 for the numerical simulation of this study. The initial water temperature for 1982 is not available. However, this study uses the value of the January 1st, 0:00, 1986, water temperature of 4°C (NRC, 1987).

The thickness of the epilimnion layer is measured by Mason (1967), Winkler (1977), Melack (1983) and NRC (1987). It increases during stratified seasons in the range of 9 - 15 m per stratified period. The top 9 m thickness always belongs to the epilimnion layer, and the value 9 m was used for the thickness of the top layer in the thermocline 3-layer sub-model in this study. From the depth of 9 m to 15 m, with a thickness of 6 m, this region sometimes belongs to the epilimnion layer and sometimes to the hypolimnion layer. Therefore, this region is used for the thickness of the middle layer in the 3-layer sub-model. The remaining part of the water column from the

depth 15 m to the bottom of the Mono Lake (average depth 17.8 m) with a thickness of 2.8 m always belongs to the epilimnion layer, and the value 2.8 m is used for the thickness of the bottom layer in the 3-layer sub-model.

The heat diffusivity term includes molecular diffusivity and eddy diffusivity. The molecular diffusivity of fresh water is $0.12 \times 10^{-2} \text{ cm}^2/\text{s}$ (Jassby, 1975), and of the saline water in Mono Lake is $0.14 \times 10^{-2} \text{ cm}^2/\text{s}$ (Mason, 1967). The eddy diffusivity varies with time and depth. In the epilimnion, the eddy diffusivity depends on wind speed, density gradient, current gradient (Kullenberg, 1971), and varies in a range of 0.1 to $500 \text{ cm}^2/\text{s}$ (Kondo, 1979). This study uses $1.5 \text{ cm}^2/\text{s}$ because the wind speed above Mono Lake is weaker in comparison to other studies (refer to Table 1, Kondo, 1979). The eddy diffusivity is almost a constant in the hypolimnion layer. Jassby (1975) determined an average value, $2 \times 10^{-2} \text{ cm}^2/\text{s}$ to be the eddy diffusivity in the hypolimnion layer in Castle Lake, CA., and that value is adopted in this study as no other information is available. Since the eddy diffusivity is 2 to 4 orders larger than the molecular diffusivity, the heat dispersion in a lake depends mainly upon the eddy diffusivity. The heat diffusivity in the top layer and the bottom layer are used in the value in the epilimnion layer and the hypolimnion layer, respectively. The eddy diffusivity in the middle layer is assumed to be the harmonic average of that of the epilimnion layer and the hypolimnion layer, expressed as

$$\frac{1}{\alpha_m} = \left(\frac{1}{\alpha_e} + \frac{1}{\alpha_h} \right) / 2 \quad (37)$$

where

α_m = heat diffusivity in the middle layer (L^2/T),

α_e = heat diffusivity in the top (epilimnion) layer (L^2/T),

α_h = heat diffusivity in the bottom (hypolimnion) layer (L^2/T),

The density of the fresh water, ρ_f , can be expressed as (Hostetler, 1987)

$$\rho_f(T) = [1 - 1.9549 \times 10^{-5} |T - 4|^{1.68}] \times 1000 \quad (38)$$

where

ρ_f = fresh water densities (kg/m^3),

T = water temperature ($^\circ\text{C}$),

The density of the saline water in Mono Lake is determined by the curve fitting from Manson's figure 19 (1967) and the table of LADWP (1986). The relation is found to be

$$\rho(T, S) = [1.0048259 + 8.66 \times 10^{-1}S - 2.867 \times 10^{-4}T + 2.472 \times 10^{-4}TS] \times 1000 \quad (39)$$

where

ρ = saline water densities (kg/m^3),

T = water temperature ($^\circ\text{C}$),

S = the salinity (kg/kg).

The specific and the latent heat of the saline water body can be calculated by adjusting the value of fresh water (Henderson-Sellers, 1986; Hostetler, 1987), written as

$$C_w(T, S) = C_{wf}(1 - S) = 4192(1 - S) \quad (40)$$

$$L_e(T, S) = L_{ef}(1 - S) = 1.91846 \times 10^6 \left[\frac{(T + 273.2)}{(T + 239.29)} \right]^2 (1 - S) \quad (41)$$

where

C_w, C_{wf} = specific heat of saline and fresh water, respectively (J/kg),

L_e, L_{ef} = latent heat of saline and fresh water, respectively (J/kg).

T = water temperature ($^\circ\text{C}$),

S = the salinity (kg/kg).

The fixation of carbon dioxide and the advection energy of Mono Lake are assumed to be negligible, i.e. $L_p F_p, A_h$ in equations (14), (15) and (17).

4.2.3 Parameters Used for the Mono Lake Simulation

Other miscellaneous data, and its source, used in determining the evaporation rate of Mono Lake, using the IEM model, are listed in Table 7.

Table 7. Constants for the Year 1982

Parameter	Value	Description and Source
D	17.80 m	average depth of Mono Lake for 1982 (LADWP, 1987)
S	92.1 g/kg	salinity of Mono Lake in 1982 (LADWP, 1986; 1987)
α	0.06	albedo of water surface (Brutsaert, 1982)
ε_s	0.97	emissivity of water surface (Brutsaert, 1982)
p	810 mb	ambient air pressure
A	1.50E+08 m ²	surface area of water body
N	1.33E-09	mass-transfer coefficient (Harbeck, 1962)
σ	5.67E-08 w m ⁻² k ⁻⁴	Stephan-Boltzman constant
L	2.47E+06 j kg ⁻¹	latent heat of Mono Lake water (Mason, 1967)
β	0.95	activity coefficient of water (Salhotra, 1985)
\bar{u}	1.44 m s ⁻¹	1982 wind speed, Lee Vining
\bar{u}_w	2.76 m s ⁻¹	over-water wind speed
C_p	1005 j kg ⁻¹ k ⁻¹	specific heat of air (Brutsaert, 1982)
C_w	3869 j kg ⁻¹ k ⁻¹	specific heat of Mono Lake water (Mason, 1967)
ρ	1078 kg m ⁻³	density of Mono Lake water (Mason, 1967)
T_{t0}	4.00 °C	initial top layer temperature (NRC, 1987)
T_{m0}	4.00 °C	initial middle layer temperature (NRC, 1987)
T_{b0}	4.00 °C	initial bottom layer temperature (NRC, 1987)
α_e	1.50E-04 m ² s ⁻¹	epilimnion heat diffusivity (Kondo, 1979)
α_h	2.14E-06 m ² s ⁻¹	hypolimnion heat diffusivity (Jassby, 1975)
z_t	9.0 m	thickness of top layer
z_m	6.0 m	thickness of middle layer
z_b	2.8 m	thickness of bottom layer
G_{bed}	0.0 j m ⁻² hr ⁻¹	heat flux into lake bed (assumed)

4.3 Results

The IEM is validated by applying it to Mono Lake, California, using 1982 hourly meteorological data. The cloud cover data are derived from the Cain Ranch station. The over-water wind speed data are calculated from the over-land wind speed measured at the Lee Vining station. Air temperature data are measured at the Lee Vining station. The humidity data are measured at the Simis station.

The results of this simulation includes the evaporation rate, the lake water temperature and the surface energy components all in diurnal and monthly time domains. The simulated diurnal results are presented using Autumn Equinox, September 22nd, 1982, as an example. These results are shown in Figures 14 to 24 and Table 8, 9.

Table 8. Simulation Monthly Results using IEM for Mono Lake, 1982

SALINITY = 92.10 G/KG

INITIAL WATER TEMPERATURE

Tt= 4.00 Tm= 4.00 Tb= 4.00 (C)

LAKE PROPERTIES

DEPTH= 17.80 Zt= 9.00 Zm= 6.00 Zb= 2.80 (M)

ALPHAt=.15E-03 ALPHAm=.42E-05 ALPHAb=.21E-05 M²/S

Month	E (mm/day)	Tt (C)	Tm (C)	Tb (C)	Rn (W/M ²)	LE (W/M ²)	H (W/M ²)	B _o	Gs (W/M ²)
1	.969	2.34	2.32	2.32	-9.	28.	45.	1.61	-82.
2	.750	.75	.66	.66	45.	22.	34.	1.54	-11.
3	1.520	2.45	.70	.56	107.	44.	12.	0.27	51.
4	2.185	5.93	1.40	.73	155.	63.	32.	0.51	60.
5	3.171	12.39	2.85	1.23	220.	91.	-4.	-0.04	134.
6	4.440	17.66	5.18	2.27	223.	126.	21.	0.17	76.
7	4.933	21.07	7.66	3.83	221.	140.	7.	0.05	75.
8	4.636	22.76	10.08	5.75	181.	131.	11.	0.08	39.
9	4.851	19.15	11.76	7.71	94.	138.	27.	0.20	-70.
10	2.734	14.12	12.13	9.30	47.	78.	29.	0.37	-59.
11	1.919	9.83	9.81	9.41	-10.	55.	39.	0.71	-104.
12	1.482	5.92	5.91	5.91	-16.	43.	46.	1.07	-105.

SIMULATED WATER TEMPERATURE AT END OF THE SIMULATION

Tt= 4.18 Tm= 4.18 Tb= 4.18 (C)

ANNUAL EVAPORATION RATE = 1.026 M/YR

EXECUTION TIME = 416.90 SEC (AT&T 6300 with math coprocessor)

Table 9. Simulation Diurnal Results using IEM for Mono Lake, Sep. 22nd, 1982

Hour	E (mm/hr)	Tt (C)	Tm (C)	Tb (C)	Rn (W/M ²)	LE (W/M ²)	H (W/M ²)	B _o	Gs (W/M ²)
0	.103	18.00	11.95	8.03	-106.	70.	26.	0.37	-202.
1	.103	17.98	11.95	8.04	-110.	70.	29.	0.41	-209.
2	.097	17.96	11.95	8.04	-112.	66.	29.	0.44	-207.
3	.103	17.94	11.95	8.04	-115.	70.	32.	0.46	-217.
4	.092	17.92	11.95	8.04	-117.	63.	30.	0.48	-209.
5	.092	17.89	11.95	8.04	-119.	62.	31.	0.50	-213.
6	.091	17.87	11.95	8.05	-121.	62.	33.	0.53	-216.
7	.096	17.86	11.95	8.05	29.	65.	34.	0.52	-71.
8	.124	17.87	11.95	8.05	178.	84.	37.	0.44	57.
9	.161	17.88	11.96	8.05	313.	110.	33.	0.30	171.
10	.183	17.91	11.96	8.06	418.	125.	23.	0.18	270.
11	.206	17.94	11.96	8.06	484.	140.	17.	0.12	327.
12	.228	17.97	11.96	8.06	511.	155.	8.	0.05	348.
13	.262	18.00	11.96	8.06	496.	178.	2.	0.01	317.
14	.278	18.03	11.96	8.07	443.	189.	-7.	-0.04	260.
15	.311	18.04	11.96	8.07	353.	212.	-12.	-0.06	153.
16	.311	18.04	11.96	8.07	229.	212.	-7.	-0.03	24.
17	.300	18.03	11.96	8.07	83.	204.	2.	0.01	-123.
18	.255	18.00	11.96	8.08	-76.	174.	17.	0.10	-267.
19	.244	17.97	11.96	8.08	-84.	166.	27.	0.16	-277.
20	.227	17.94	11.97	8.08	-88.	155.	32.	0.21	-276.
21	.173	17.92	11.97	8.08	-93.	118.	30.	0.25	-241.
22	.151	17.89	11.97	8.09	-98.	103.	31.	0.30	-231.
23	.124	17.87	11.97	8.09	-103.	84.	29.	0.34	-216.

4.3.1 Water Thermal Structure

The simulated monthly water temperature is shown in Figure 14. The thermal structure derived from this model shows that during 1982 the lake stratified from February until November and the water surface temperature ranged from 0 °C to 23 °C. The surface water temperature decreases to its coolest temperature in February, then increases to its highest in August. After August, the water temperature decreases again. Comparatively, water temperature in the middle and bottom levels reach their highest temperature in October. These values have been confirmed by several field studies in other years (1982 data are not available) (Mason, 1967; Winkler, 1977; Melack, 1983; NRC, 1987).

The simulated diurnal water temperature on September 22nd, 1982, is shown in Figures 15, 16, 17 and 18. In the top layer, the water temperature shows a small diurnal variation and a seasonal decreasing trend. In the middle and bottom layers only a seasonal trend and no diurnal variation is determined. The diurnal variation of surface water temperature is only 0.1 °C. This small variation justifies neglecting the diurnal effect of evaporation since the temperature only increases the saturated water vapor by 0.7 %. That is, the incorporation of hourly data only increases the accuracy of the daily average data by 0.7%. The highest temperature occurs at 3 PM. The lowest temperature occurs at 7 AM when the sun is just rising. The seasonal trend decreases surface water temperature at about 0.2 °C per day and increases the temperature of the middle and the bottom layers at about 0.1 °C per day.

4.3.2 Evaporation Rate

Table 10 compares the simulated annual evaporation rate and that of the evaporation pan method (Vorster, 1985) and a annual normal-year reference evapotranspiration from the area around Mono Lake (Pruitt et al., 1987). The simulated annual saline evaporation rate is 1.03 m/yr (40.4 in/yr) while that from the pan method is 39.7 in/yr. The simulated annual fresh water evaporation rate is 1.08 m/yr (42.4 in/yr) while that from the pan method is 1.06 m/yr (41.8 in/yr) (Vorster, 1985). In addition, comparing an annual evapotranspiration of 1.12 m/yr (44.2 in/yr) (Pruitt et al., 1987) for an area just east of Lee Vining, the agreement among these values is quite remarkable.

The simulated monthly saline evaporation rate for Mono Lake during 1982, compared with the monthly evaporation pan data (without pan-to-lake adjustment) at the Simis station (Vorster, 1985) and a normal-year reference evapotranspiration from the area around Mono Lake (Pruitt et al., 1987) is shown in Figure 19. The simulated monthly evaporation from IEM ranges from a low of 0.8 mm/day in February to a high of 4.9 mm/day in July. In August, although the simulated water surface temperature reaches its highest, due to a weaker wind speed, the evaporation rate shows a relative decrease in comparison with July and September. High evaporation rates in these months are most likely caused by the combination effects of higher water surface temperature and higher wind speed. This figure also illustrates the differences in response of the three types of surfaces with the great lag in lake evaporation behind the evaporation of evaporation pan and the evapotranspiration of grass. The simulated time lag of evaporation is about one month at Mono Lake.

According to the simulation, the salinity of the lake decreases the evaporation rate by 4.8%. This is very close to Vorster's (1985) estimation of 5.4%. Using the IEM method as a calibration, the evaporation pan coefficient of the Simis station for Mono Lake is determined to be 0.72.

Figure 20 shows the simulated diurnal evaporation rate during Sep. 22nd, 1982 when the evaporation rates vary from 0.09 mm/hr to 0.31 mm/hr. Before the sun rises, the evaporation rate is almost a constant. After sunrise, the evaporation rate begins to increase. The peak evaporation rate occurs at 4 PM during the highest wind speed, then the rate decreases until midnight.

Table 10. A Comparison of Evaporation Rate between those Simulated by the IEM & Using the Evaporation Pan Method

1982 Evaporation Rate		
Methodology	Fresh Water (in/yr)	Saline Water (in/yr)
IEM	42.4	40.4
Pan Method ¹	41.8	39.7
Evapotranspiration around Mono Lake = 44.2 in/yr (Pruitt et al., 1987)		
1. Using Simis station with a pan coefficient = 0.71 and salinity adjustment coefficient = 5.4 % (Vorster, 1985).		

4.3.3 Distribution of Energy

The simulated monthly and diurnal (September 22nd, 1982) energy components of Mono Lake are shown in Figures 21 and Figure 22, respectively. The simulated monthly net solar radiation, downward/upward long-wave radiation and net radiation fluxes are shown in Table 11. The subsurface energy flux, G_s , shows a significant seasonal and diurnal variation. Most of the absorbed solar energy becomes energy flux, G_s , and is stored in the water body. The upward long-wave radiation and the sensible heat are relatively constant during the day. The latent heat shows a significant seasonal and diurnal variation. The variation of latent heat is primarily caused by the combination effects of water surface temperature and wind speed.

The simulated monthly Bowen ratio at Mono Lake for 1982 is shown in Figure 23 and varies from -0.04 to 1.61. The low values occur during the summer, and the high values during the winter. The only minus ratio occurs in May. The calculated diurnal Bowen ratio on September 22nd, 1982 is shown in Figure 24. It varies from -0.06 to 0.53. The minus ratios occur at afternoon and the high values at dawn.

A comparison between IEM simulated Bowen ratio derived from equation (18) and that calculated from Penman's approach (Brutsaert, 1982) as discussed in equation (20) is also presented in Figures 23 and 24. γ in equation (20) is equal to 0.53 mb/°K for mean barometric pressure, P , of 810 mb over Mono Lake. The equation (20b) can be written as

$$B_o = 0.414 \frac{1}{de'/dT_a} - 0.22 \quad (42)$$

From the comparisons, the Bowen ratio derived from Penman's approach, which uses air temperature only, is shown highly in agreement to the theoretical formula of equation (18). This result also implies that the Bowen ratio over water bodies depends greatly on the value of air temperature in comparison with humidity and water temperature.

**Table 11. Simulated Monthly Radiation Energy Fluxes at
Mono Lake, 1982**

Month	Net Solar Radiation	Downward Long-wave Radiation	Upward Long-wave Radiation	Net Radiation
	W/M ²	W/M ²	W/M ²	W/M ²
J	79	232	320	-9
F	132	221	308	45
M	181	246	320	107
A	244	244	333	155
M	293	285	358	220
J	310	290	378	223
J	305	309	393	221
A	271	313	402	181
S	192	296	394	94
O	149	270	373	47
N	98	249	356	-10
D	69	249	335	-16

5. Model Uncertainties

This section discusses the uncertainties of the IEM as a function of the change in the frequency of the input meteorological data and changes of lake parameters such as heat diffusivity and the thickness of each layer.

5.1 Uncertainty due to the Change of the Frequency of the Input Meteorological Data

Most evaporation and water thermocline simulation studies (e.g. Hostetler, 1987; Babajimopoulos, 1982; Aldama, 1989; Croley, 1989) use daily meteorological data as inputs to the numerical models. These calculations assume that diurnal effects are not important. However, the solar radiation follows a diurnal cycle. Therefore, an annual simulation of the IEM model using both daily and hourly average meteorological data is performed. A comparison of daily and hourly surface water temperature is presented in Figure 25. A similar comparison of evaporation is shown in Figure 26.

The simulated water temperatures are initially similar, but they gradually separate as shown in Figure 25. During the summer, the surface water temperature, using daily data, is about 1°C less than that using hourly data. After the summer, the simulated temperatures of these two data sets becomes closer. This also occurs in Figure 26 regarding evaporation rates. During the summer, the simulated evaporation rate using daily data is 8% less than that using hourly data. After the summer, the simulated evaporation rates of these two data sets becomes closer. During the entire year, the simulated annual evaporation rate using daily data is 5.5 % less than that using hourly data.

The daily evaporation deviation of the result of daily data to the hourly data as a function of the simulated period is present in Figure 27. The deviations vary from 0% at the begining stage to -8% after 3 - 6 months' simulation. But the deviation does not increase with time. The daily deviation decreases to -3.5% after one year's simulation. By using daily data, although the simulated

annual evaporation rate is 5.5 % less than that using hourly data, the results are accurate enough for a shorter period simulation. From Figure 27, the deviation is less than -1% for a simulation period of less than a month. Also, from the diurnal water temperature of the top layer, as shown in Figures 15 and 16, the diurnal variation of water temperature is only about 0.1 °C. This small variation increases the saturated water vapor by 0.7 % according to the equation (2). That is, the incorporation of hourly data only increases the accuracy of the evaporation estimation over that of the daily average data by 0.7%. This justifies neglecting the diurnal effect of evaporation for short-term estimation (Brutsaert, 1982; Henderson-Sellers, 1987b)

In summary, the deviation is less than one percent using daily data as an input for a period of less than a month, but for longer periods the use of daily data will cause a small variation in the simulated values of evaporation and water temperature.

5.2 Uncertainty due to Lake Parameters

The thermal diffusivities and the thickness of each layers are two simplified terms in the thermocline 3-layer simulation sub-model. They are not constant during the entire year. A sensitivity is tested by changing these values. The results are presented in Figures 28 and 29. If the thickness of the top layer varies from 2 meters to 16 meters while the proportion of the thickness of the middle to the bottom layer remain unchanged, the evaporation rates change from 2.5 % to -2.0 % in comparison with the current thickness of 9 meters. If the heat diffusivities of the epilimnion layer and the hypolimnion layer change from 0.1 to 10 times of the current values, it affects the evaporation from 0.3 % to 0 % and 4.6 % to -2 %, respectively. In summary, the simplified estimation of the thermal diffusivities and thickness causes the inaccuracy within 5 %. This conclusion justifies the use of the simplified 3-layer thermocline simulation module.

6. Application

This section discusses the utilization of IEM to characterize the phenomenon of evaporation and includes the time lag effect of deep water bodies, climatic variation on evaporation and salinity effect on evaporation. In addition, a technique combines IEM and the evaporation pan method is used to determine long-term evaporation rate from Mono Lake.

6.1 Time Lag Effect

The ocean and other bodies of water are the major response systems to the insolation of solar energy. Two thirds of the earth's surface is covered by water. Therefore, the water receives two thirds of the solar energy, responding to it in two ways. First, the water changes the energy into two phases: sensible heat and the latent heat. Secondly, the water redistributes the diurnal and seasonal variation of solar energy into a more homogeneous time frame. That is, the water absorbs the solar energy during the hot summer months and releases it during the cold winter months. The water also absorbs the solar energy during the day and releases it during the night. Since the minus values of net radiation energy, latent heat and sensible heat is very small in comparison with plus values, the net incoming energy into water body can be roughly approximate to the net radiation energy, and the net outgoing energy from the water body was roughly equal to the latent heat plus sensible heat (Tables 8 and 9). A comparison between the incoming energy, i.e. net radiation energy, R_n , and the returning energy, i.e. $LE+H$, in the air-water interface is simulated with IEM and is shown in Figure 30. Figure 19 compares the seasonal evaporation pattern from Mono Lake, the pan evaporation rates at Simis station (Vorster, 1985) and the evapotranspiration for the area around Mono Lake (Pruitt et al., 1987). Although the incoming energy follows a significant seasonal cycle, the energy return is relatively constant during the entire year. As indicated in these figures there is a time delay of the energy returning to the atmosphere from Mono Lake. The highest insolation occurs in June, but the peak energy returning to the atmosphere is delayed until September. The

main variance of this time lag effect is the depth of water body. For a shallow water body such as an evaporation pan or soil, the time lag effect is not obvious. Similar phenomenon has been found in field studies (Hounam, 1973)

6.2 Sensitivity to Climatic Variations

The sensitivity of evaporation to climate variability has been studied by Hostetler (1987) (Figure 30) using an eddy diffusion model, and by Croley (1989) using a verifiable evaporation model. Both of these models found that solar radiation energy is the most sensitive component to evaporation.

Four sensitivity tests are performed in this study to assess how perturbations in the model climatic inputs variables using hourly data affect the simulated annual lake evaporation. Sensitivity tests are obtained by modifying the 1982 Mono Lake solar radiation, wind speed, air temperature and water vapor pressure data. Each of these data sets is separately perturbed over a range of $\pm 10\%$ relative to the 1982 data (Figure 32). Assuming independence, a 10 % increase in solar radiation energy corresponds to approximately a 10.6 % increase in lake evaporation; a 10 % increase in wind speed corresponds approximately to a 4.5 % increase in lake evaporation, and a 10 % increase in Celsius air temperature corresponds approximately to about a 3.8 % increase in lake evaporation. But, a 10 % increase in water vapor pressure corresponds approximately to a 2.7 % decrease in lake evaporation. Therefore, the solar radiation is the most sensitive input in determining evaporation using the IEM, with wind speed is next and temperature as the third most sensitive term. These results are consistent with the above studies (Hostetler, 1987 and Croley 1989). Humidity is the only factor which has a negative effect on evaporation.

Perturbations of various meteorological data result in the change of evaporation rates (or latent heat released), and in the redistribution of energy fluxes over time. For example, increasing wind speed decreases the simulated ending water temperature. Consequently, this cooler water temperature decreases the evaporation rate of the next year. Therefore, a change in wind speed shifts the evaporation rates between the following and the present year. Changes in air temperature and water vapor pressure will change the Bowen Ratio. Therefore, these shift the energy between the sensible and the latent heat. The change of solar radiation energy changes the incoming energy. Consequently, a correspondent change of outgoing energy includes the sensible and the latent heat.

6.3 Maximum & Minimum Evaporation Rate

The seasonal evaporation rates under the different fractional cloud covers at Mono Lake are shown in Table 12 and Figure 33. Under clear sky, the evaporation rate is 1.22 m/yr (48.0 in/yr). This is an approximate maximum evaporation rate which could have occurred during 1982. Under an overcast condition, the simulated evaporation rate is 0.57 m/yr (22.4 in/yr). This is an approximate minimum evaporation rate which could have occurred during 1982. The actual evaporation rates under these two extreme cloud conditions would be slightly different, accounting for the change of air temperature, wind speed and humidity.

**Table 12. % of Annual Evaporation
Each Month as a Function of Fractional Cloud Cover, Mc**

Mc	J %	F %	M %	A %	M %	J %	J %	A %	S %	O %	N %	D %	Tot m/yr
0.0	3.2	2.6	4.9	6.5	9.3	11.4	14.1	13.2	14.6	9.0	6.2	5.0	1.22
0.1	3.5	2.7	5.0	6.5	9.1	11.1	13.8	13.0	14.7	9.2	6.4	5.1	1.13
0.2	3.8	2.9	5.2	6.6	9.1	11.1	13.9	13.1	15.3	9.7	7.0	6.3	1.05
0.4	4.3	3.1	5.4	6.4	8.4	10.2	12.8	12.1	15.2	9.8	7.0	5.5	0.87
0.6	4.9	3.4	5.7	6.3	7.8	9.4	11.9	11.4	15.5	10.3	7.6	5.9	0.75
0.8	5.7	3.7	6.1	6.3	7.1	8.6	10.8	10.5	15.8	10.8	8.2	6.4	0.64
1.0	6.4	4.1	6.6	6.3	6.5	7.7	9.6	9.5	16.0	11.4	8.9	7.1	0.57

6.4 Evaporation and Wind Speed

The relation between wind speed and the variation of inter-annual water temperature is shown in Figure 34 where, in 1982, wind increased water temperature about 0.18°C and $\pm 10\%$ perturbation of wind speed caused a change of inter-annual variation of water temperature $\mp 0.6^{\circ}\text{C}$. While the wind speed is 3% larger than current model wind speed, the inter-annual water temperature variation is zero as the figure shows. This implies that there are no shifts in energy from year to year. The wind speed, 3% larger than the current value, is equal to 2.84 m/s. The correspondent evaporation rate of the increased wind speed, (Figure 32), is 1.04 m/yr (41.0 in/yr), and can be interpreted as a steady state for a long term value from the lake. The wind speed value of 2.84 m/s can be used for the calibration of Nu_2 term as discussed in Section 3.3. Then the annual mean Nu_2 is 3% larger than the current data. If the wind speed is correct, the mass transfer coefficient should increase from the value, 1.29×10^{-9} , derived from the Harbeck's formula, to 1.33×10^{-9} . The correspondent evaporation rate will also increase about 1.5%, or 1.04 m/yr (41.0 in/yr). However, this evaporation value is not adopted for further estimation since the 0.6°C water temperature variation is negligible. A small variation of inter-annual water temperature is reasonable, and the 1.04 m/yr evaporation rate is very close to the 1.03 m/yr, our 1982 IEM result.

6.5 Sensitivity to Salinity

The IEM numerical model can be used to evaluate the effect of salinity on evaporation. A fresh water evaporation rate from Mono Lake is also simulated using a salinity of 0. The simulated annual fresh water evaporation rate is 1.08 m/yr. Being that the simulated annual saline evaporation rate is 1.03 m/yr from Mono Lake during 1982, the salinity of the lake decreases the evaporation rate for 4.8%. In addition, the relation between evaporation and various salinities is simulated using the IEM. The salinity adjustment ratios of saline water evaporation rate from a fresh water evaporation rate is presented in Figure 35. The figure shows that the simulated results are consistent with other studies (Bonython, 1956; Turk, 1970; Loeffler, 1977; Salhotra, 1985), especially, to Loeffler's (1977) study which was based on Mono Lake. Although this study showed a high agreement with the others, the assumption of the β coefficient of Mono Lake should be noted. This study derives the β coefficient of Mono Lake with the assumption of NaCl to be the only composition of the solute of saline water. The chemical compositions of the Mono Lake include Ca, Mg, Na, K, SO_4 , Cl, As, SiO_2 , Fe, B, PO_4 , F and CO_3 (LADWP, 1986, 1987).

6.6 Pan Coefficient

In 1982, the pan evaporation rate at the Simis station was measured as 1.51 m/yr (Vorster, 1985). Using the IEM method as a calibration, the simulated evaporation pan coefficient of the Simis station for Mono Lake was determined to be 0.72. Recalling the simulated fresh water evaporation rate from Mono Lake is 1.08 m/yr (Table 9), this coefficient is very close to the value, 0.70, as suggested in various other studies (e.g. Viessman, 1977; Dunne, 1978)

6.7 Long-Term Evaporation

This section determines the long term evaporation rate from Mono Lake. As previously noted, IEM can only be used in the year 1982 due to the data availability to simulate the evaporation rate from Mono Lake. In order to determine the long-term average evaporation rate, the IEM model is combined with the evaporation pan method. Two pan stations are available in the Mono Basin. One evaporation pan operated at the Mono Lake on-shore Simis station from 1980 to 1983 (Vorster, 1985), and another evaporation pan has been operating at Grant Lake, ten kilometers from Mono Lake, since 1940 (LADWP, 1987).

The procedure is as follows: First, the new pan coefficient derived in 1982's simulation, is adjusted to the evaporation pan data measured at Grant Lake and at the Simis station. Second, using the IEM simulation these data are adjusted by the derived salinity affect. Finally, the long term variation of evaporation rates are checked with the maximum and minimum benchmarks. The new pan coefficient used is 0.72. The salinity decreases the evaporation rate by 4.8%. The maximum evaporation rate is determined to be 1.22 m/yr (48.0 in/yr), and the minimum evaporation rate 0.57 m/yr (22.4 in/yr).

Using the Simis station data, the evaporation rates at Mono Lake from 1981 to 1983 are shown in Figure 36. They vary from 1.02 m/yr (40.4 in/yr) to 1.17 m/yr (46.1 in/yr). The three-year average rate is 1.08 m/yr (42.5 in/yr). The calculated evaporation rates are within the range of the approximate maximum - minimum values. However, the reliability of these results are based upon only the three-year period which the Simis station recorded.

Although the Grant Lake station has a longer period of record than the Simis station, its pan site is over 700 feet higher than the surface of Mono Lake and is six miles away. Therefore, an extrapolation of the relationship between the Grant Lake station and the Simis station data is derived and used in this study (similar to LADWP, 1984a). Using the Grant Lake evaporation pan data and a pan conversion relationship, the evaporation rates at Mono Lake from 1940 to 1985 are shown in Figure 37. The lowest evaporation rate is 0.85 m/yr (33.5 in/yr) in 1952. The highest evaporation

rate is 1.29 m/yr (50.8 in/yr) in 1978. This maximum value contradicts the approximate maximum value for Mono Lake (see section 6.3). Therefore, it can be concluded that the evaporation data measured at Grant Lake should not be applied to Mono Lake. Two reasons may explain this: First, a floating evaporation pan was used at Grant Lake from 1942 to 1969 and then a land evaporation pan was used from 1968 to the present (Vorster, 1985). Secondly, and more importantly, there is a large difference in the topography between the two lakes.

The long-term saline evaporation rates from Mono Lake are determined to be 1.08 m/yr (43.0 in/yr) using the adjusted Simis station data. This evaporation rate can be compared with the values of 45 in/yr suggested by Vorster (1985) and 40 in/yr suggested by LADWP (1987).

7. Conclusion

This study validates IEM methodology by applying it to Mono Lake, California. Using 1982 meteorological data, the IEM simulates the lake thermal structure and evaporation rate. The simulated evaporation rate from Mono Lake during 1982 is determined to be 1.03 m/yr (40.6 in/yr). This evaporation rate is close to the values obtained using the evaporation pan method (Vorster, 1985). The thermal structure derived from the IEM model indicates that the lake stratified from March until November, 1982, and the water surface temperature ranged from 0°C to 23°C. This phenomenon has been confirmed in other years (Mason, 1967; Winkler, 1977; Melack, 1983; NRC, 1987). Although the thermocline simulation module is a simplified model, from the uncertainty analysis of heat diffusivities and thickness of each layers, the resulting inaccuracy from the simplified model is less than 5 %.

Using the IEM methodologies to investigate the phenomenon of evaporation, the study found the following features:

1) The diurnal variation of water surface temperature is not significant. Therefore, a daily average meteorological data would be sufficient for the calculation of evaporation for short periods to monthly simulation. But, for annual simulation, the accumulated small difference of water temperature would result in a 5.5 % less estimation of evaporation rate by using daily average data. However, daily meteorological data are used as inputs to most evaporation and water thermocline simulation studies (e.g. Hostetler, 1987; Babajimopoulos, 1982; Aldama, 1989; Croley, 1989).

2) The lake with a depth of 17.8 m postpones the energy response from the highest net incoming radiation flux in June to the peak returning energy in September.

3) From the sensitivity analysis, the solar radiation energy is the most sensitive term among meteorological data, and, hence, must be carefully noted.

4) The approximate maximum and minimum evaporation rates can be derived under clear sky condition and overcast condition using the IEM model. These evaporation rates can be used as benchmarks for the inspection of evaporation rates estimated by less accurate methodologies, such as the evaporation pan method.

5) A lake salinity of 92.1 g/kg can reduce evaporation rate by 4.8%. The salinity effects on the reduce of evaporation by using IEM shows favorable results compared with other studies.

6) Since meteorological input data for the IEM model are not available for more than one year, a technique combining the IEM, the pan method and the maximum and minimum evaporation benchmarks is developed in order to determine the long-term evaporation rate from Mono Lake. The long-term saline evaporation rates are Mono Lake were determined to 1.08 m/yr (42.5 in/yr). However, this value is based on only three years of data at the Simis station and based on an estimation of the solar radiation and over-water wind speed in 1982. Additional data should be obtained for further testing of the long-term value.

The IEM model not only reflects inter-annual evaporation variation but can also calculate monthly evaporation rates. The cost of the IEM is significantly less than that of the mass transfer method and the energy budget method. In addition, the IEM model is more accurate than the evaporation pan method. All these features make the IEM worthy of implementation and further improvement. Moreover, the IEM offers an opportunity for other applications, such as the determination of the evaporation pan coefficient, determining the affect of salinity on evaporation, determining its use as an input to a global circulation model, and determining the impact of evaporation rate changes due to global climatic warming.

8. Future Research

The IEM, as currently written, is valid only for temperature-stratified saline lakes. The year which the model used for the Mono Lake simulation, 1982, was fortuitous due to a large influx of fresh water in 1983, induced by the Pacific El Niño climatic conditions, which resulted in chemical stratification of the water column (LADWP, 1984b). This stratification persisted until 1988 when the lake overturned (November, 1988) in response to the recent drought years. Therefore, it is unlikely that the current model would work as well during this period. Between 1983 to 1988 Mono Lake would not conform to the temperature-stratified thermocline simulation model, described in Section 3.1.4. Chemical or density stratification of saline water bodies is common. The Great Salt Lake has been, and remains, stratified. This is also due to anthropogenic activities, such as occurred to Big Soda Lake, Nevada, which became stratified due to the inflow of irrigation water. A more general model for simulating evaporation rates in saline lakes must include the effects of density stratification. A density-stratified model would most logically be an extension of the three-layer model. In order to simulate the density structure of a water body, salt, as well as temperature, structures are required. This also requires calculating salinity distribution along the water column.

Fortunately, an advantage of the IEM is the use of four function modules. This offers a flexibility for future modification when improvements are made to each function modules. Currently, the mass transfer module can be improved by the incorporation of atmospheric boundary layer theory (e.g. Brutsaert, 1982; Croley, 1989). An eddy diffusivity model can be substituted for the water thermocline simulation module (e.g. Babajimopoulos, 1986; Hostetler, 1987). The eddy diffusivity model has potential to determine the heat diffusivity in three-layer sub-model inclusion density-stratified effect, hence, remedying the current failure of simulation during density-stratified periods.

Acknowledgments

The work was funded by the University of California, Water Resources Center, Riverside, California, under grant number W-706. The authors gratefully acknowledge the Great Basin Unified APCD for offering meteorological data at the Lee Vining station, the USBLM for offering meteorological data at the Simis station, the LADWP for offering meteorological data at the Cain Ranch station, and the Center for Remote Sensing and Environmental Optics at UCSB for offering solar radiation data at Mammoth Mountain. Special thanks to Professor M. Wurtele, UCLA, and three anonymous reviewers, for their comments and assistance.

Notation Index

A	water body surface area (m^2)
$A(z)$	water body area at depth z (L^2),
B_0	Bowen ratio,
C_w	specific heat of the water (j/kg),
d	zero plane displacement,
E	saline evaporation rate (L/T),
e_a	vapor pressure in the air (mb),
E_{∞}	solar constant, w/m^2 ,
e^*	saturation vapor pressure above a water surface as a function of salinity (S), and water surface temperature (T_s) (mb),
G_{bed}	specific energy flux leaving the layer at the hypolimnion and entering the lake bed (w/m^2).
G_s	specific energy flux from the water surface into the water body (w/m^2),
G_m	specific energy flux leaving the top layer and entering the middle layer (w/m^2),
H	sensible heat (w/m^2),
h	height of the measurement point,
L	latent heat of vaporization (j/kg),
m_c	fractional cloud cover (%),
N	mass transfer coefficient for a specific lake,
R_{ld}	downward long-wave atmospheric radiation (w/m^2),
R_{lsc}	atmospheric radiation under clear skies (w/m^2),
R_{lu}	upward long-wave radiation (w/m^2).
R_n	net radiation flux density at the air-water interface (w/m^2),
R_s	downward solar radiation energy flux on the water surface (w/m^2),
R_e	extraterrestrial radiation (w/m^2), that is, the solar radiation which would reach a horizontal surface in the absence of the atmosphere,
S	surface lake salinity (g/kg),
t_j	the Julian date (number of the year) in the year.
t_h	the local apparent solar time (using a 24-hour clock).
T_a	air temperatures ($^{\circ}C$ or $^{\circ}K$),
T_t, T_m	temperature in the top and the middle layers, respectively ($^{\circ}C$ or $^{\circ}K$),

T_b	temperature in the bottom layer ($^{\circ}\text{C}$ or $^{\circ}\text{K}$),
T'_t	temperature in the top layer after time lag Δt ($^{\circ}\text{C}$ or $^{\circ}\text{K}$),
T'_b	temperature in the bottom layer after time lag Δt ($^{\circ}\text{C}$ or $^{\circ}\text{K}$),
T'_m	temperature in the middle layer after time lag Δt ($^{\circ}\text{C}$ or $^{\circ}\text{K}$),
T_s	water surface temperature ($^{\circ}\text{C}$ or $^{\circ}\text{K}$),
t_R	$1-(373.15/T_s)$,
T_w	water temperature, ($^{\circ}\text{C}$ or $^{\circ}\text{K}$),
T'_w	water temperature after time lag Δt , ($^{\circ}\text{C}$ or $^{\circ}\text{K}$),
$\partial T_w/\partial t$	the rate of change of the water temperature ($^{\circ}\text{C}/\text{T}$ or $^{\circ}\text{K}/\text{T}$),
$\partial T_w/\partial z$	the gradient of the water temperature ($^{\circ}\text{C}/\text{L}$ or $^{\circ}\text{K}/\text{L}$),
u_2	average wind speed measured 2 meters above the water surface (L/T),
$\partial W/\partial t$	rate of energy storage per unit area in the layer (w/m^2).
x	downwind distance.
u_w	wind speed related to the observed land wind speed (u_l) at the same height,
u_l	observed land wind speed,
z_{ow}	water surface roughness,
Z	average depth of a water body, m,
Z_t, Z_m, Z_b	thickness of the top, the middle and the bottom layers, respectively (m),
z_{ol}	land surface roughness,
α	albedo of the water surface.
α_t	heat diffusivity in the top (epilimnion) layer (L^2/T),
α_{tm}	heat diffusivity in the layer between the top and the middle layers (L^2/T),
α_m	heat diffusivity in the middle layer (L^2/T),
α_{mb}	heat diffusivity in the layer between the middle and the bottom layers (L^2/T),
α_b	heat diffusivity in the bottom (hypolimnion) layer (L^2/T).
β	activity coefficient of water for a specific salinity,
δ	Earth's declination,
δ	the thickness of the boundary layer at a distance, x , downwind,
ε_{ac}	emissivity of the atmosphere.

ϵ_s emissivity of the water surface, 0.97 (Brutsaert, 1982),
 θ latitude,
 ρ water density (M/L^3),
 σ Stephan-Boltzman constant, $5.6697 \times 10^{-8} \text{ W m}^{-2} \text{ K}^{-4}$,
 ϕ hour angle,
 Δt time interval (hours).

Bibliography

- Abdulmumin, S., L. O. Myrup and J. L. Hatfield, "An Energy Balance Approach to Determine Regional Evapotranspiration- Based on Planetary Boundary Layer Similarity Theory and Regularly Recorded data", Water Resources Research, Vol. 23, No. 11, pp 2050-2058, Nov. 1987.
- Aldama, A.A., D. R. F. Harleman and E. Adams, "Hypolimnetic Mixing in a Weakly Stratified Lake", Water Resources Research, Vol. 25, No. 5, pp. 1014- 1024, May 1989.
- Anderson, E.R., "Energy-Budget Studies", U. S. Geol. Surv. Prof. Pap. 269, pp 71-119, 1954.
- Babajimopoulos, C. and F. Papadopoulos, " Mathematical Prediction of Thermal Stratification of Lake Ostrovo (Vegoritis), Greece", Water Resources Research, Vol. 22, No. 11, pp. 1590- 1596, 1986.
- Black, L.G., Report on the Mono Lake Investigation. Unpub. report for the Los Angeles Department of Water and Power, 1958.
- Briscoe, F., and P. Shaw, "Spread And Evaporation of Liquid", Prog. Energy Combustion Sci., Vol. 6, 127- 140, 1980.
- Brutsaert, W. and G. Yeh, "Implications of a Type of Empirical Evaporation Formula for Lakes and Pans", Water Resources Research, Vol. 6, No. 4, pp. 1202- 1215, 1970.
- Brutsaert, W. H., Evaporation into the Atmosphere, D. Reidel Publish Company, 299 pp., 1982.
- Calder, R., and C. Neal, "Evaporation from saline lakes: A combination equation approach", J. Hydrol. Sci., 29(1), 89- 97, 1984.
- Croley II, T.E., "Verifiable Evaporation Modeling on the Laurentian Great Lakes", Water Resources Research, Vol. 25, No. 5, pp 781- 792, 1989.
- Crow, F. R. and S. D. Hottman, "Network Density of Temperature Profile Stations and Its Influence on the Accuracy of Lake Evaporation Calculations", Water Resources Research, Vol. 9, No. 4, pp. 895- 899, Aug. 1973.
- de Bruin, H.A., "A Simple Model for Shallow Lake Evaporation", J. of Applied Meteorology, Vol. 17, pp. 1132- 1134, 1978.
- Dunne, T. and L. Leopold, Water in Environmental Planning, W. H. Freeman and Co., San Francisco, pp. 818, 1978.
- Faeth, G. M., "Evaporation and Combustion of Sprays", Prog. Energy Combustion Sci., Vol. 9, pp. 1- 76, 1983.
- Ficke, J. F., D. B. Adams, and T.W. Danielson, "Evaporation from Seven Reservoirs in the Denver Water-Supply System, Central Colorado", U.S. Geophysical Survey Water-Resources Investigations, 76- 114, 170 pp., 1977.
- Ficke, J. F., "Comparison of Evaporation Computation Methods, Pretty Lake, Lagrange County, Northeastern Indiana", Geological Survey Professional Paper 686 -A, 44 pp., 1972.
- Goldman, C. R. and A. J. Horne, Limnology, McGraw-Hill Book Company, pp., 1983.
- Haney, R.L. and R.W. Davies, "The Role of Surface Mixing in the Seasonal Variation of the Ocean Thermal Structure", J. of Physical Oceanography, Vol. 6, pp. 504- 510, July 1976.
- Harbeck, G. E., "The effect of salinity on evaporation", U.S. Geol. Surv. Prof. Pap. 272-A, 1955.
- Harbeck, G. E., "A practical field technique for measuring reservoir evaporation utilizing mass-transfer theory", U.S. Geol. Surv. Prof. Pap. 272-E, pp. 101 -105, 1962.

- Henderson-Sellers, B., Engineering Limnology, 356 pp., Pitman, London, 1984.
- Henderson-Sellers, B., "New Formulation of Eddy Diffusion Thermocline Models", Appl. Math. Modelling, Vol. 9, pp. 441- 446, Dec. 1985.
- Henderson-Sellers, B., "Calculating the Surface Energy Balance for Lake and Reservoir Modeling: A Review", Reviews of Geophysics, Vol. 24, No. 3, pp. 625- 649, 1986.
- Henderson-Sellers, B., "One Dimensional Models for the Thermal Stratification: Review of use in Oceans and Lakes" Environ. Software, pp. 78-84, 1987.
- Hostetler, S., "Simulation of lake evaporation with an energy balance-eddy diffusion model of lake temperature: model development and validation, and application to lake-level variations at Harney-Malheur Lake, Oregon, Ph.D. thesis, University of Oregon, 1987.
- Hounam, C. E., Comparison between Pan and Lake Evaporation, WMO # 354, pp. 52, 1973.
- Hutchinson, A Treatise on Limnology, John Wiley & Sons, Inc., New York, 1015 pp., 1957.
- Jassby, A. "Vertical Patterns of Eddy Diffusion During Stratification in Castle Lake, California" Limnology and Oceanography, V. 20 (4), pp 530- 543, July 1975
- Keijman, J. Q. and R.W.R. Koopmans, "A Comparison of Several Methods of Estimating the Evaporation of Lake Flevo", Hydrology of Lakes, Helsinki Symposium, International Association of Hydrological Sciences, Publication 109, pp. 225- 232, 1973.
- Kohler, M. A. "Lake and Pan Evaporation", Water-loss investigations: Lake Hefner Studies. Tech. Report. Prof. Paper 269, Geol. Survey, U.S. Dept. Interior, pp. 127- 148, 1954.
- Kohler, M.A., T.J. Nordenson, and W.E. Fox, Evaporation from Pans and Lakes, U.S. Weather Bureau, Research Paper 38, 20 pp., 1955.
- Kohler, M.A., T.J. Nordenson, and D.R. Baker, Evaporation Maps for the United States, U.S. Weather Bureau, Technical Paper 37, 13 pp., 1959.
- Kohler, M.A. and L.H. Parmele, "Generalized Estimates of Free-Water Evaporation", Water Resources Research, Vol. 3, No. 4, pp. 997- 1005, 1967.
- Kondo, J. and Y. Sasano, and T. Ishii, "On Wind-Driven Current and Temperature Profiles with Diurnal Period in the Oceanic Planetary Boundary Layer", J. of Applied Meteorology, Vol. 9, pp. 360- 372, Mar. 1979.
- Kullenberg, G., "Vertical Diffusion in Shallow Waters", Tellus, Vol. 23, pp. 129- 135, 1971.
- LADWP, Background Report on Mono Basin Geology and Hydrology, 1984a.
- LADWP, Briefing Document, March, 1984b.
- LADWP, "Report on Mono Lake Salinity", Nov. 1986.
- LADWP, Mono Basin Geology and Hydrology, Los Angeles, CA. 1987.
- Law, C. K., "Recent Advances in Droplet Vaporization and Combustion", Prog. Energy Combustion Sci., Vol. 8, pp. 171- 201, 1982.
- Lean, J., "Contribution of Ultraviolet Irradiance Variations to Changes in the Sun's Total Irradiance", Science, Vol. 244, No. 4901, pp. 197- 200, 14 April 1989.
- Linacre, E.T., "A Simple Formula for Estimating Evaporation Rates in Various Climates, Using Temperature data Alone", Agricultural Meteorology, 18, pp. 409- 424, 1977.
- Marciano, J. J., and Harbeck, G. E., Jr., 1952, Mass-transfer studies in Water-loss investigations: lake Hefner studies, technical report, U.S. Geol. Survey Prof. Paper 269, pp. 46- 70, 1954.

- Mason, D. T., Limnology of Mono Lake, California, U. California Publish Zoology, 83, 110 pp., 1967.
- McCormick, M. J. and D. Scavia, "Calculation of vertical profiles of lake-averaged temperature and diffusivity in lakes Ontario and Washington", Water Resour. Res., 17, 305- 310, 1981.
- Meehl, G.A., "A Calculation of Ocean Heat Storage and Effective Ocean Surface Layer Depths for the Northern Hemisphere", J. of Physical Oceanography, Vol. 14, pp. 1747- 1761, Nov. 1984.
- Melack, J. M., "Large, Deep Salt Lakes: A Comparative Limnological Analysis", Hydrobiologia, 105, 223- 230, 1983.
- Milly, P. C. D., "A Linear Analysis of Thermal Effects on Evaporation From Soil", Water Resources Research, Vol. 20, No. 8, pp. 1075-1085, Aug. 1984a.
- Milly, P. C. D., "A Simulation Analysis of Thermal Effects on Evaporation From Soil", Water Resources Research, Vol. 20, No. 8, pp. 1087-1098, Aug. 1984b.
- Milly, P.C.D. and P.S. Eagleson, "Effects of Spatial Variability on Annual Average Water Balance", Water Resources Research, Vol. 23, No. 11, pp. 2135- 2143, Nov. 1987.
- National Research Council, The Mono Basin Ecosystem - Effects of Changing Lake Level, Mono Basin Ecosystem Study Committee, National Academy Press, Washington, D.C., 272 pp., 1987.
- Niiler, P.P. and Kraus, E.B., "One-Dimensional Models of the Upper Ocean", Chapter 10 in Modelling and Prediction of the Upper Layers of the Ocean, ed. E.B. Kraus, 1977, Pergamon.
- Oke, T.R., Boundary Layer Climates, 2 ed, Methuen: London & New York, 435 pp., 1987.
- Persaud, C., Potential Evapotranspiration in Different Climatic Regions of Guyana, McGill University, Climatological Research Series #11, pp. 101, Oct. 1977.
- Priestley, C.H.B. and R.J. Taylor, "On the Assesment of the Surface Heat Flux and Evaporation Using Large Scale Parameters", Mon. Weather Rev., 100, pp. 81- 92, 1972.
- Pruitt, W.O., E. Fereres, K. Kaita, and R. L. Snyder, Reference Evapotranspiration (ET₀) for California, Div. of Agric. and Nat. Resources, University of California, Bulletin 1922. 14 pp + 12 Maps, 1987.
- Richards, J.M., "Simple Expression for the Saturation Vapour Pressure of Water in the Range -50°C to 140°C", Brit. J. Appl. Phys., Vol. 4., L15- L18, 1971.
- Salhotra, A. M., E. Adams, and D. R. F. Harleman, "Effect of Salinity and Ionic Composition on Evaporation: Analysis of Dead Sea Evaporation Pans", Water Resources Research, Vol. 21, No. 9, pp. 1336- 1344, Sep., 1985.
- Salhotra, Atul M., E. Adams, and D. R. F. Harleman, "The Alpha, Beta, Gamma of Evaporation From Saline Water Bodies", Water Resources Research, Vol. 23, No. 9, pp. 1769- 1774, Sep., 1987.
- Sirignano, W. A., "Fuel Droplet Vaporization and Spray Combustion Theory", Prog. Energy Combustion Sci., Vol. 9, pp. 291- 322, 1983.
- Sod, G.A., Numerical Methods in Fluid Dynamics: Initial and Boundary-Value Problems, Cambridge U. Press, 446 pp., 1985.
- Spigel, R. H. and J. Imberger, "The Classification of Mixed-Layer Dynamics in Lakes of Small to Medium Size", J. of Physical Oceanography, Vol. 10, pp. 1104- 1121, July 1980.
- Stewart, R. B. and W. R. Rouse, "A Simple Method for Determining the Evaporation From Shallow Lake and Ponds", Water Resources Research, Vol. 12, No. 4, pp. 623- 628, Aug. 1976.

- Stewart, R. B., "Substantiation of the Priestley and Taylor Parameter = 1.26 for Potential Evaporation in High Latitudes", I. of Applied Meteorology, Vol. 16, pp. 649- 650, June 1977.
- van de Griend, A.A. and J.H. van Boxel, "Water and Surface Energy Balance Model with Multilayer Canopy Representation for Remote Sensing Purposes", Water Resources Research, Vol. 25, No. 5, pp. 949- 971, May 1989.
- Vorster, P., A Water Balance Forecast Model for Mono Lake, CA., MS. Thesis, Ca. State Univ. Hayward, pp. 350, 1985.
- Warnaka, K. and L. Pochop, "Analyses of Equations for Free Water Evaporation Estimates", Water Resources Research, Vol. 24, No. 7, pp. 979-984, July 1988.
- Welch, P. S., Limnology, McGraw-Hill Book Company, 1935.
- Wetzel, R. G., Limnology, 2nd ed., CBS College Publishing: 383 Madison Ave., New York, NY 10017, 850 pp., 1983.
- Williams, F. A., Combustion Theory, The Benjamin/Cummings Company, Inc., 680 pp., 1985.
- Winter, T. C., "Uncertainties in Estimating the Water Balance of Lakes", Water Resources Bulletin, Vol. 17, No. 1, pp. 82- 115, 1981.
- Winkler, D. W., An Ecological Study of Mono Lake, California, Institute of Ecology Publication, No. 12, U. of California, Davis, 190 pp., June 1977.
- Yonts, W.L., G.L. Giese, and E.F. Hubbard, "Evaporation from Lake Michie, N. Carolina 1961-71", U.S. Geological Survey Water-Resources Investigations 38- 73, 27 pp., 1973.

Appendix

Program Code

```
PROGRAM IEM
C \11\20\89
parameter (nMON=12, NDAY = 365, ihour=0, nhour=23)
DIMENSION DU2(nMON,ihour:nhour),DEA(nMON,ihour:nhour)
dimension DTA(nMON,ihour:nhour),DXMC(nMON,0:nhour)
REAL TE,TM,TH,E,RN
C GET TIME
C MICROSOFT FORTRAN ONLY
  CALL GETTIM(IHRB,IMINB,ISECB,I100B)
C
C INITIAL CONDITIONS
OPEN (UNIT=30,FILE='MONO.PAR')
READ (30,*) S,TEINI,TMINI,THINI,C_MTM,C_NSRM,C_TA,C_EA
OPEN (UNIT=20,FILE='MONO.OUT')
OPEN (UNIT=25,FILE='MONOJ264.OUT')
WRITE (20,3900) S*1000.,TEINI,TMINI,THINI,C_MTM,C_NSRM,C_TA,C_EA
WRITE (*,3900) S*1000.,TEINI,TMINI,THINI,C_MTM,C_NSRM,C_TA,C_EA
C CONSTANT TABLE (SI:MKS UNITS)
C ATMOSPHERIC PRESSURE
CP = 1005.
P = 810.
C LOCATION (LATITUDE)
THETA = 38.*3.14159/180.
C LAKE PARAMETERS
READ (30,*) Z,ZE,ALPHAE,ALPHAH
close (30)
A = 1.5E+8
C ze= 9.
C zm=6.
C zh = 2.8
zm= (z-ze)*6./(6.+2.8)
zh= (z-ze)*2.8/(6.+2.8)
C ALPHAE= 1.5E-4
C alphah= 2.14e-6
alphaM= 2./(1./ALPHAE+1./ALPHAH)
Z0W=0.0004
WRITE (20,3905) Z,ZE,ZM,ZH,ALPHAE,ALPHAM,ALPHAH
WRITE (*,3905) Z,ZE,ZM,ZH,ALPHAE,ALPHAM,ALPHAH
C WATER PROPERTIES
Cw= 4192.*(1-S)
BETA = ACTVTY(S)
ALBEDO = 0.06
C OVER WATER WIND SPEED CONSTANT TABLE
Z0L=0.4
Z0=4.
C INITIAL VARIABLES OF THE YEAR
ESUMYR=0.
JD=0
C READ METEOROLOGICAL DATA
```

```

CALL METE(nMON,ihour,nhour,A,Z0W,Z0L,Z0,DU2,DEA,DTA,DXMC)
C END METEOROLOGICAL DATA
C
C  OUTPUT TITLE
  WRITE (20,3910)
  WRITE (*,3910)
  WRITE (25,3920)
C
  TEOLD=TEINI
  TMOLD=TMINI
  THOLD=THINI
  DO 999 MON= 1,nMON
  IF (MON .EQ.1) THEN
    NDAYTH=31
  ELSE IF (MON .EQ. 2) THEN
    NDAYTH=28
  ELSE IF (MON .EQ. 3) THEN
    NDAYTH=31
  ELSE IF (MON .EQ. 4) THEN
    NDAYTH=30
  ELSE IF (MON .EQ. 5) THEN
    NDAYTH=31
  ELSE IF (MON .EQ. 6) THEN
    NDAYTH=30
  ELSE IF (MON .EQ. 7) THEN
    NDAYTH=31
  ELSE IF (MON .EQ. 8) THEN
    NDAYTH=31
  ELSE IF (MON .EQ. 9) THEN
    NDAYTH=30
  ELSE IF (MON .EQ. 10) THEN
    NDAYTH=31
  ELSE IF (MON .EQ. 11) THEN
    NDAYTH=30
  ELSE IF (MON .EQ. 12 ) THEN
    NDAYTH=31
  ENDIF
C  INITIAL VALUE OF THE MONTH
  ESUM=0.
  TEAVG=0.
  TMAVG=0.
  THAVG=0.
  RNAVG=0.
  XLEAVG= 0.
  HAVG=0.
  GSAVG=0.
  DO 888 DAY=1,NDAYTH
    JD = JD+1
    DO 777 NHR = ihour,nhour
      DT = 3600.

```

```

C   CHANGE DIMENSION METEOROLOGICAL DATA INTO SINGLE VARIABLE
    TA = DTA(MON,NHR)*C_TA
    EA = DEA(MON,NHR)*C_EA
    U2 = DU2(MON,NHR)
    XMC= DXMC(MON,NHR)

C   CALL NSRM(C_NSRM,ALBEDO,THETA,JD,NHR,
+           XMC,EA,TA,TEOLD,RN)
    TE=TEOLD
    DO 100 I=1,3
        CALL MTM(C_MTM,U2,BETA,EA,A,TE,E)
        CALL SEBM(CP,P,TE,TA,EA,BETA,
+           RN,E,XLE,H,GS)
        CALL WTSM(DT,S,CW,ZE,ZM,ZH,
+           ALPHAM,ALPHAH,GS,TEOLD,TMOLD,THOLD,TE,TM,TH)
100  CONTINUE
    TEOLD=TE
    TMOLD=TM
    THOLD=TH
    ESUM=ESUM+E*DT*1000./FLOAT(NDAYTH)
    TEAVG=TEAVG+TE/FLOAT(NDAYTH)/24.
    TMAVG=TMAVG+TM/FLOAT(NDAYTH)/24.
    THAVG=THAVG+TH/FLOAT(NDAYTH)/24.
    RNAVG=RNAVG+RN/FLOAT(NDAYTH)/24.
    XLEAVG=XLEAVG+XLE/FLOAT(NDAYTH)/24.
    HAVG =HAVG +H/FLOAT(NDAYTH)/24.
    GSAVG=GSAVG+GS/FLOAT(NDAYTH)/24.

C   IF (JD .EQ. 264) THEN
    WRITE (25,4000) NHR,E*DT*1000.,TE,TM,TH,RN,XLE,H,GS
    WRITE (*,4000) NHR,E*DT*1000.,TE,TM,TH,RN,XLE,H,GS
    ENDIF
777  CONTINUE
888  CONTINUE
    ESUMYR=ESUMYR+ESUM*FLOAT(NDAYTH)
    WRITE(20,4000) MON,E-
    SUM,TEAVG,TMAVG,THAVG,RNAVG,XLEAVG,HAVG,GSAVG
    WRITE(*,4000)
    MON,ESUM,TEAVG,TMAVG,THAVG,RNAVG,XLEAVG,HAVG,GSAVG
999  CONTINUE
    WRITE (*,4100) TE,TM,TH
    WRITE (20,4100) TE,TM,TH
    WRITE (*,5000) ESUMYR*1E-3
    WRITE (20,5000) ESUMYR*1E-3
3900 FORMAT (' SALINITY = ',F6.2,' G/KG',
+           /, ' INITIAL WATER TEMPERATURE',
+           /, ' TE= ',F6.2,2X,' TM= ',F6.2,2X, ' TH= ',
+           F6.2,2X,'(C)',/,
+           ' CORRECTION FACTORS',/,
+           ' C_MTM= ',F6.2,2X,'C_SEBM= ',F6.2,2X,'C_TA= ',f6.2,2x,

```

```

+ 'C EA= ',f6.2,2x,/)
3905 FORMAT (' LAKE PROPERTIES',
+ /, 'DEPTH= ',F6.2,2X,'ZE= ',F6.2,2X,'ZM= ',F6.2,2X,
+ 'ZH= ',F6.2,2X,'(M)',
+ /, 'ALPHAE= ',E7.2,2X,'ALPHAM= ',E7.2,2X,
+ 'ALPHAH= ',E7.2,2X,'M^2/S',/)
3910 FORMAT (' ', 'Month',1X,' E ',2X,' TE ',2X,' TM ',2X,
+ ' TH ',2X,' Rn ',2X,' LE ',2X,' H ',2X,' Gs ',
+ ' 2X/,' ',6X,'(mm/day)',2X,' (C)',2X,' (C)',2X,
+ ' (C)',2X,'(W/M2)',2X,'(W/M2)',2X,
+ '(W/M2)',2X,'(W/M2)',2X)
3920 FORMAT (' ', 'Hour',2X,' E ',2X,' TE ',2X,' TM ',2X,
+ ' TH ',2X,' Rn ',2X,' LE ',2X,' H ',2X,' Gs ',
+ ' 2X/,' ',6X,'(mm/hr)',2X,' (C)',2X,' (C)',2X,
+ ' (C)',2X,'(W/M2)',2X,'(W/M2)',2X,
+ '(W/M2)',2X,'(W/M2)',2X)
4000 FORMAT (' ',I4,2X,F8.3,2X,3(F6.2,2X),4(F6.0,2X))
4100 FORMAT (/,' SIMULATED WATER TEMPERATURE AT END OF THE SIMU-
LATION',
+ /, 'TE= ',F6.2,2X,'TM= ',F6.2,2X,'TH= ',
+ ' F6.2,2X)
5000 FORMAT (' ANNUAL EVAPORATION RATE = ',F8.3,'M/YR')
C GET TIME
C MICROSOFT FORTRAN ONLY
  CALL GETTIM(IHRE,IMINE,ISECE,I100E)
  EXETIM= (IHRE-IHRB)*3600+(IMINE-IMINB)*60+(ISECE-ISECB)+  

+ (I100E-I100B)/100.
  WRITE (*,5100) EXETIM
  WRITE (20,5100) EXETIM
  CLOSE (20)
  CLOSE (25)
5100 FORMAT (' EXECUTION TIME = ',F8.2, 'SEC')
  STOP
  END
CC
CC
SUBROUTINE METE(nmon,ihour,nhour,A,Z0W,Z0L,Z0,U2,EA,TA,XMC)
DIMENSION U2(nmon,ihour:nhour),EA(nmon,ihour:nhour)
DIMENSION TA(nmon,ihour:nhour),XMC(nmon,ihour:nhour)
C  OVER WATER WIND SPEED FETCH LENGTH
R=SQRT(A/3.14159)
  DELTA=0.86*R**0.8*Z0L**0.2
C
  OPEN (UNIT=10,FILE='MONO.MET')
  DO 1100 MON= 1,NMON
    DO 1200 NHR=IHOUR,NHOUR
      READ (10,*) TA(MON,NHR),EA(MON,NHR),U,XMC(MON,NHR)
C
C  OVER WATER AND HEIGHT ADJUSTMENT OF WIND SPEED
  U2(MON,NHR)= U*LOG(2/Z0W)*LOG(DELTA/Z0L)/LOG(Z0/Z0L)

```

```

+ /LOG(DELTA/ZOW)
C
C
1200  CONTINUE
1100  CONTINUE
  CLOSE (10)
  RETURN
  END
C END OF PROCESSING METEOROLOGICAL DATA
CC
CC
C   SUBROUTINE MTM(C_MTM,u2,beta,ea,A,Ts,E)
C   Mass Transfer Module
C
C   CONSTANT TABLE
XN= 3.367e-9*A**(-0.05)
E=C_MTM*XN*u2*(beta*e_sat(Ts)-ea)
RETURN
END
CC
CC
C   Net Solar Radiation Module
Subroutine NSRM(C_NSRM,ALBEDO,theta,
+                JD,NHR,XMC,EA,TA,TS,RN)
C   ****
C   Constant Tables
C   ****
Eb0 = C_NSRM*1367.
C   BRUTSAERT, MAY NOT BE ACCURATE FOR EA < 10MB
C   Eac = 1.24*(ea/(Ta+273.2))**1.7.
C   SATTERLUND
EAC =1.08*(1-EXP(-EA**((TA+273.2)/2016.)))
Es = 0.97
sigma = 5.6697e-8
C   ****
C   CHANGE JULIAN DAY AND HOUR TO EARTH'S DECLINATION AND HOUR
ANGLE
  DELTA = 23.5*3.14159/180.*SIN((FLOAT(JD)-81.)*2.*3.14159/365.)
  PHI = (FLOAT(NHR)-12.)*15.*3.14159/180.
C
  Rsd=(1-ALBEDO)*(0.75-0.5*Xmc)*Eb0*(cos(phi)*
+ COS(theta)*COS(DELTA)+sin(theta)*sin(delta))
  IF (RSD .LT. 0.) THEN
    RSD = 0.
  END IF
  Rld=Eac*sigma*(Ta+273.2)**4*(1+0.22*XMc**2)
  Rlu = Es*sigma*(Ts+273.2)**4
  Rn = Rsd+Rld-Rlu
  Return
  END

```

```

CC
CC
C  Surface Energy Balance Module
Subroutine SEBM(CP,P,TS,TA,EA,BETA,
+           RN,E,XLE,H,GS)
CALL BOWEN(CP,P,TS,TA,EA,BETA,B0)
XLE = DTY F(TS)*XLATNT(TS)*E
H = XLE*B0
Gs=Rn-XLE-H
RETURN
END

CC
CC
CC  WATER THERMOCLINE SIMULATION MODULE
SUBROUTINE WTSM (DT,S,CW,ZE,ZM,ZH,ALPHAM,
+           ALPHAH,GS,TEOLD,TMOLD,THOLD,TE,TM,TH)
CALL STRATF(Dt,S,Cw,ze,zm,zh,alphaM,
+           ALPHAH,Gs,TeOLD,TmOLD,ThOLD,Te,Tm,Th)
IF (DENTY(TE,S) .GT. DENTY(TM,S)) THEN
  CALL TURN1(ZE,ZM,TE,TM)
  IF (DENTY(TM,S) .GT. DENTY(TH,S))
+  THEN
    CALL TURNOV(ze,zm,zh,TE,TM,TH)
  ENDIF
ENDIF
RETURN
END

CC
CC  SUBMODEL 1: STRATIFIED PERIOD
SUBROUTINE STRATF(Dt,S,Cw,ze,zm,zh,alphaM,
+           ALPHAH,GS,TeOLD,TmOLD,ThOLD,Te,Tm,Th)
C
  TE=(Gs/DENTY(TEOLD,S)/Cw-ALPHAM*(TEOLD-TMOLD)/
+ ((zE+zM)/2.))*Dt/zE+TEOLD
  Tm=(ALPHAM*(TeOLD-TmOLD)/((ze+zm)/2.-
+ ALPHAH*(TmOLD-ThOLD)/((zm+zh)/2.))*Dt/zm+TmOLD
  Th=(ALPHAH*(TmOLD-ThOLD)/((zm+zh)/2.))*Dt/zh+ThOLD
  RETURN
END

C
C  SUBMODULE 2: TURN OVER PERIOD
SUBROUTINE TURNOV(ze,zm,zh,TE,TM,TH)
z = ze+zm+zh
Tw=(Te*ze+Tm*zm+Th*zh)/z
Te=Tw
Tm=Tw
Th=Tw
RETURN
END

```

```

C
C   SUBMODULE 3: SURFACE LAYER TURN OVER PERIOD
C   SUBROUTINE TURN1(ZS,ze,TS,TE)
C   z = ZS+ze
C   Tw=(TS*ZS+Te*ze)/z
C   TS=TW
C   Te=Tw
C   RETURN
C   END
CC
CC   BOWEN RATIO OF SALINE WATER , FRESH WATER BETA=1
C   SUBROUTINE BOWEN(CP,P,TS,TA,EA,BETA,B)
C   B=CP*P/0.622/XLATNT(TS)*(TS-TA)/(BETA*E_SAT(TS)-EA)
C   RETURN
C   END
CC
CC   REAL FUNCTION e_sat(Ts)
C   REAL TS
C   tR=1-(373.15/(Ts+273.2))
C   e_sat = 1013.25*exp(13.3185*tR-1.9760*tR**2-0.6445*tR**3
C   + -0.1299*tR**4)
C   RETURN
C   END
CC
CC   REAL FUNCTION DIF_EA(TA)
C   REAL TA
C   TR=1-(373.15/(TA+273.2))
C   DIF_EA= 373.15*E_SAT(TA)/(TA+273.2)**2*(13.3185-3.952*TR-
C   + 1.9335*TR**2-0.5196*TR**3)
C   RETURN
C   END
CC
CC   REAL FUNCTION DENTY(TS,S)
C   TS,C,S:DIMENSIONLESS
C   MONO LAKE ,1964
C   DENTY = (1.061867-0.000303*TS)*1000
C   DENTY = (1.0048259+8.66E-1*S-2.867E-4*TS+2.472E-4*TS*S)*1000
C   RETURN
C   END
CC
CC   REAL FUNCTION DTY_F(TS)
C   FRESH WATER
C   DTY_F = (1-1.9549E-5*(ABS(TS-4))**1.68)*1000
C   RETURN
C   END
CC
CC   REAL FUNCTION XLATNT(TS)

```

```
C FRESH WATER
XLATNT=(1.91846E6*((TS+273.2)/(TS+239.29))**2)
RETURN
END
CC
CC
REAL FUNCTION ACTVTY(S)
C LAGRANGE INTERPOLATION FOR NaCl
ACTVTY = 1.*(S-0.05)*(S-0.1)*(S-0.2)/(-1.E-3) +
+ 0.975*S*(S-0.1)*(S-0.2)/3.75E-4 +
+ 0.940*S*(S-0.05)*(S-0.2)/(-5.E-4) +
+ 0.840*S*(S-0.05)*(S-0.1)/3.E-3
RETURN
END
```

Figure 1. Typical Day-Time One Dimensional Energy Balance Schematic Diagram of Water Body.

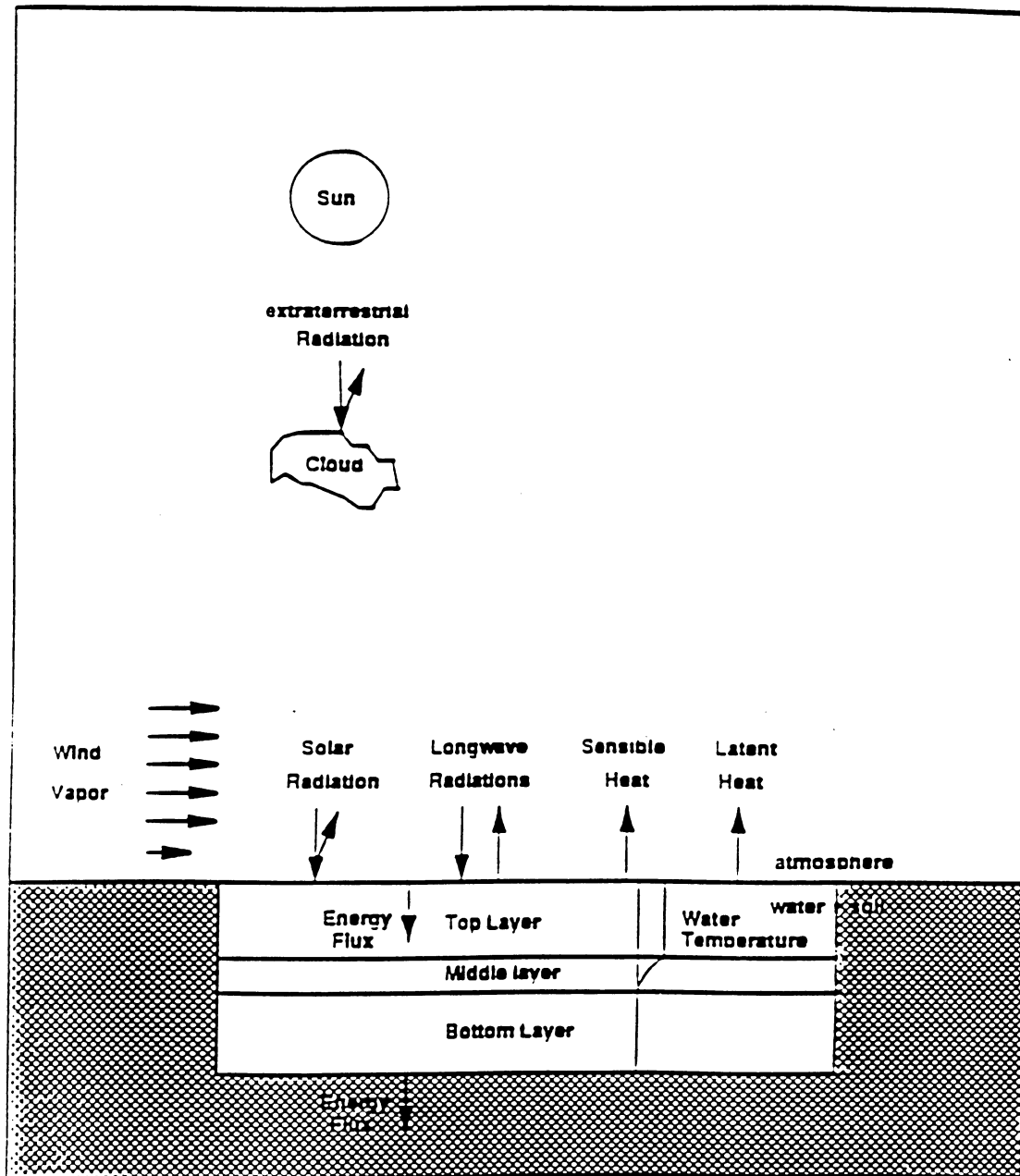


Figure 2.

The interconnection flow chart among the mass transfer module, the net solar radiation module, the surface energy budget module and the water thermocline module of the integrated evaporation methodology, where E = evaporation rate, Rsd = downward net solar radiation, Rld = downward long-wave radiation, Rlu = upward long-wave radiation, Rn = net radiation, LE = latent heat, H = sensible heat, G = energy flux into water and Tw = water temperature.

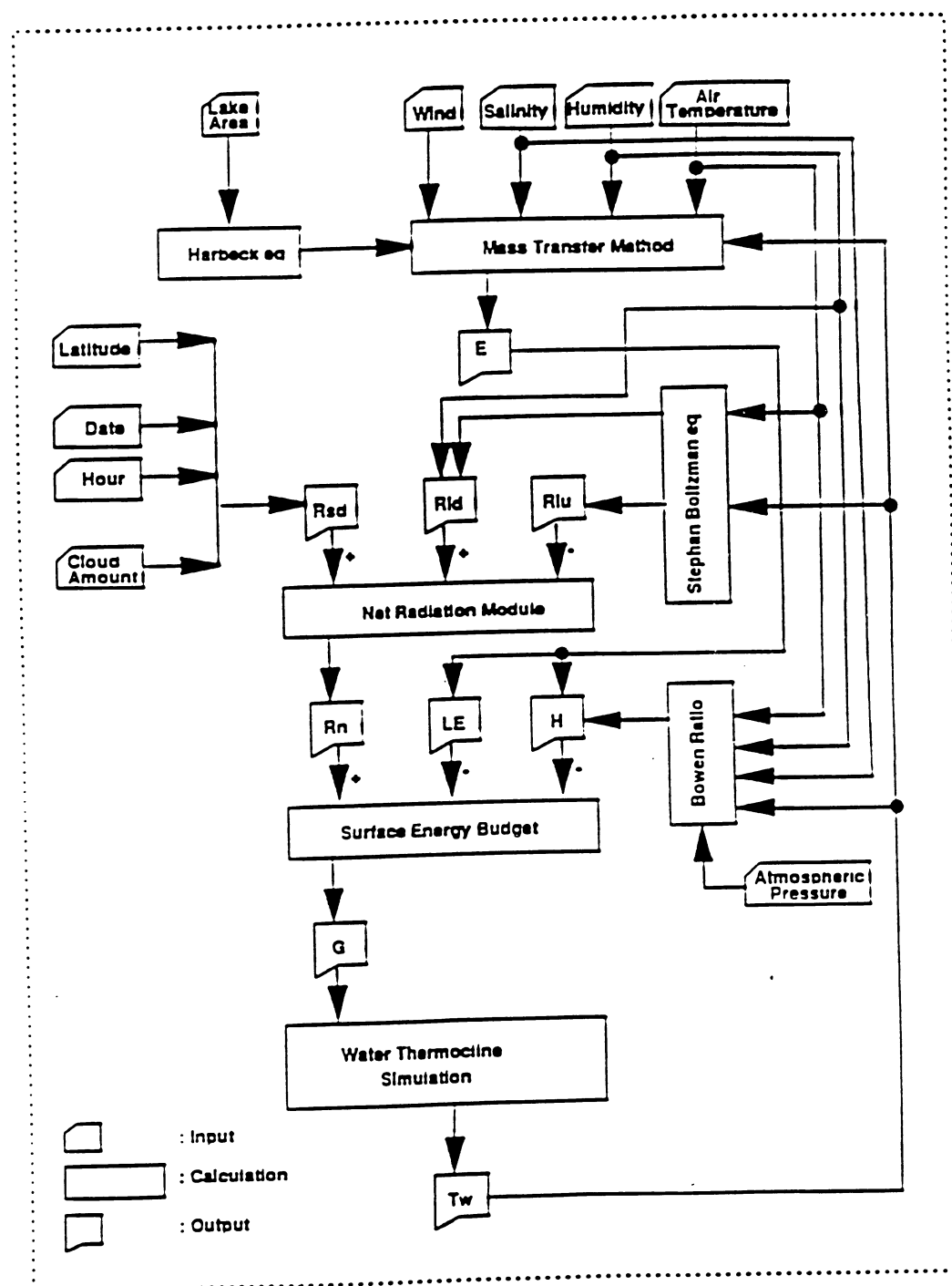


Figure 3. The flow chart of the water thermocline simulation module.

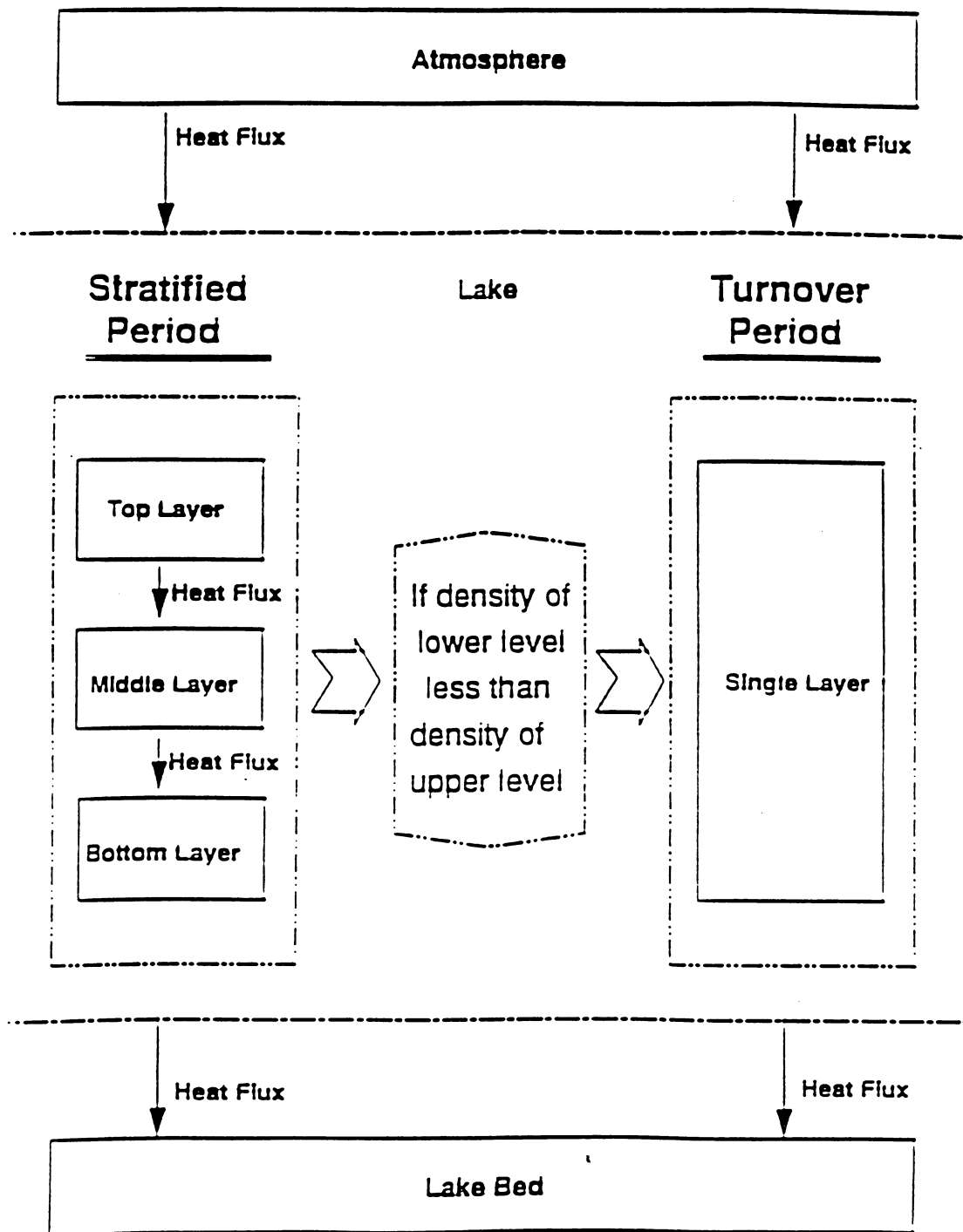
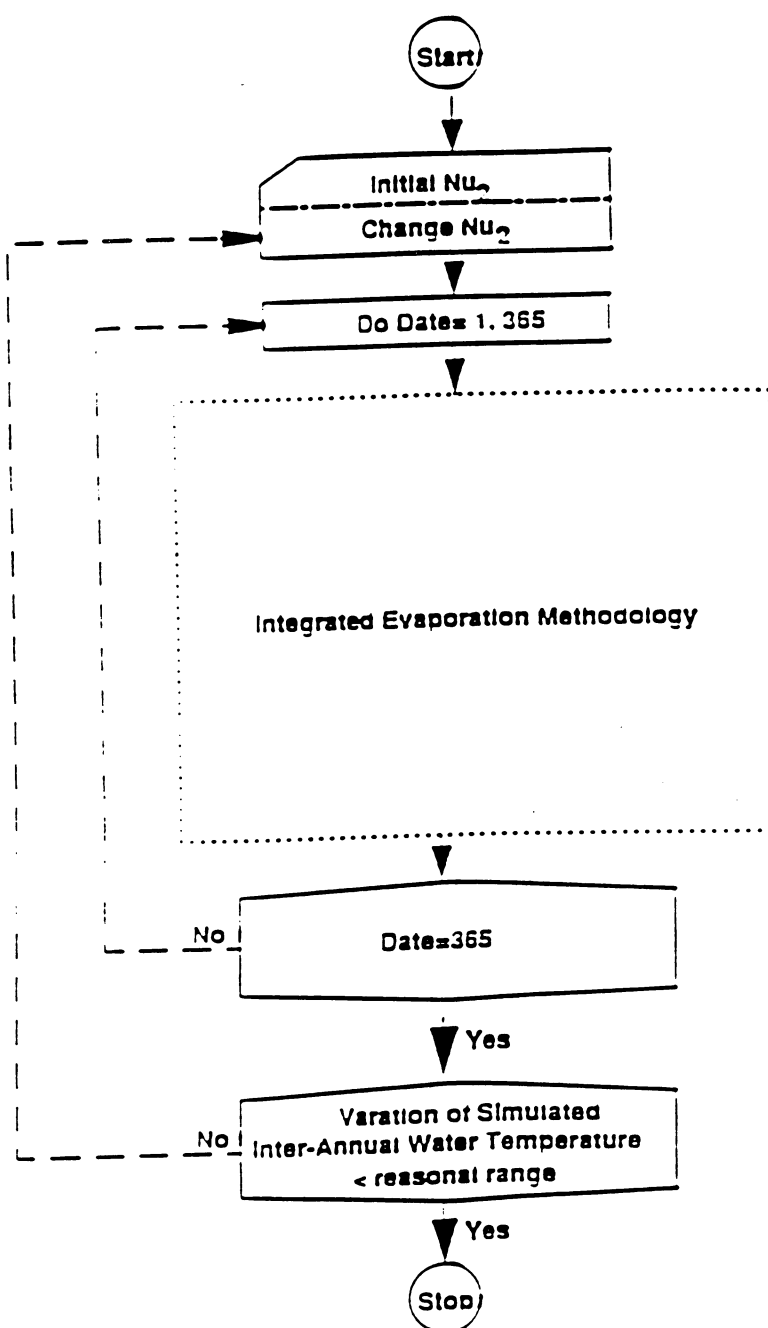


Figure 4.

The flow chart of model calibration to meet the criterion of the simulated inter-annual water temperature within reasonable range.



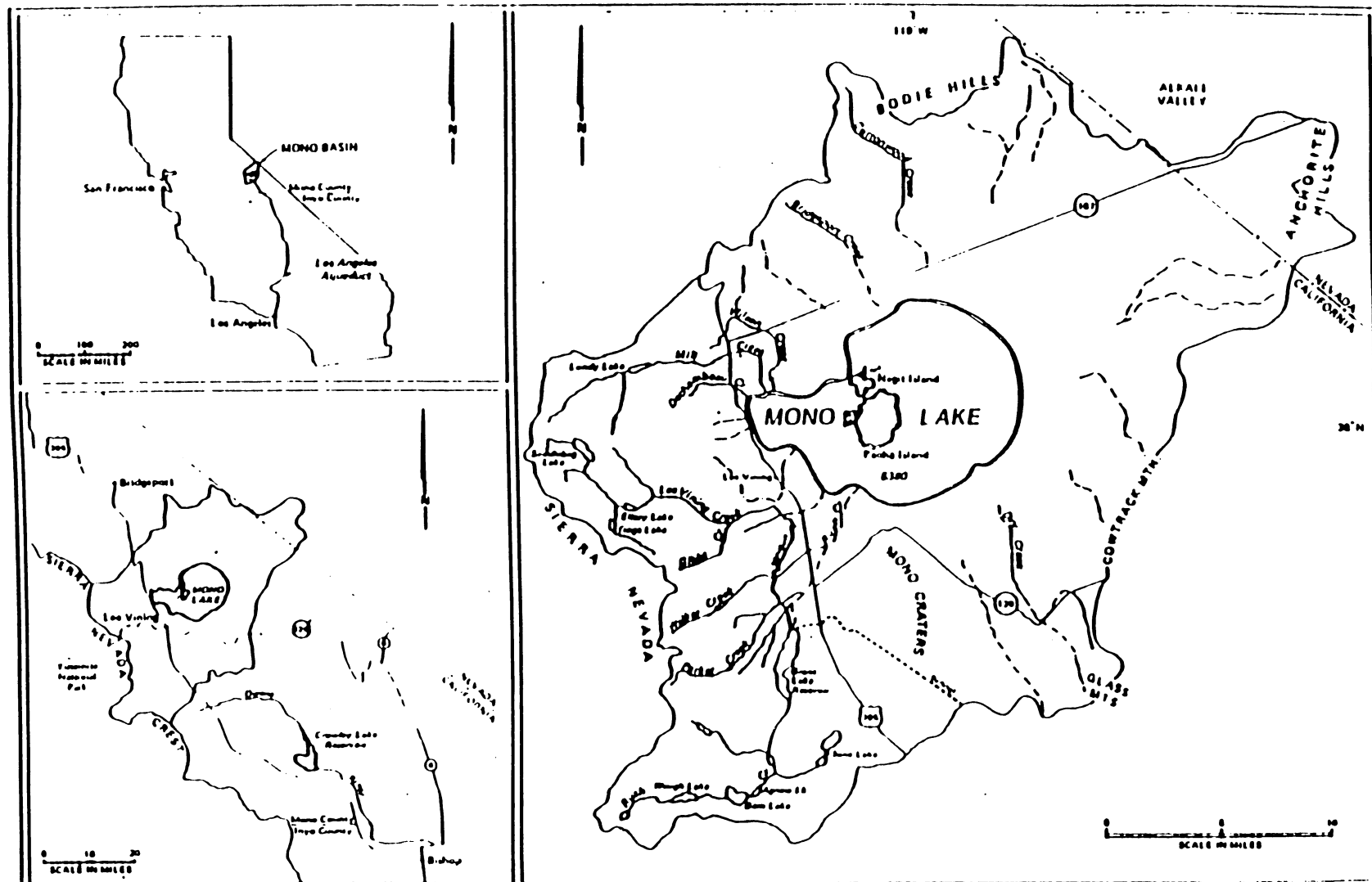


Figure 5. Location and Hydrology Map of Mono Lake, California (from Vorster, 1985).

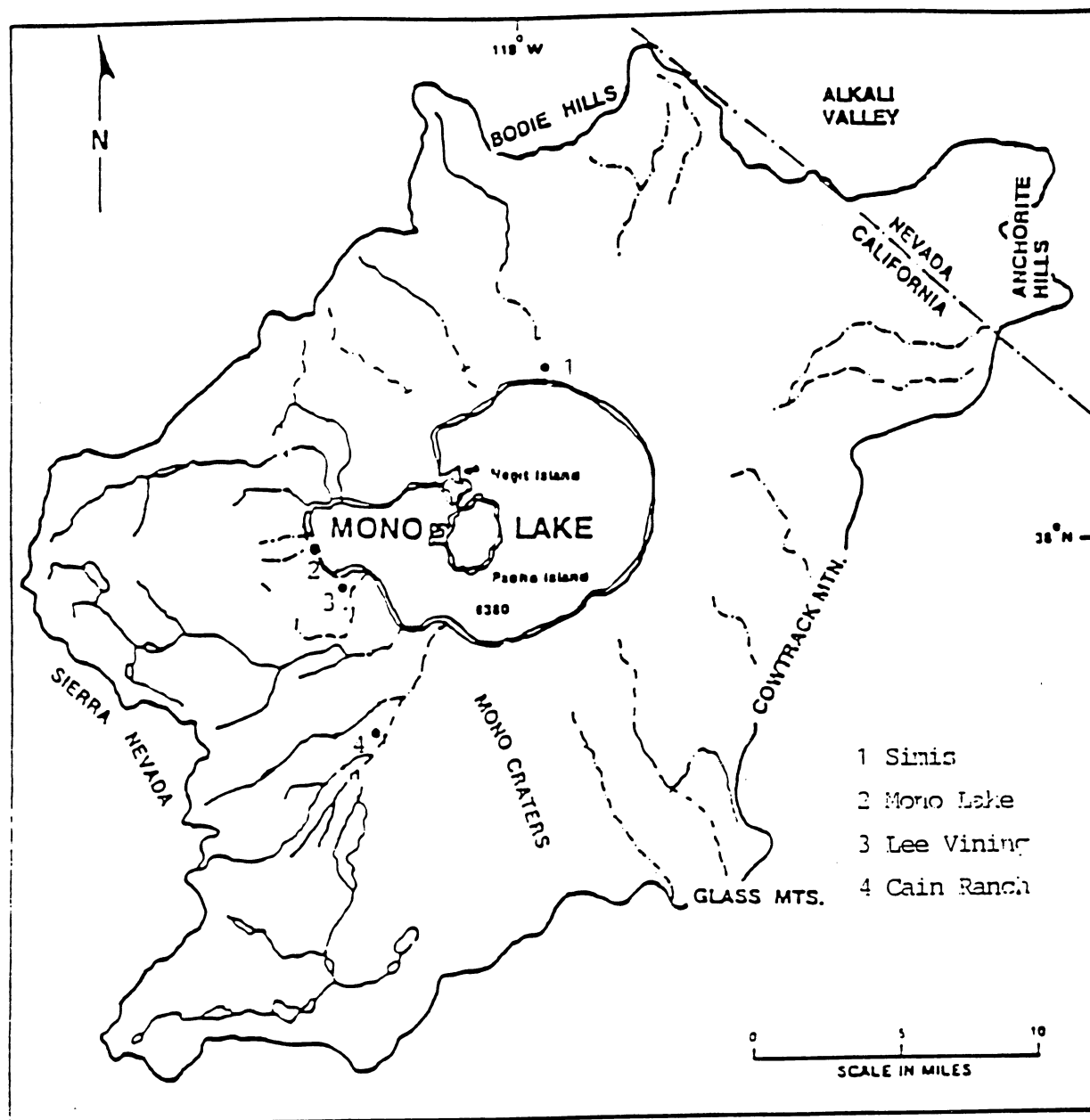


Figure 6. Climatic Measurement Sites, Mono Lake, California (adapted from Vorster, 1985).

Fractional Cloud Cover

Cala Ranch Station, 1982

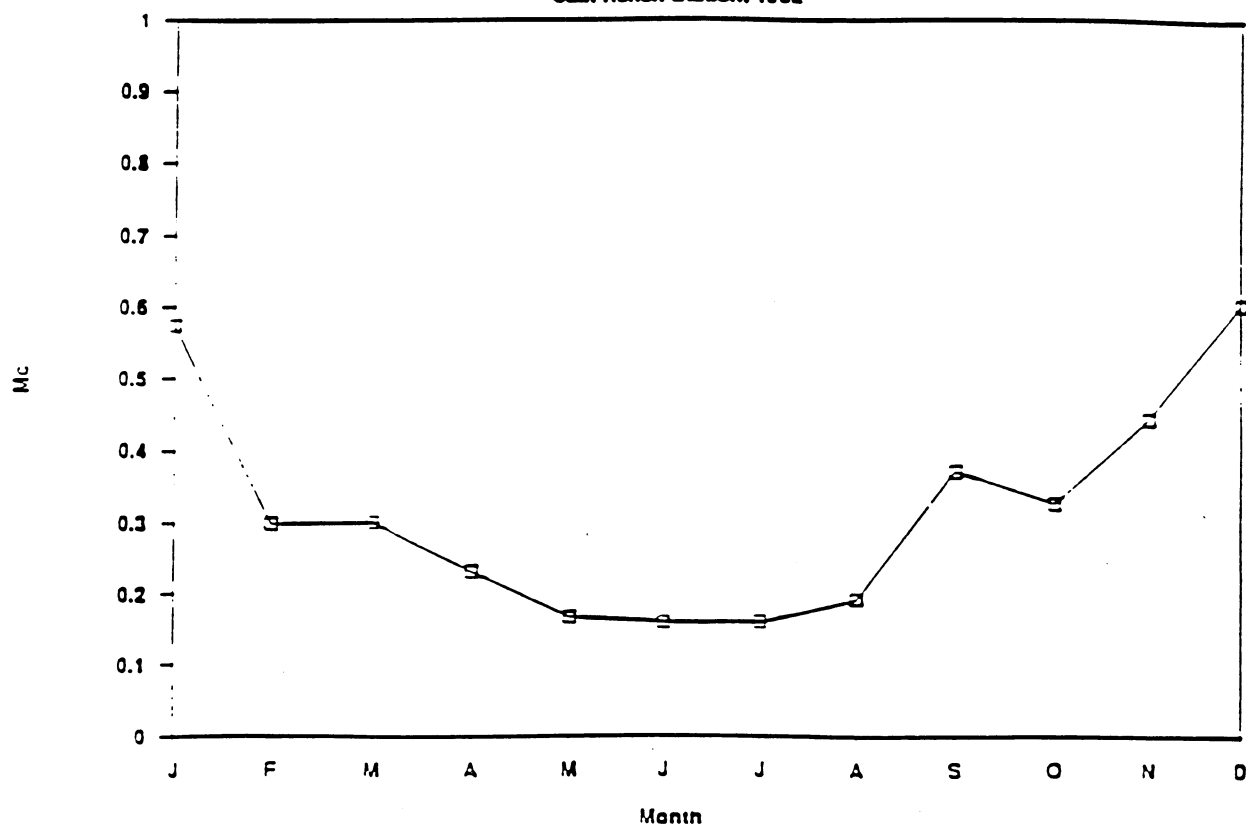


Figure 7. Equivalent Fractional Cloud Cover Information during 1982.

Wind Speed

Lee Vining Station, 1982

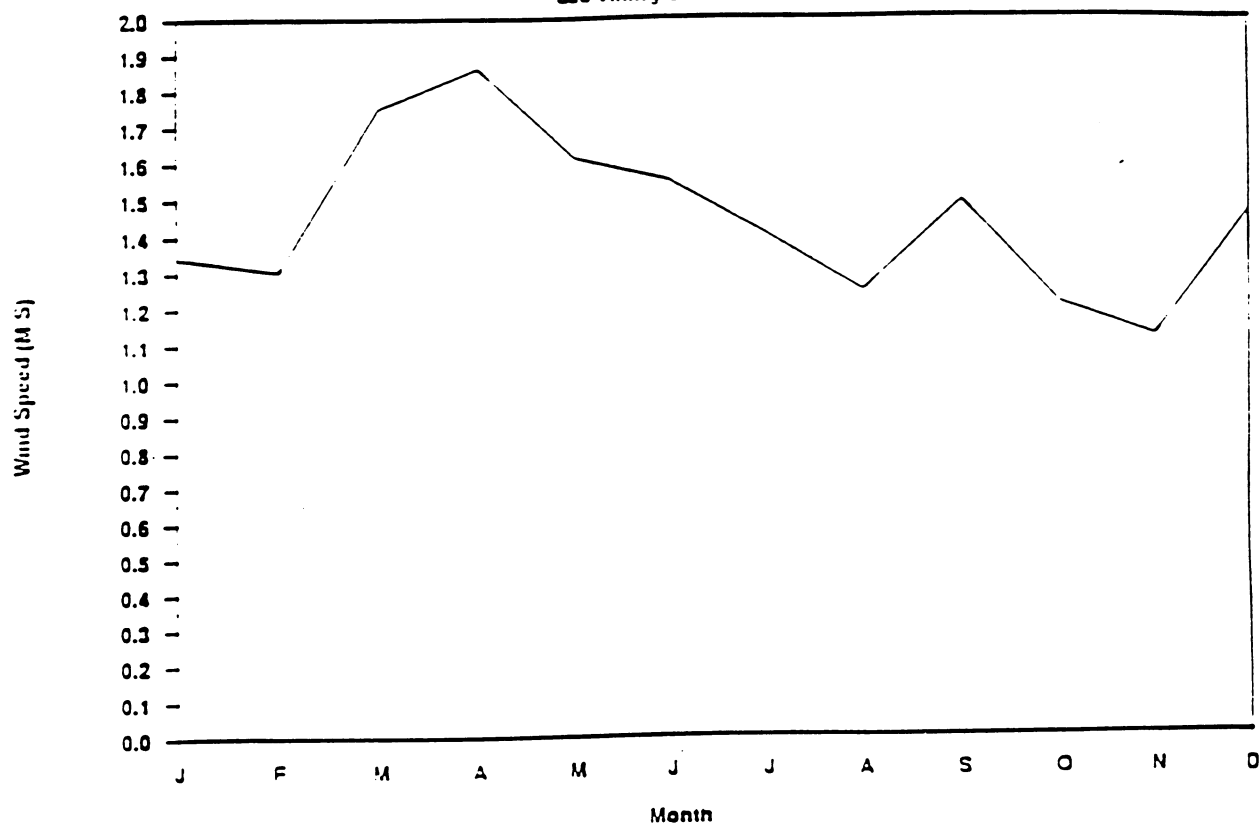


Figure 8. Monthly Wind Speed at the Lee Vining Station during 1982.

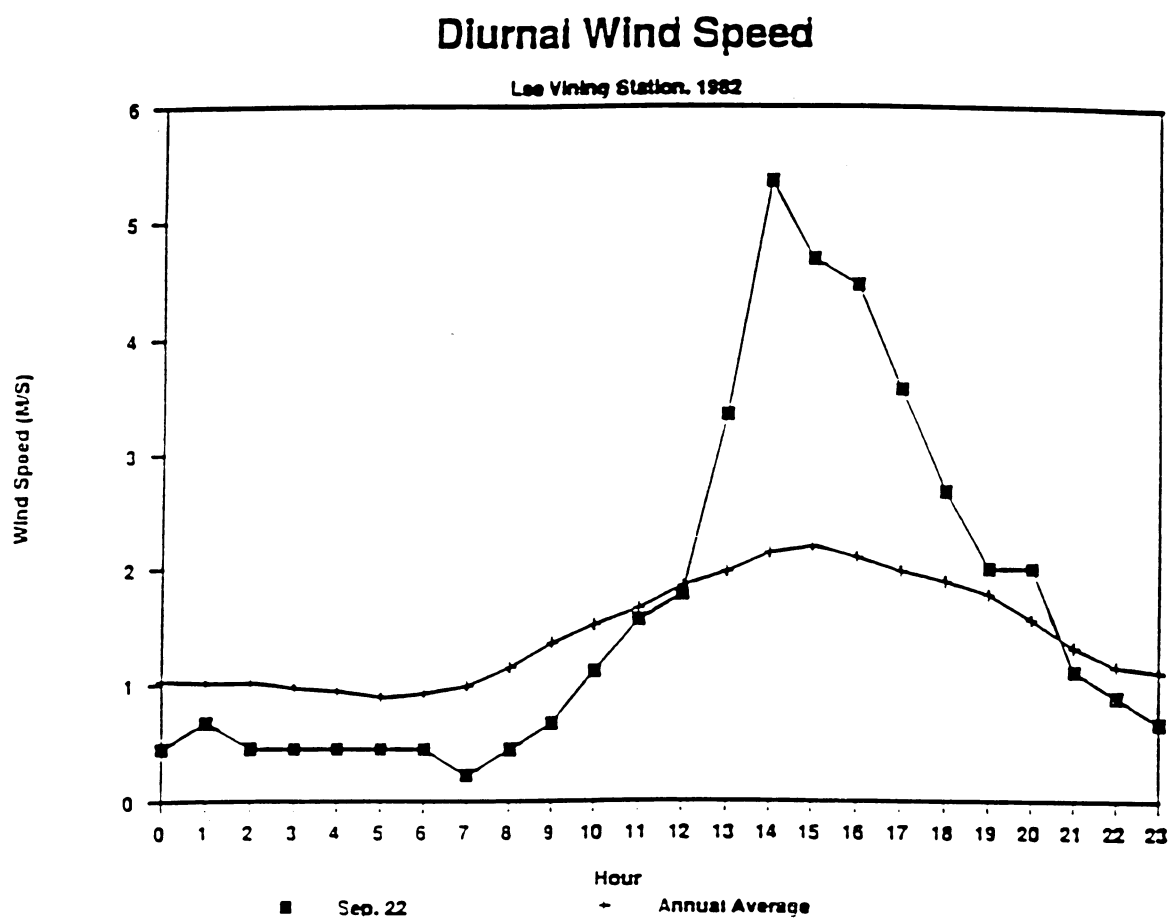


Figure 9. September-22nd and Annual Average Diurnal Wind Speed at the Lee Vining Station, 1982.

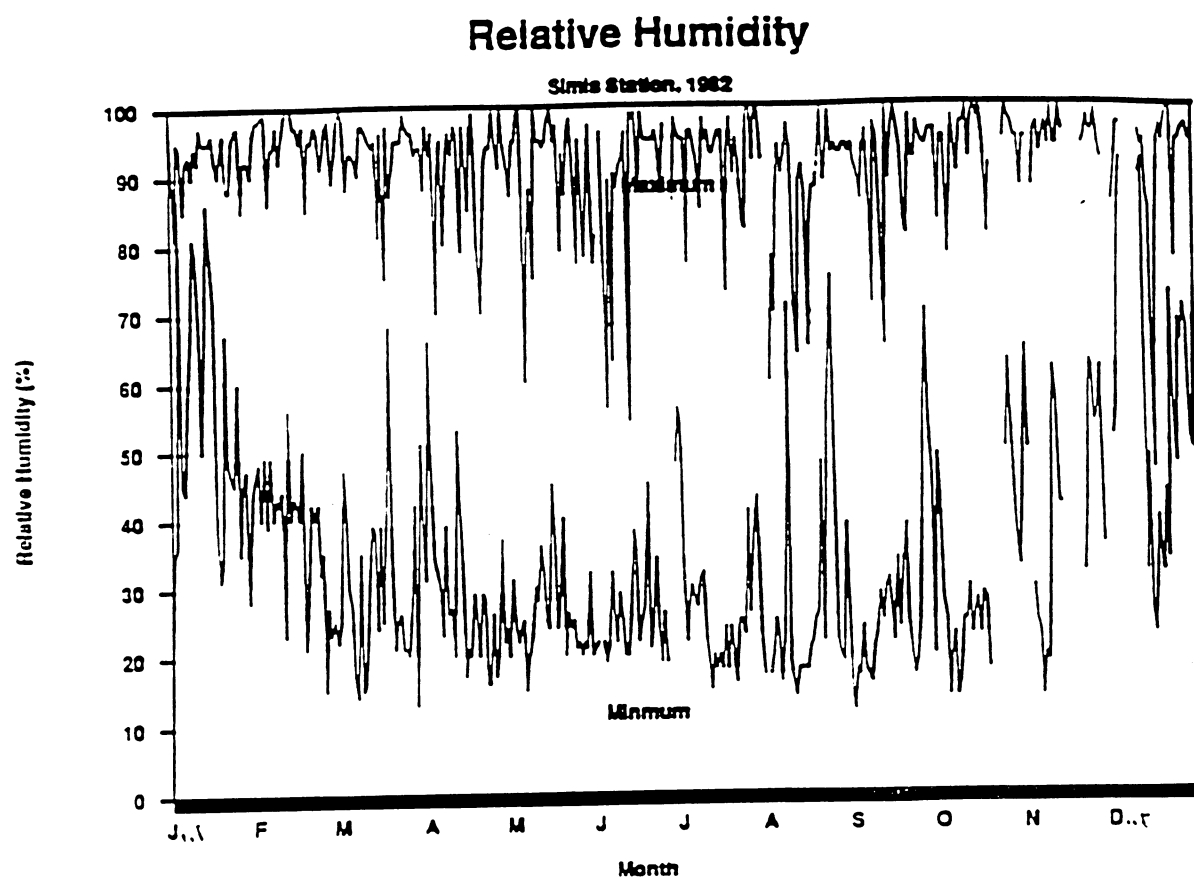


Figure 10. Daily Relative Maximum and Minimum Humidity at the Simis Station throughout 1982.

Absolute Humidity

Simis Station, 1982

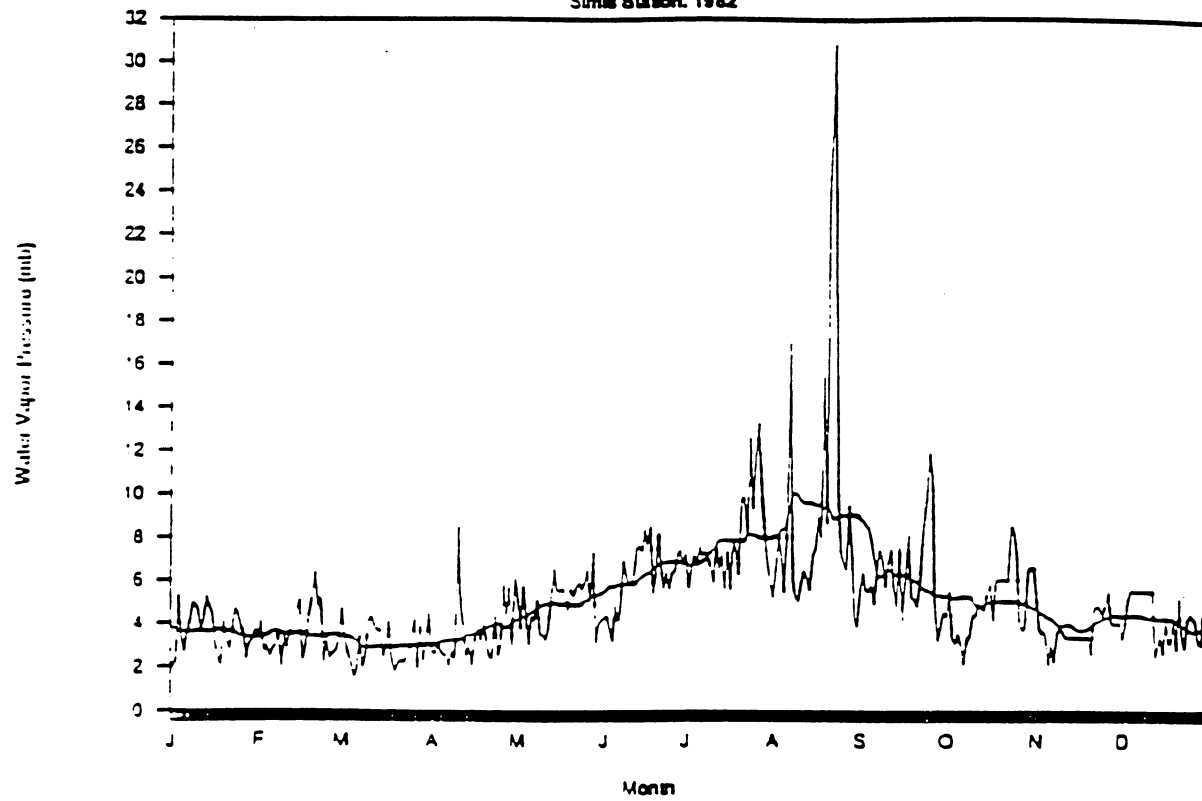


Figure 11. Daily Absolute Humidity at the Simis Station throughout 1982. Smooth curve is a running mean of 30 days of data.

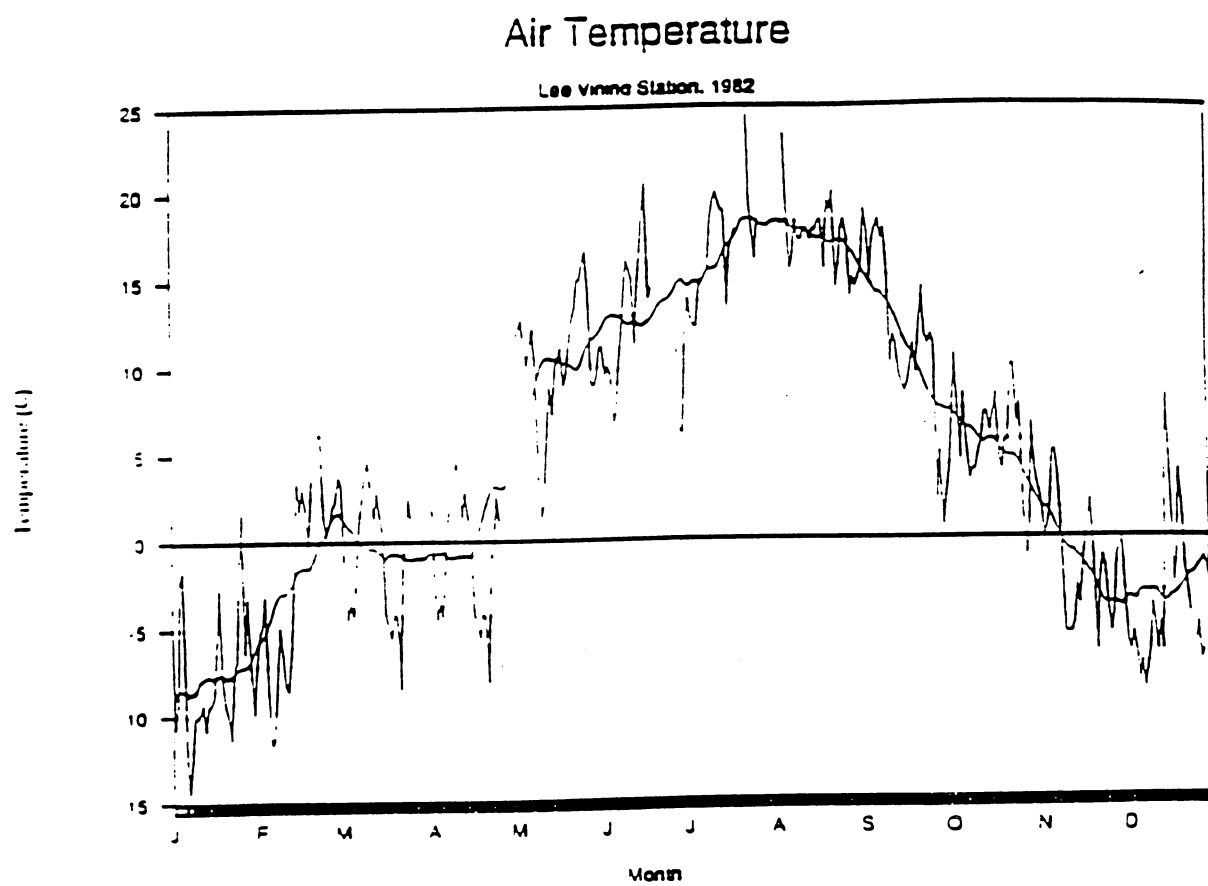


Figure 12. Daily Air Temperature at the Lee Vining Station throughout 1982. Smooth curve is a running mean of 30 days of data.

Diurnal Air Temperature

Lee Vining Station, 1982

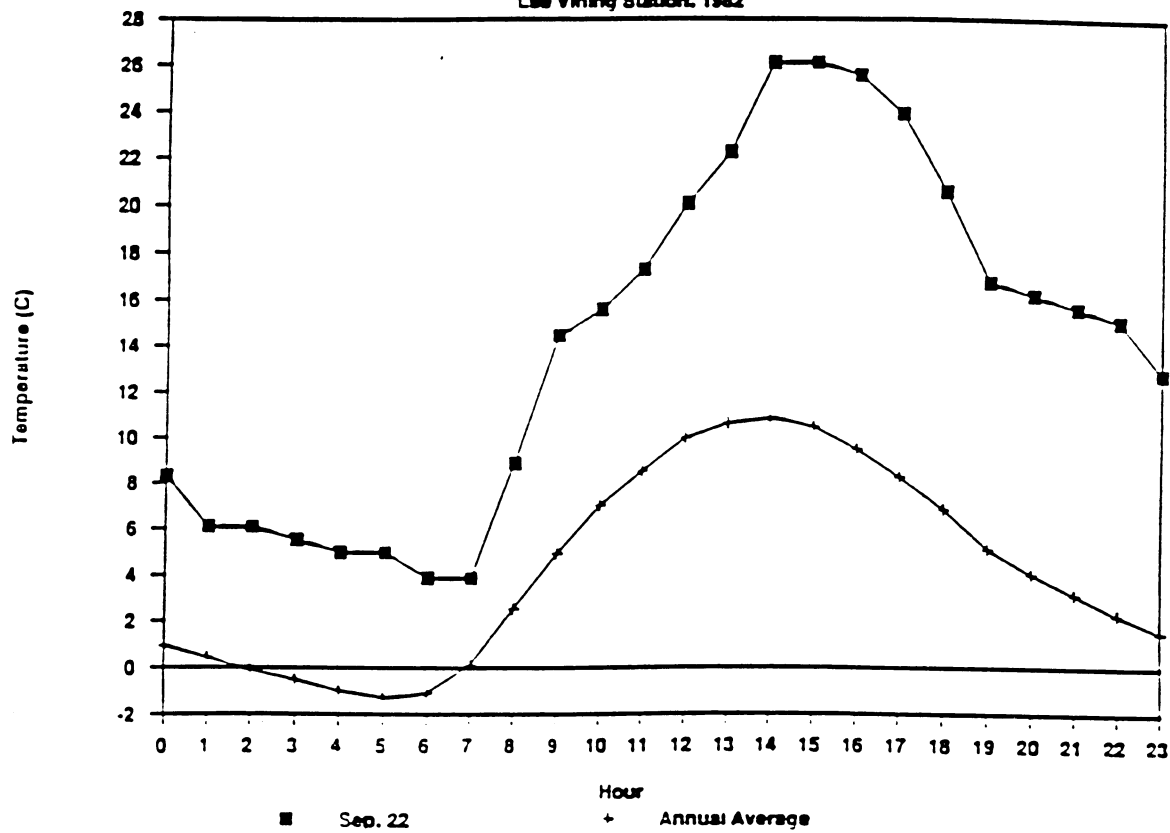


Figure 13. September-22nd and Annual Average Diurnal Air Temperature at the Lee Vining Station, 1982.

Water Temperature

Mono Lake, 1982

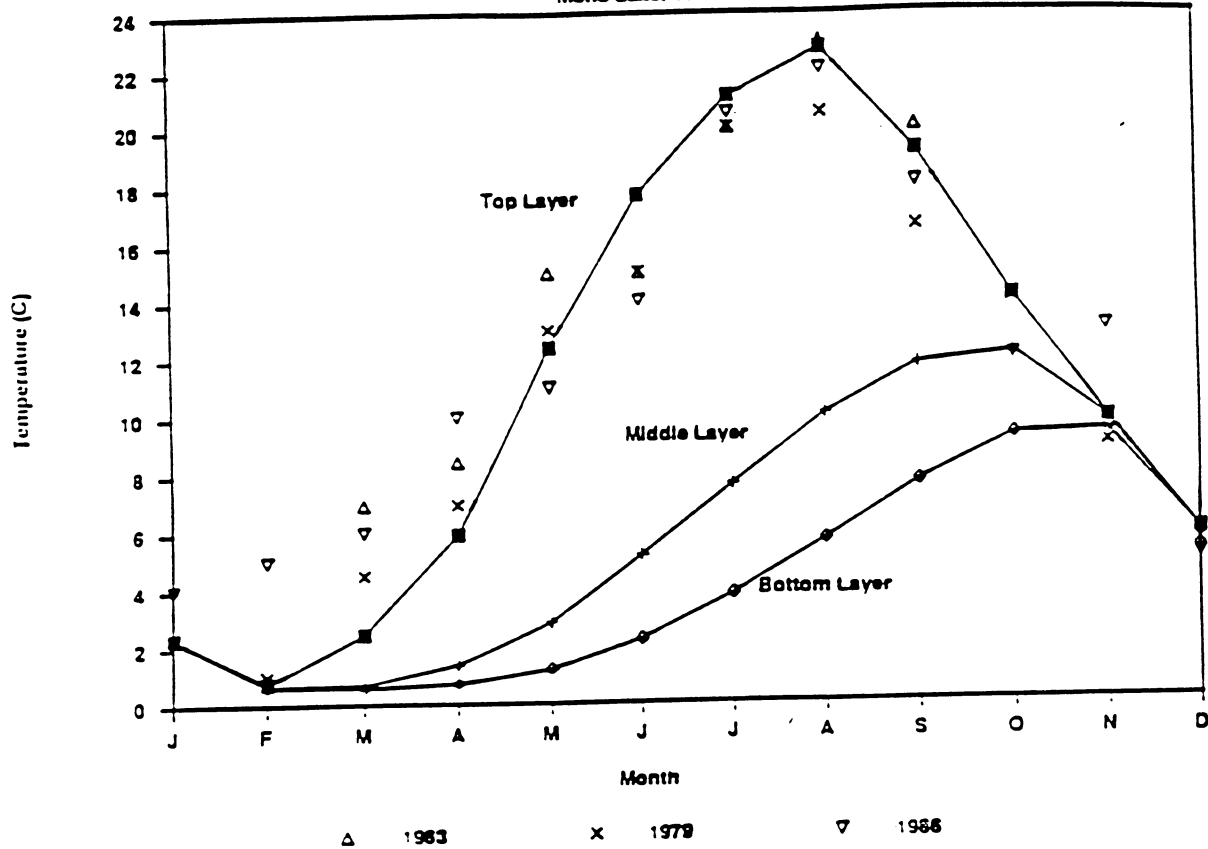


Figure 14. Simulated Seasonal Water Temperature of Mono Lake in 1982, where the solid lines are simulated results and the symbols are field data of surface water temperature in other years. The top layer was from depth 0 - 9 m, the middle layer was from depth 9 - 15 m and the bottom layer was from depth 15 - 17.8 m. From the simulation, it was found that water was thermally stratified from February to November, and turned over from November to February. The simulated water surface temperature was compared reasonably with several field data in other years (1982 data are not available).

Diurnal Water Temperature

Mono Lake, September 22, 1982

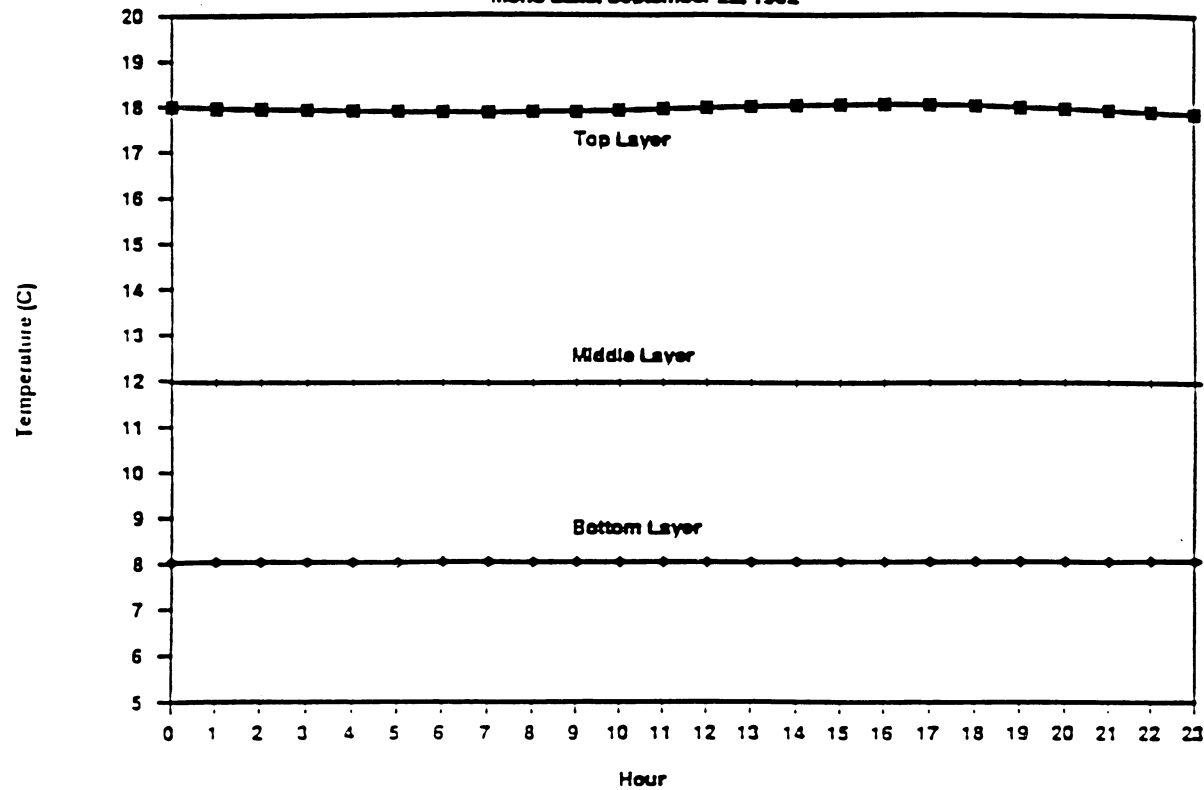


Figure 15. Simulated Diurnal Water Temperature of Mono Lake on September 22nd, 1982.

Diurnal Water Temperature in the Top Layer

Mono Lake, September 22, 1982

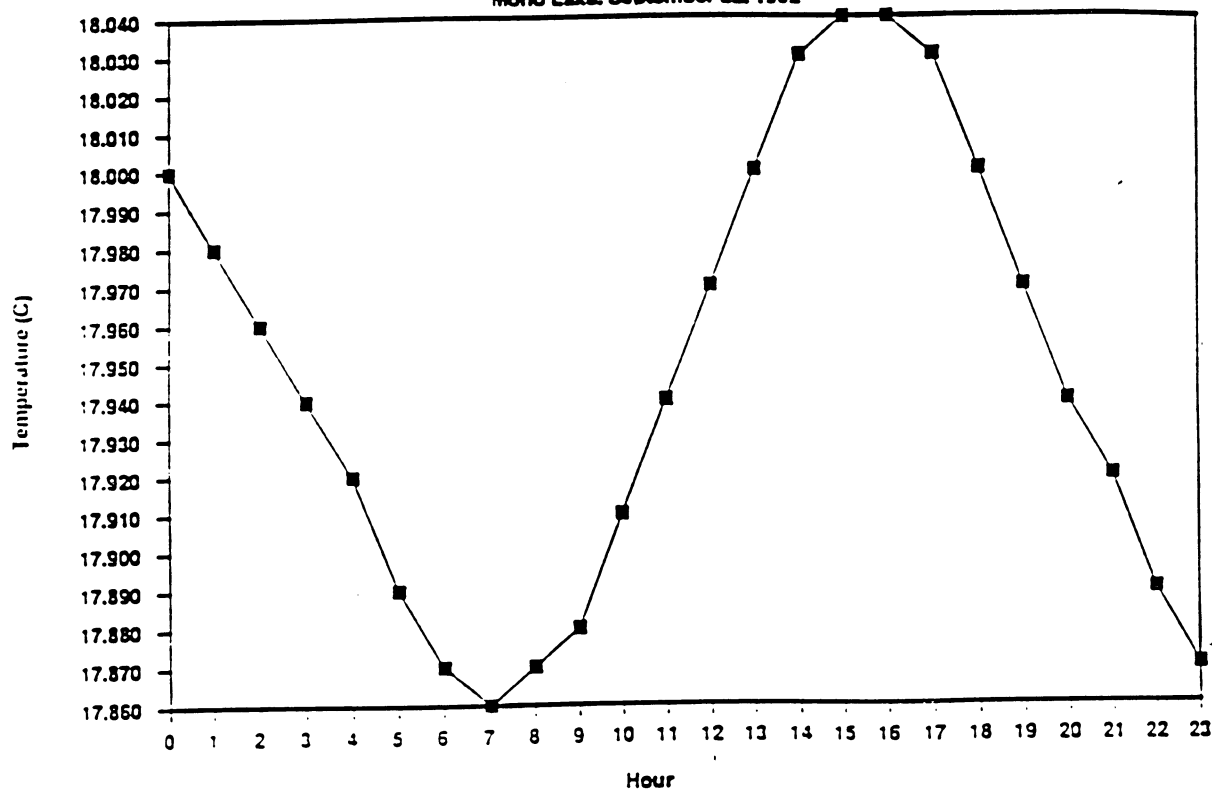


Figure 16. Simulated Diurnal Water Temperature in the Top Layer of Mono Lake, September 22nd, 1982.

Diurnal Water Temperature in the Middle Layer

Mono Lake, September 22, 1982

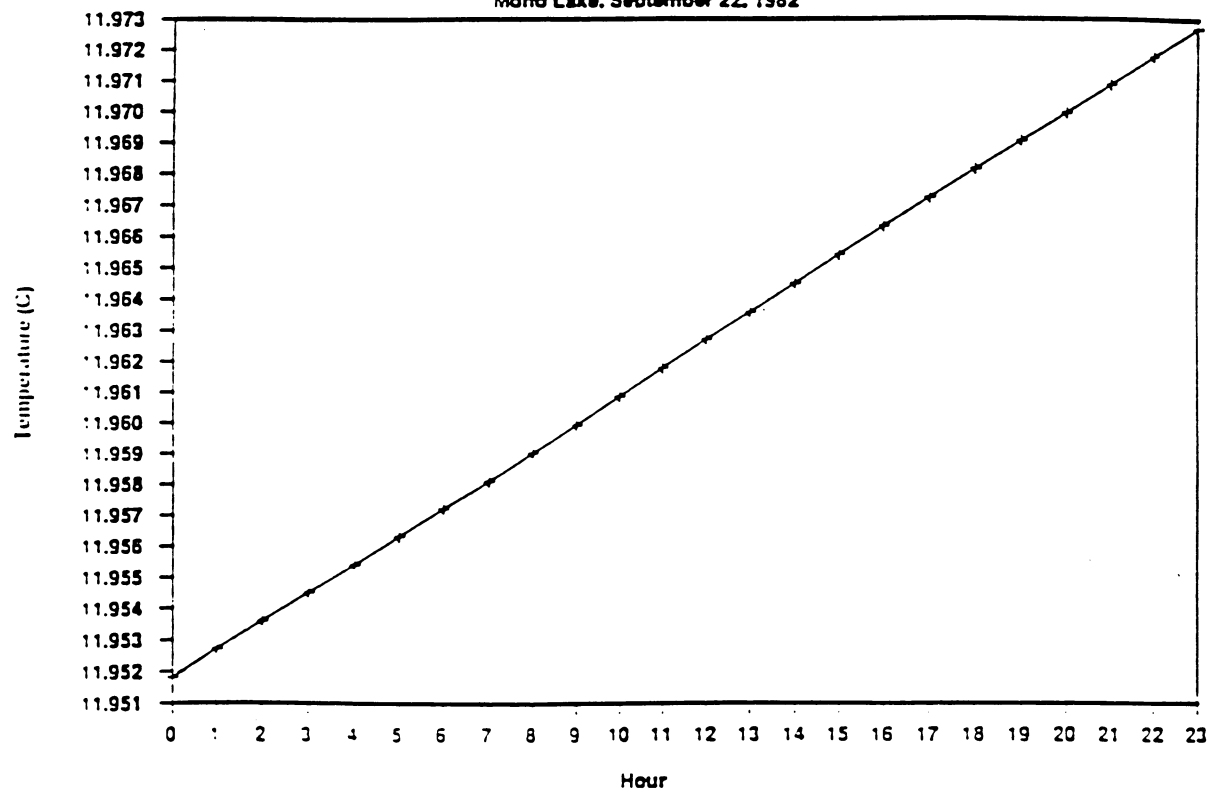


Figure 17. Simulated Diurnal Water Temperature in the Middle Layer of Mono Lake, September 22nd, 1982.

Diurnal Water Temperature in the Bottom Layer

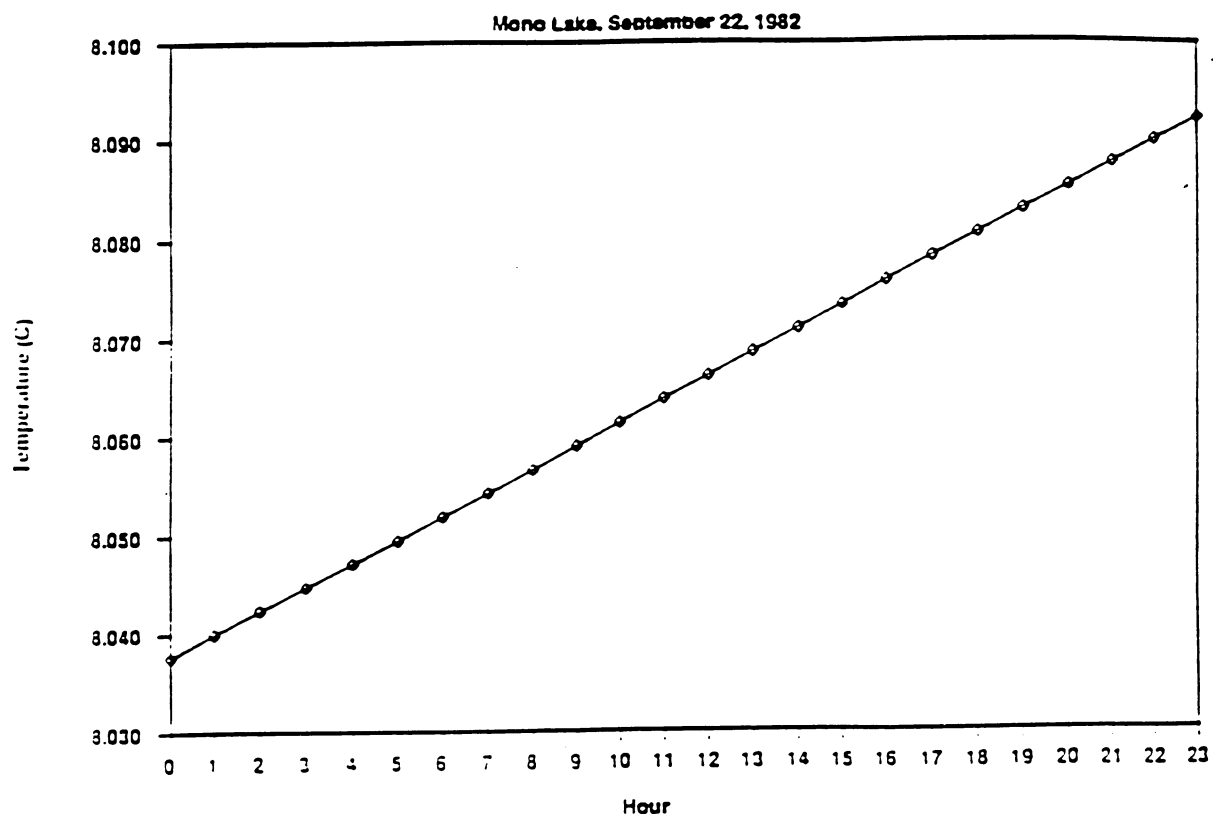


Figure 18. Simulated Diurnal Water Temperature in the Bottom Layer of Mono Lake, September 22nd, 1982.

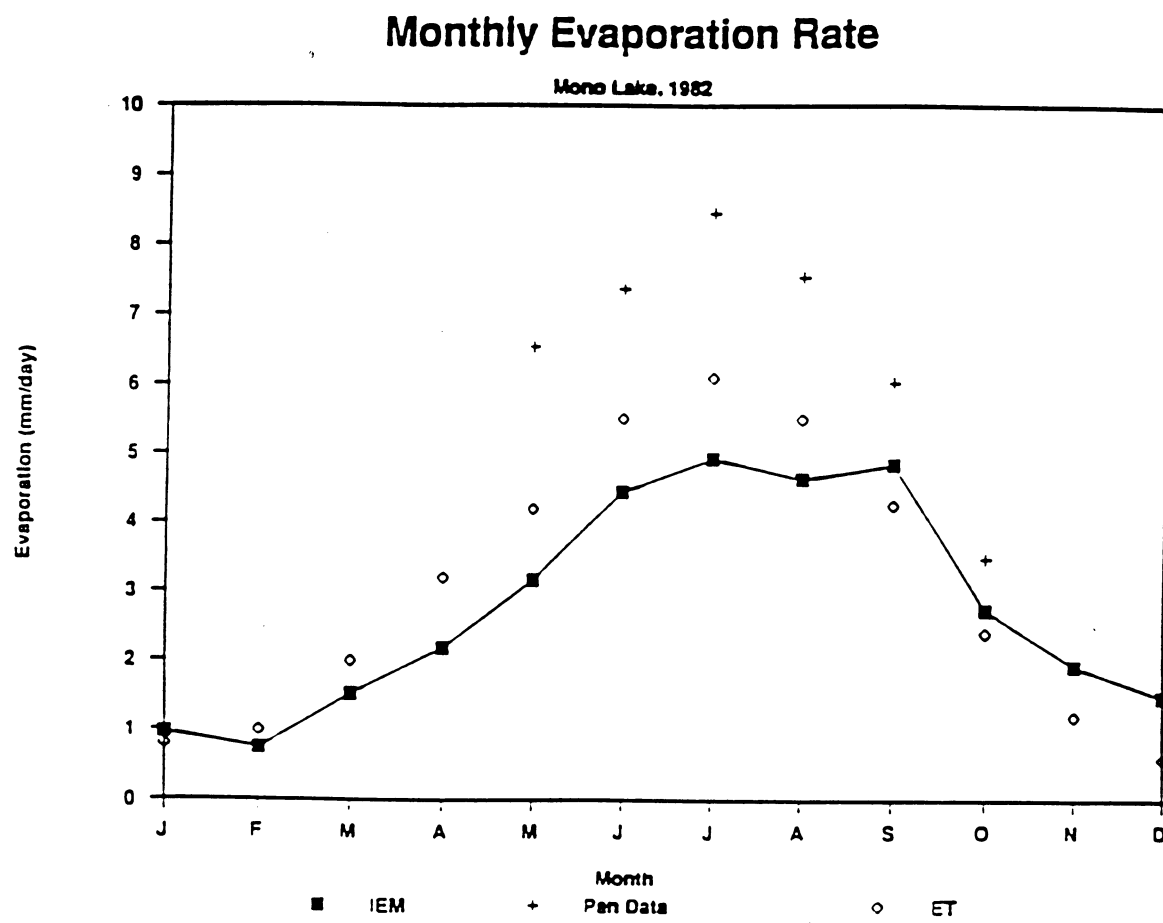


Figure 19. Simulated Monthly Saline Water Evaporation Rate from Mono Lake, 1982, compared with evaporation pan data (without pan coefficient adjustment) at the Simis station (Vorster, 1985) and normal-year reference evapotranspiration, ET, for the area around Mono Lake (Pruitt et al., 1987).

Diurnal Evaporation Rate

Mono Lake, September 22, 1982

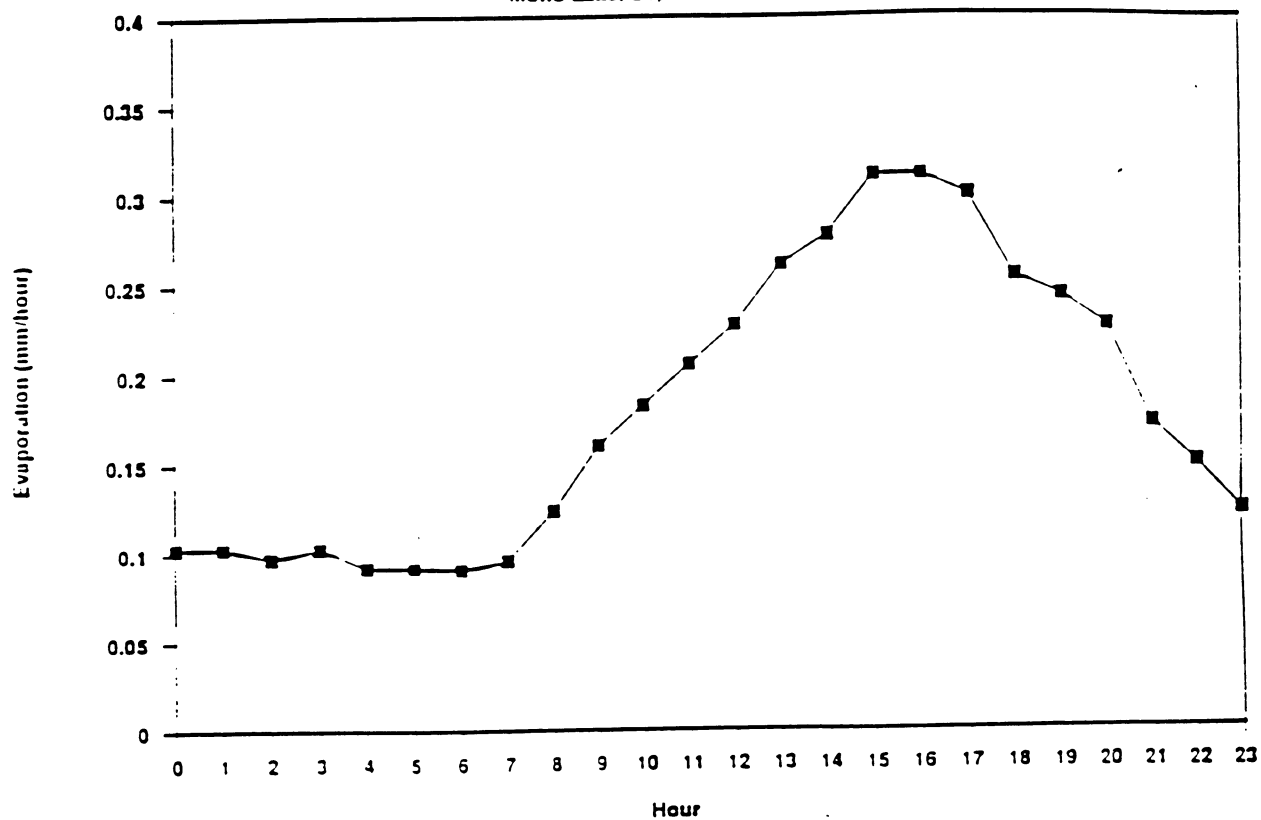


Figure 20. Simulated Diurnal Saline Water Evaporation Rate from Mono Lake on September 22nd, 1982.

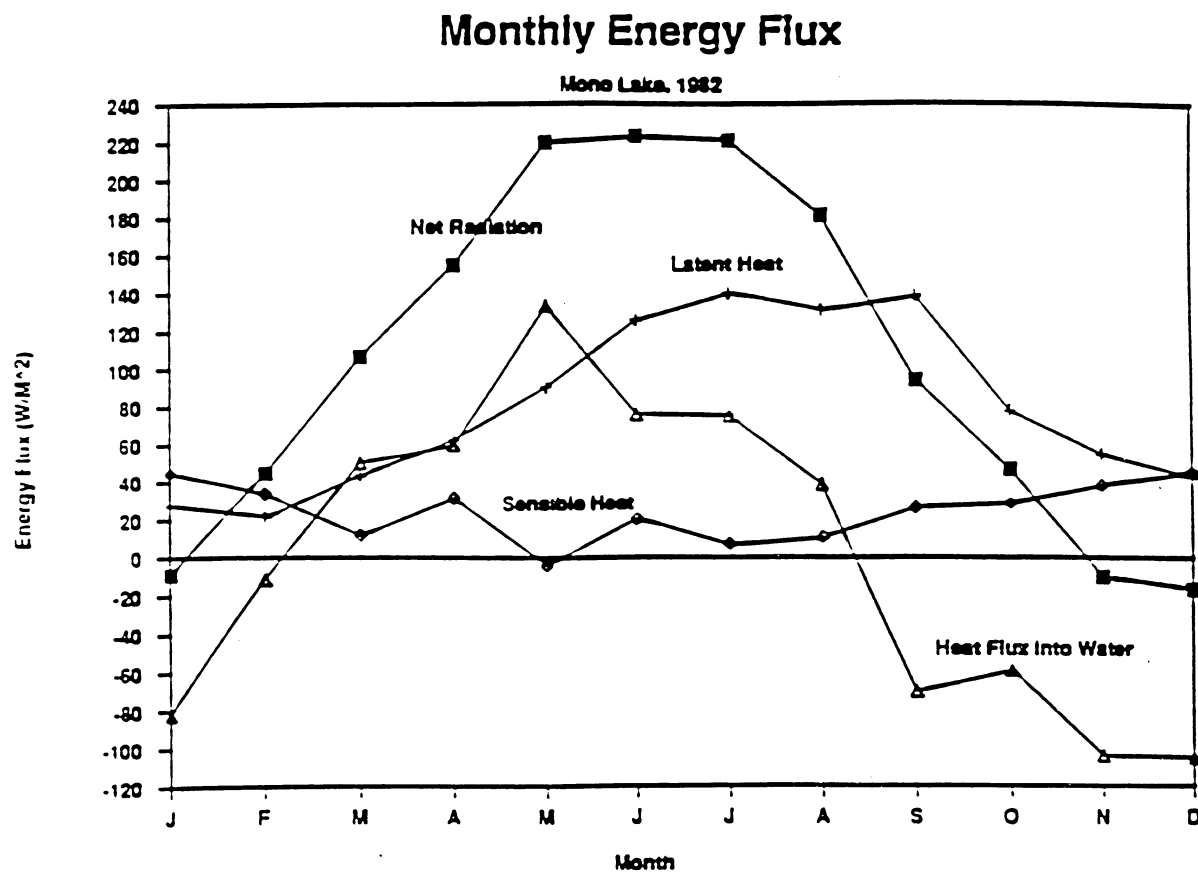


Figure 21. Simulated Monthly Energy Fluxes of Mono Lake, 1982.

Diurnal Energy Flux

Mono Lake, September 22, 1982

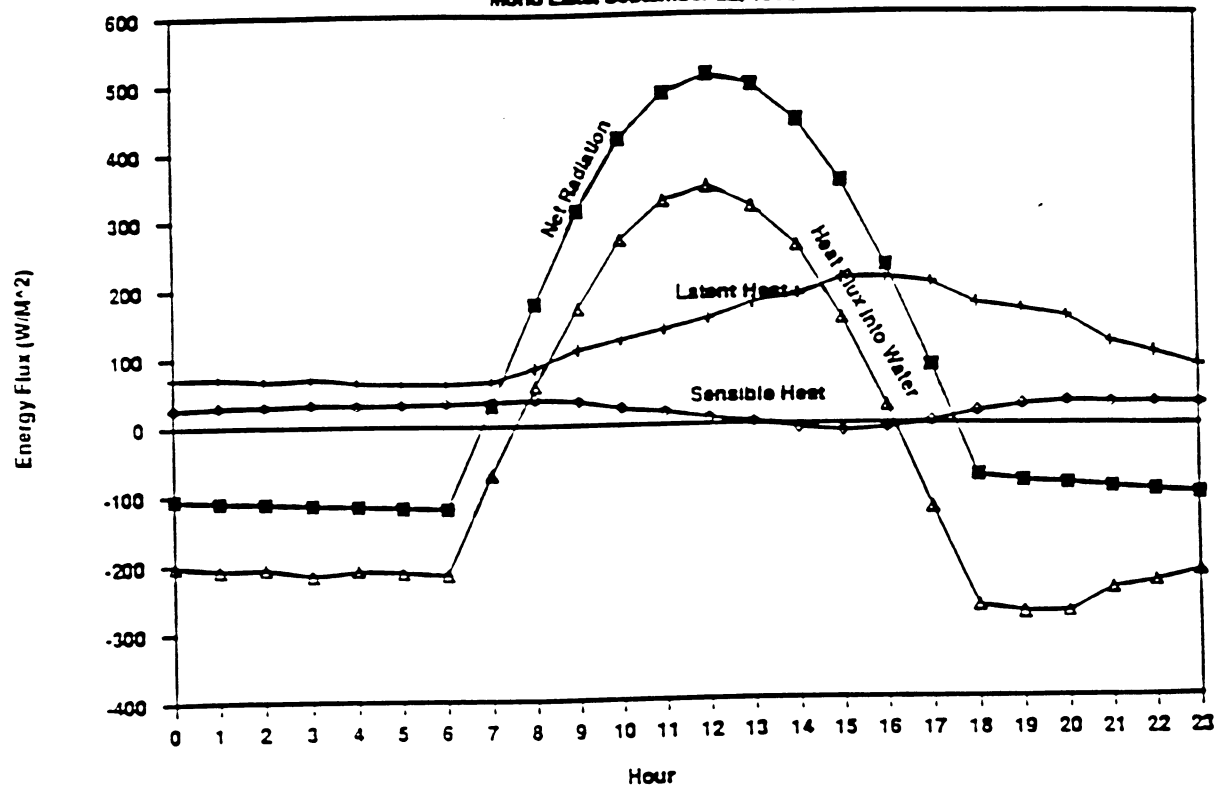


Figure 22. Simulated Diurnal Energy Fluxes of Mono Lake on September 22nd, 1982.

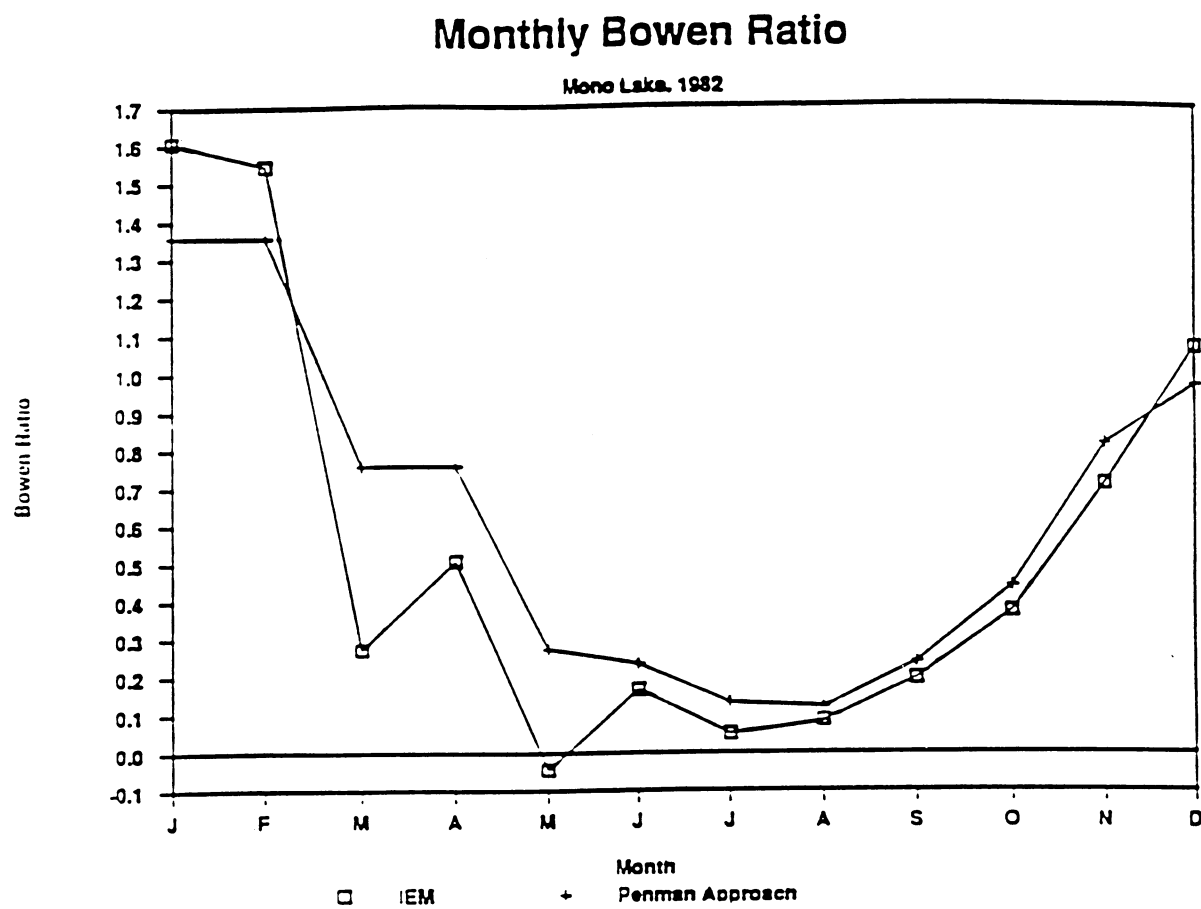


Figure 23. Simulated Monthly Bowen Ratio at Mono Lake, 1982, where IEM used theoretical equation (18) with water temperature calculated from IEM, other meteorological data from field and Penman approach as mentioned in equation (42), only air temperature is required.

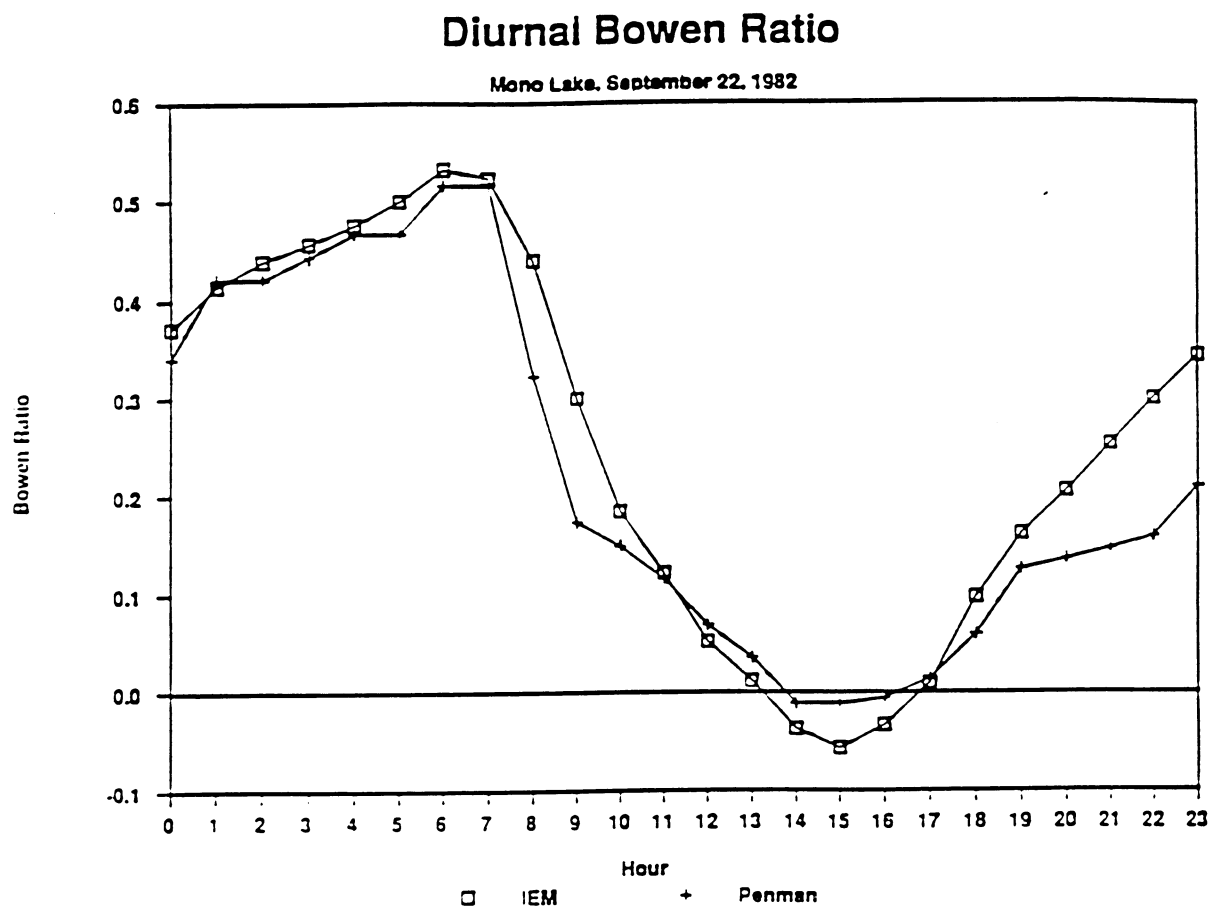


Figure 24. Simulated Diurnal Bowen Ratio at Mono Lake on September 22nd, 1982, where IEM used theoretical equation (18) with water temperature calculated from IEM, other meteorological data from field and Penman approach as mentioned in equation (42), only air temperature is required.

Comparison of Water Surface Temperature

Mono Lake, 1982

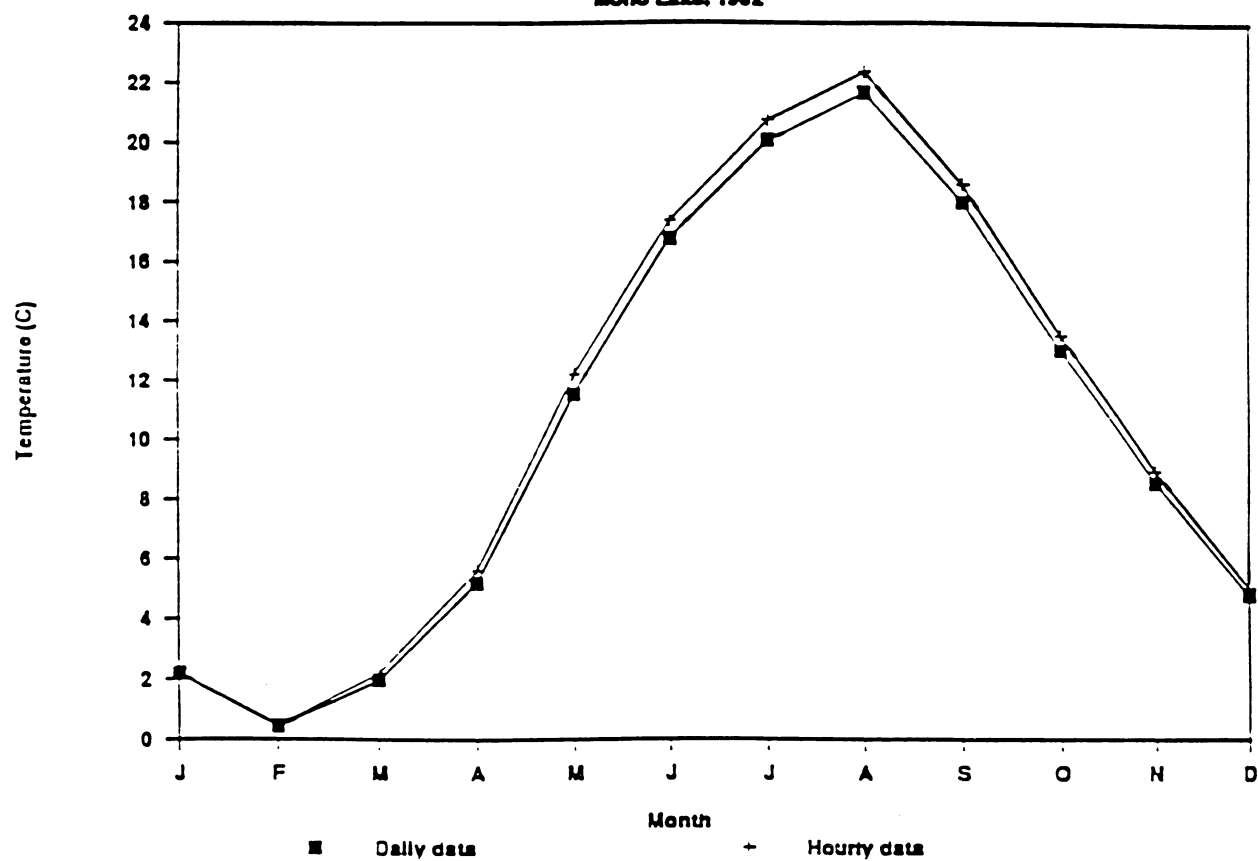


Figure 25. The difference of simulated water surface temperature between daily data and hourly data inputs.

Comparison of Monthly Evaporation Rate

Mono Lake, 1982

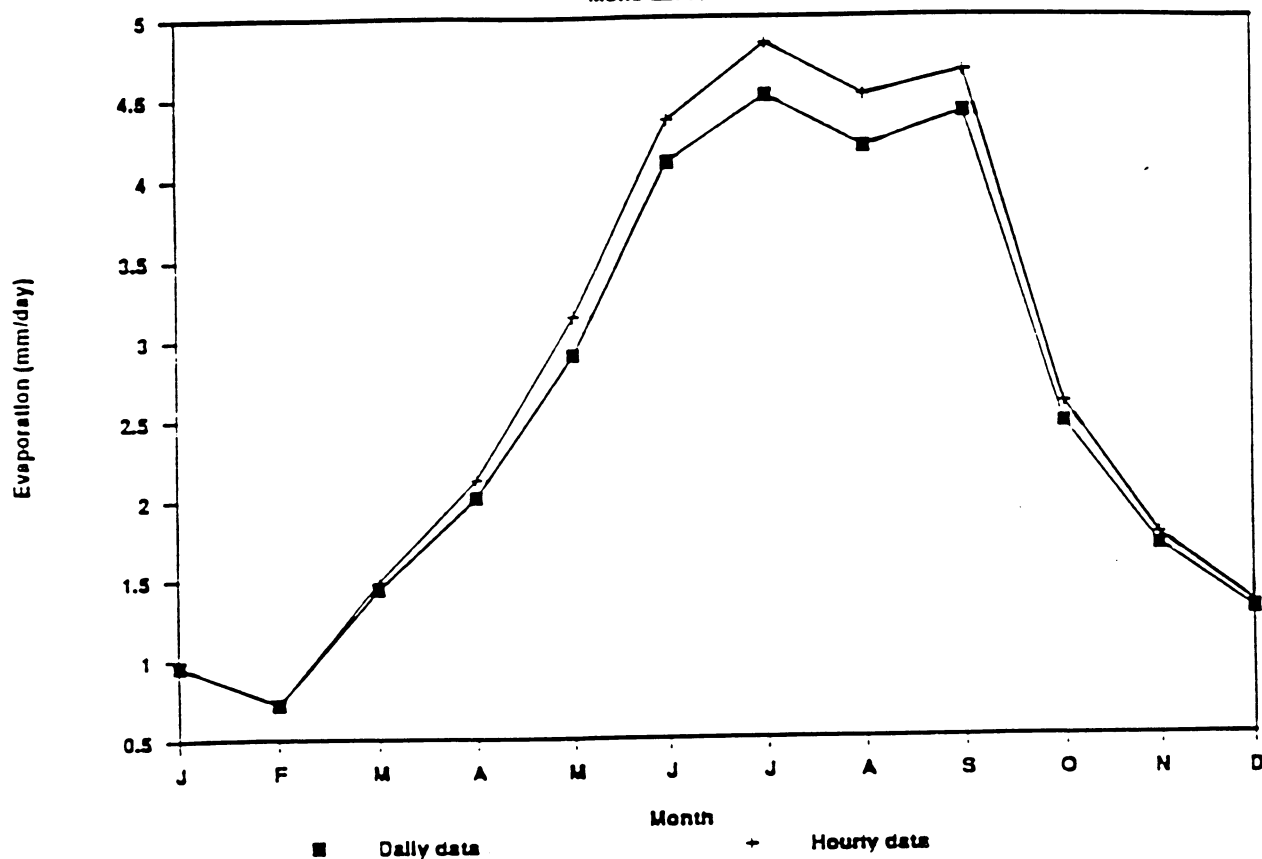


Figure 26. The difference of simulated evaporation rate between daily data and hourly data inputs.

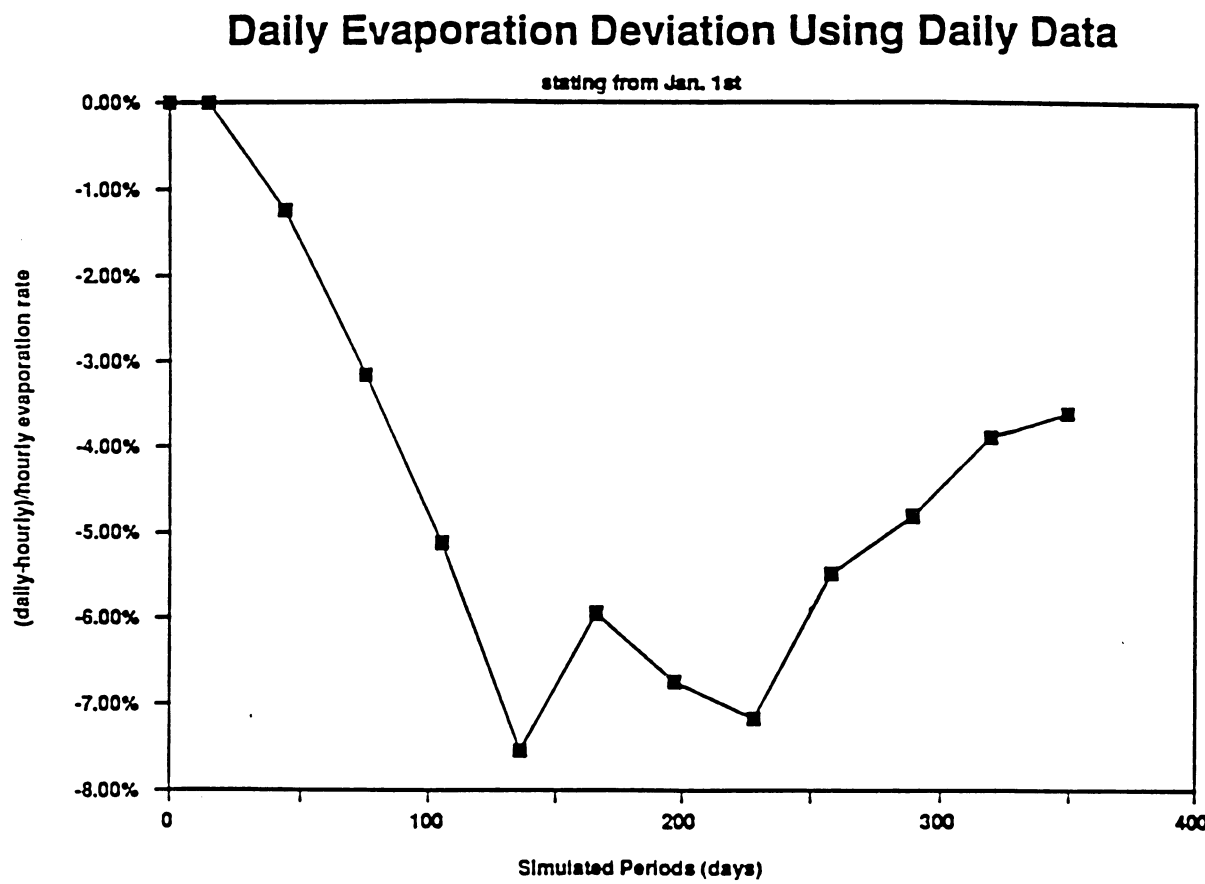


Figure 27. The daily evaporation deviation of hourly to daily data input was a function of simulated periods. The simulation started from January 1st, 1982.

Heat Diffusivity Sensitivity Analysis

Mono Lake, 1982

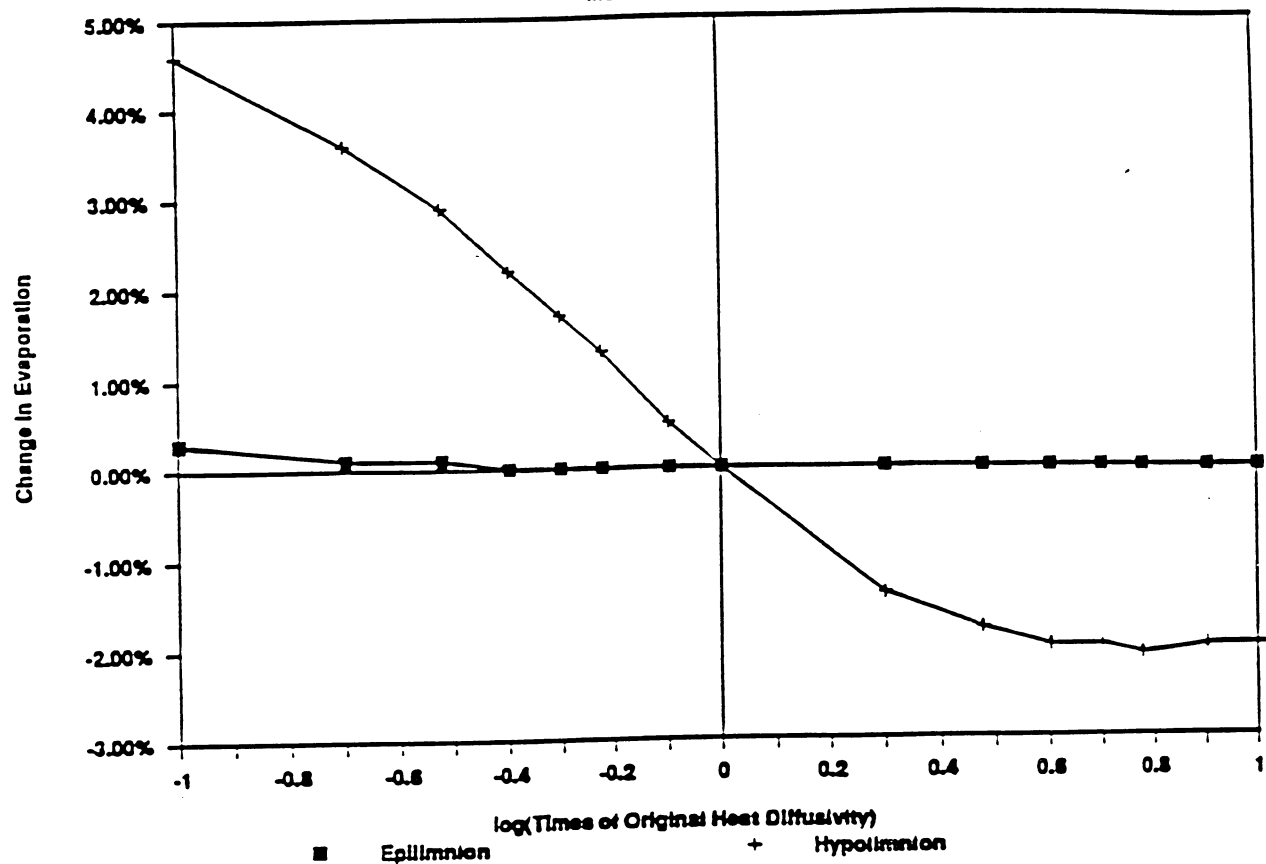


Figure 28. The sensitivity analysis of evaporation to water thermal diffusivities including those of epilimnion and hypolimnion layers.

Sensitivity Analysis

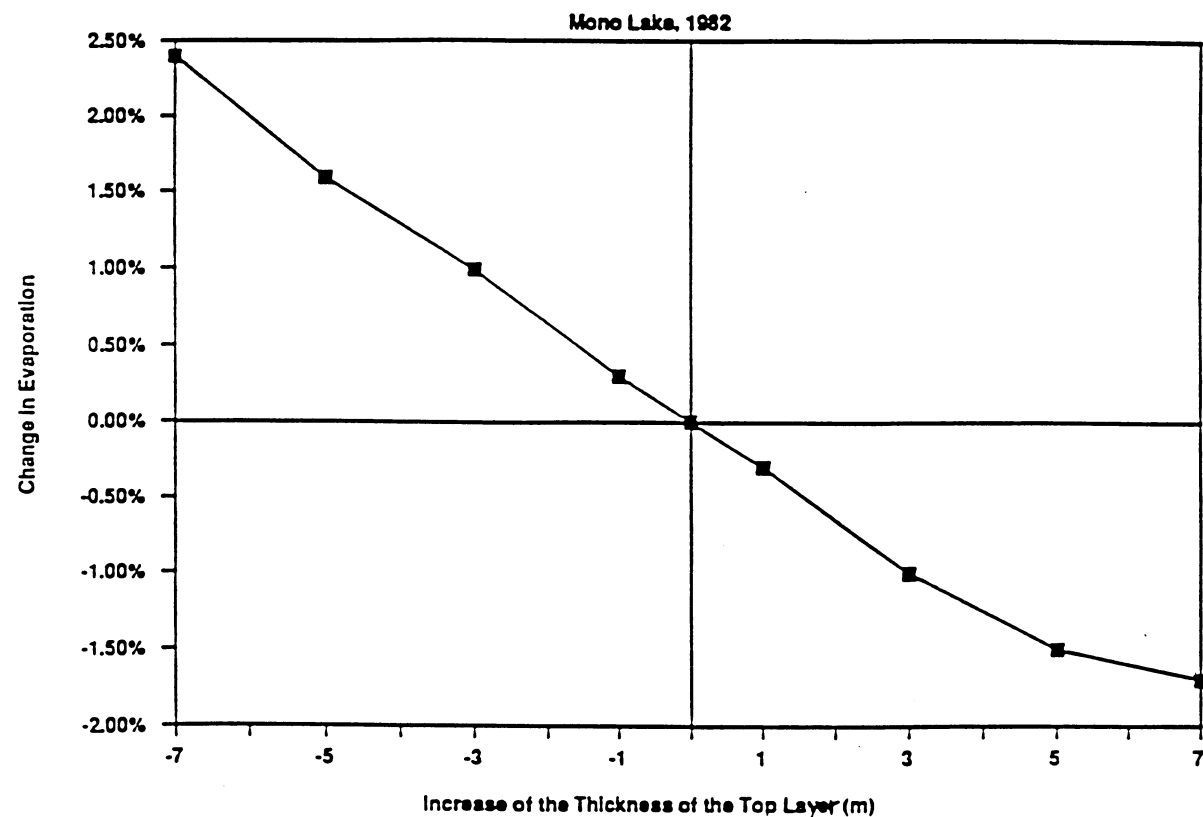


Figure 29. The sensitivity analysis of evaporation to the thickness of the top layer, while the proportion of the thickness of the middle layer to that of the bottom layer remained unchanged.

Incoming & Outgoing Monthly Energy Flux

Mono Lake, 1982

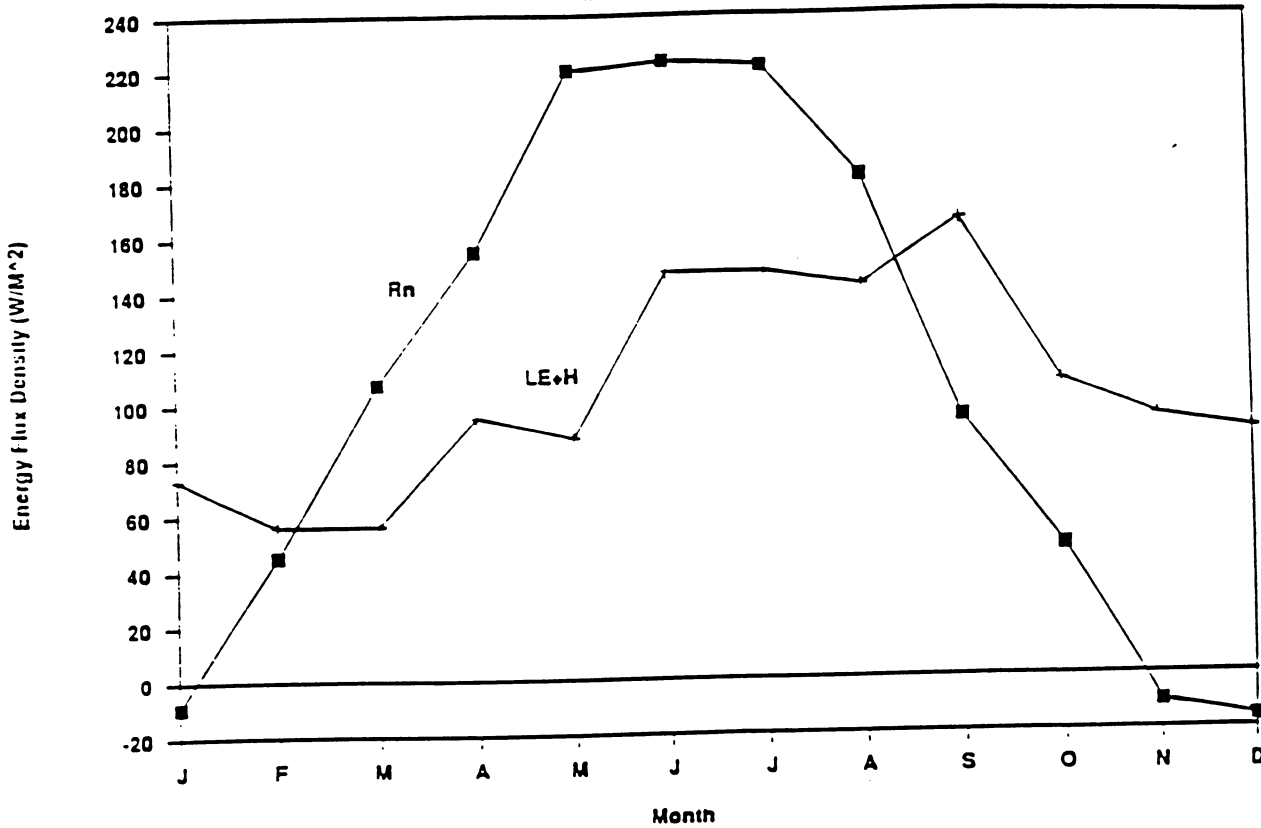


Figure 30. A Comparison Between the Monthly Incoming Energy, i.e. net radiation energy (R_n), and the Outgoing Energy Fluxes, i.e. latent heat (LE) + sensible heat (H), in Air-Water Interface of Mono Lake during 1982. A time lag effect between the incoming energy and the outgoing energy was simulated by IEM. The main contribution of this lag is the depth of water body, which of Mono Lake was 17.8 m.

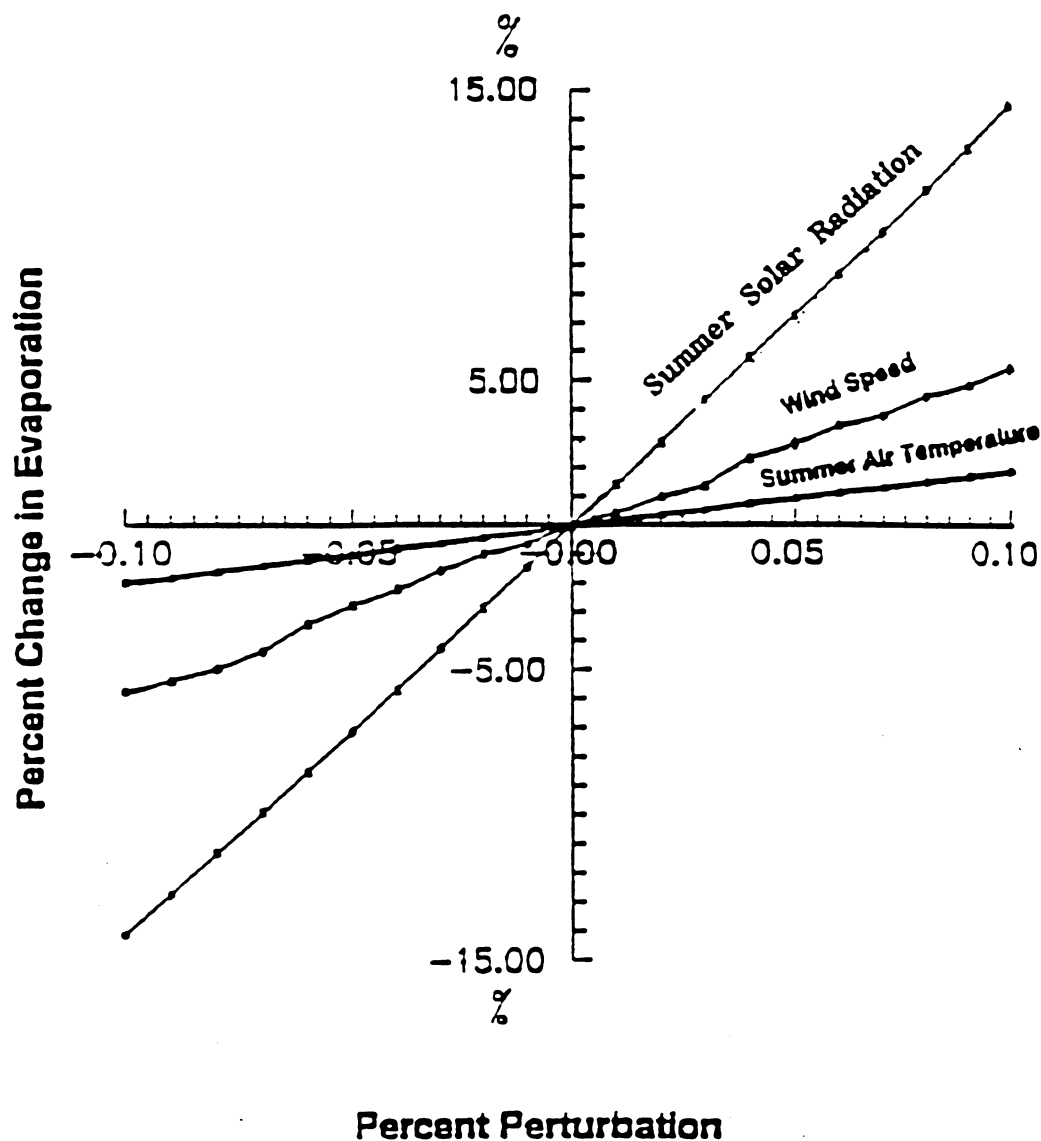


Figure 31. The sensitivity analysis of summer evaporation to climatic variabilities including summer solar radiation, wind speed and summer air temperature by Hostetler (1987). From this study, solar radiation energy is the most sensitive meteorological factor on evaporation. Wind speed is the second sensitive term.

Sensitivity Analysis

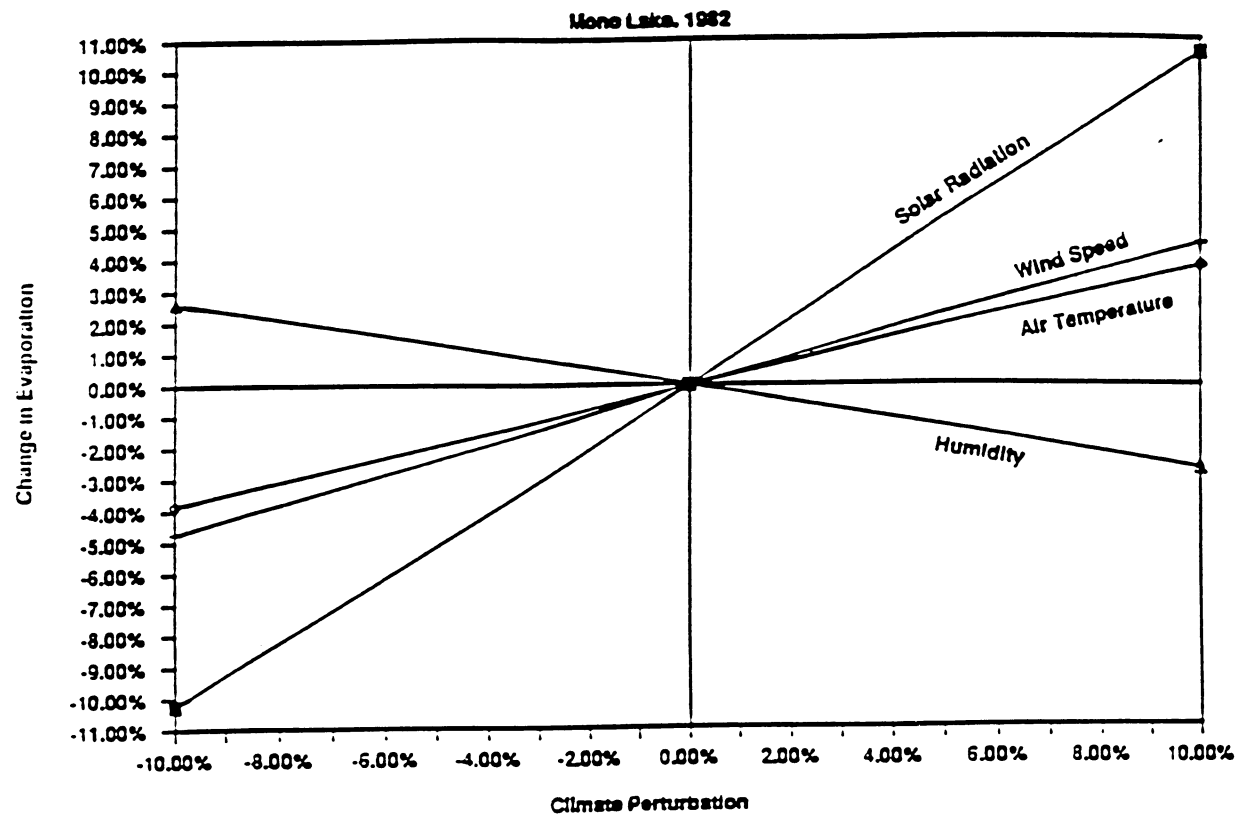


Figure 32. The sensitivity analysis of annual evaporation to climatic variabilities including solar radiation, wind speed and air temperature and absolute humidity using IEM. From the simulation, solar radiation energy is the most sensitive meteorological factor on evaporation. Wind speed is the second sensitive term. Air temperature is the third. Humidity is the only one which has a negative effect on evaporation.

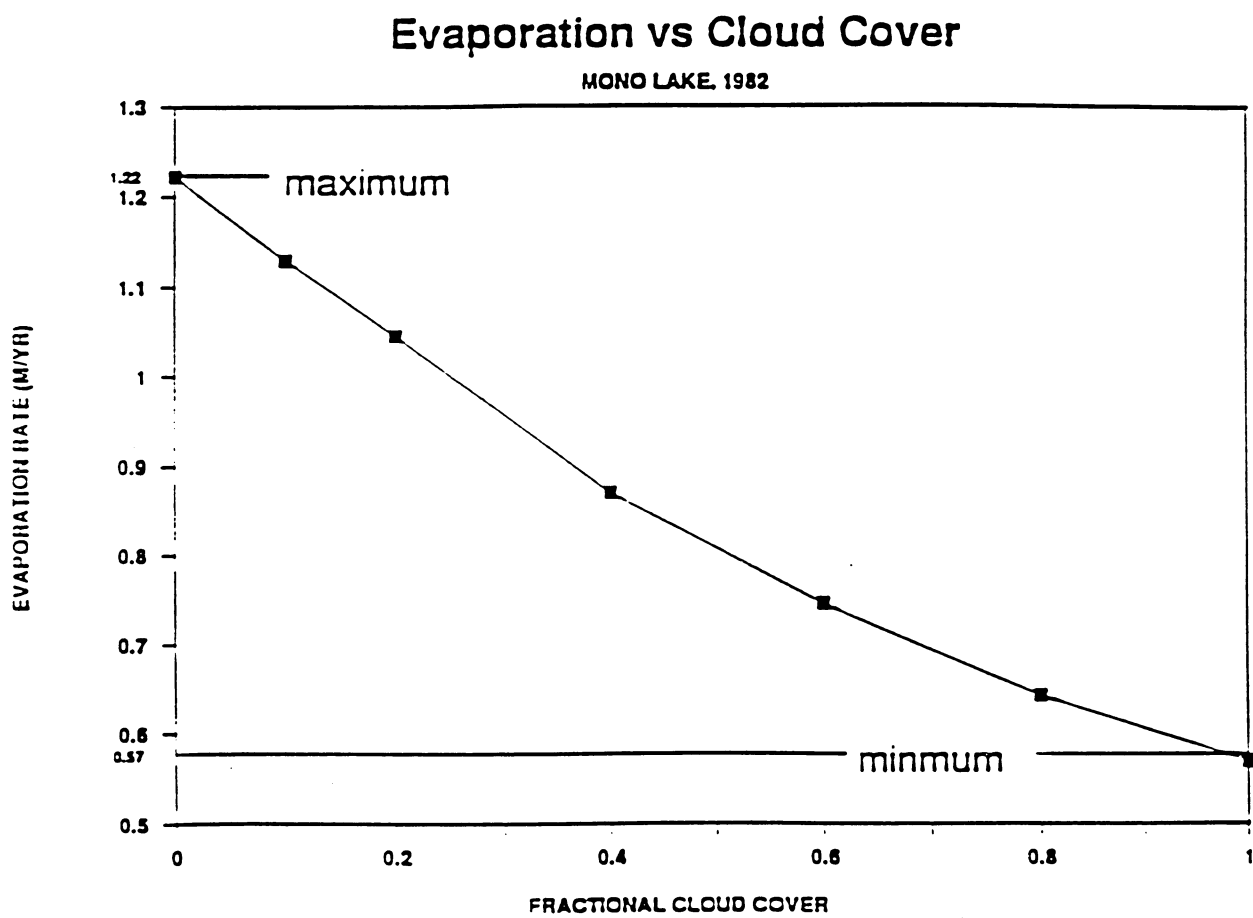


Figure 33. Simulated Annual Evaporation Rates from Mono Lake due to Different Cloud Cover Inputs, using 1982 Meteorological Conditions. Since evaporation rates are the most sensitive to solar radiation energy. Approximate maximum/minimum evaporation rates were determined under clear sky and overcast conditions.

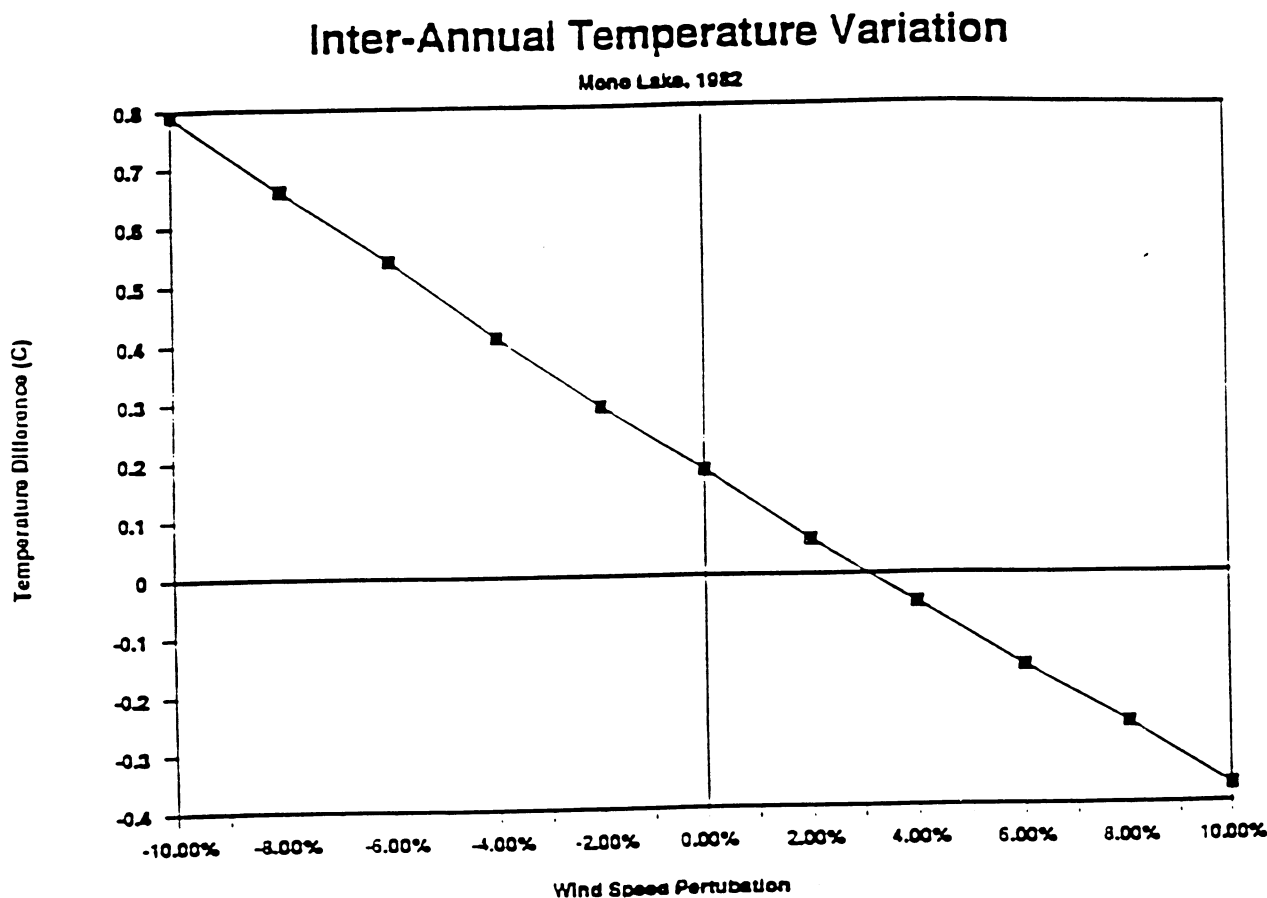


Figure 34. The relationship between wind speed and inter-annual water temperature variation. Wind speed is the second sensitive term to evaporation. It shifts energy inter-annually. 1982 wind increased water temperature about 0.18°C . $\pm 10\%$ perturbation of wind speed causes a change of inter-annual variation of water temperature $\pm 0.6^{\circ}\text{C}$. If 1982 wind speed increased 3 %, there would be no simulated inter-annual water temperature variation.

Comparsion of Salinity Adjustment Ratio

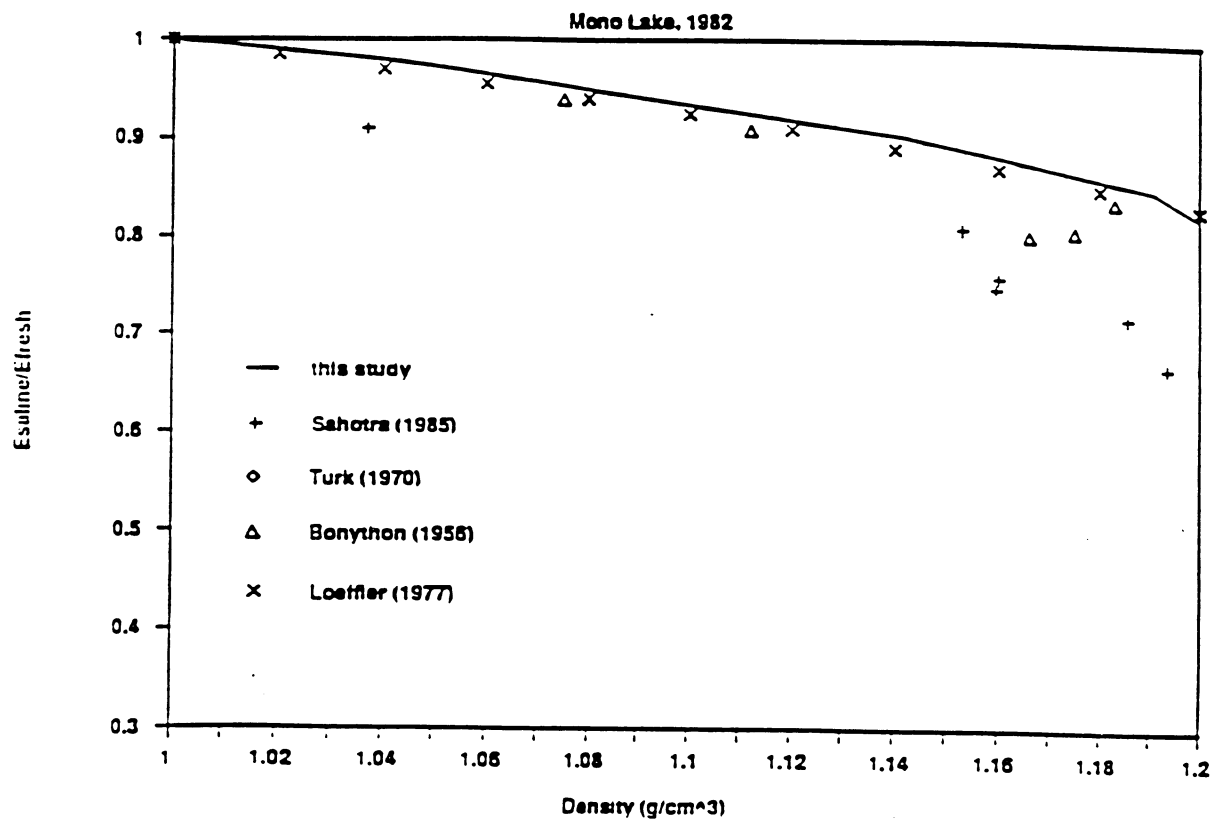


Figure 35. Comparison of saline / fresh water evaporation rates from IEM model and data reported by Bonython (1956), Turk (1970), Loeffler (1977) and Sahotra (1985). The salinity effect on evaporation was determined with IEM. From the figure, the result is good, especially, in comparison to Loeffler (1977). Loeffler's study also used the water of Mono Lake.

EVAPORATION RATE FROM MONO LAKE

USING SIMIS DATA

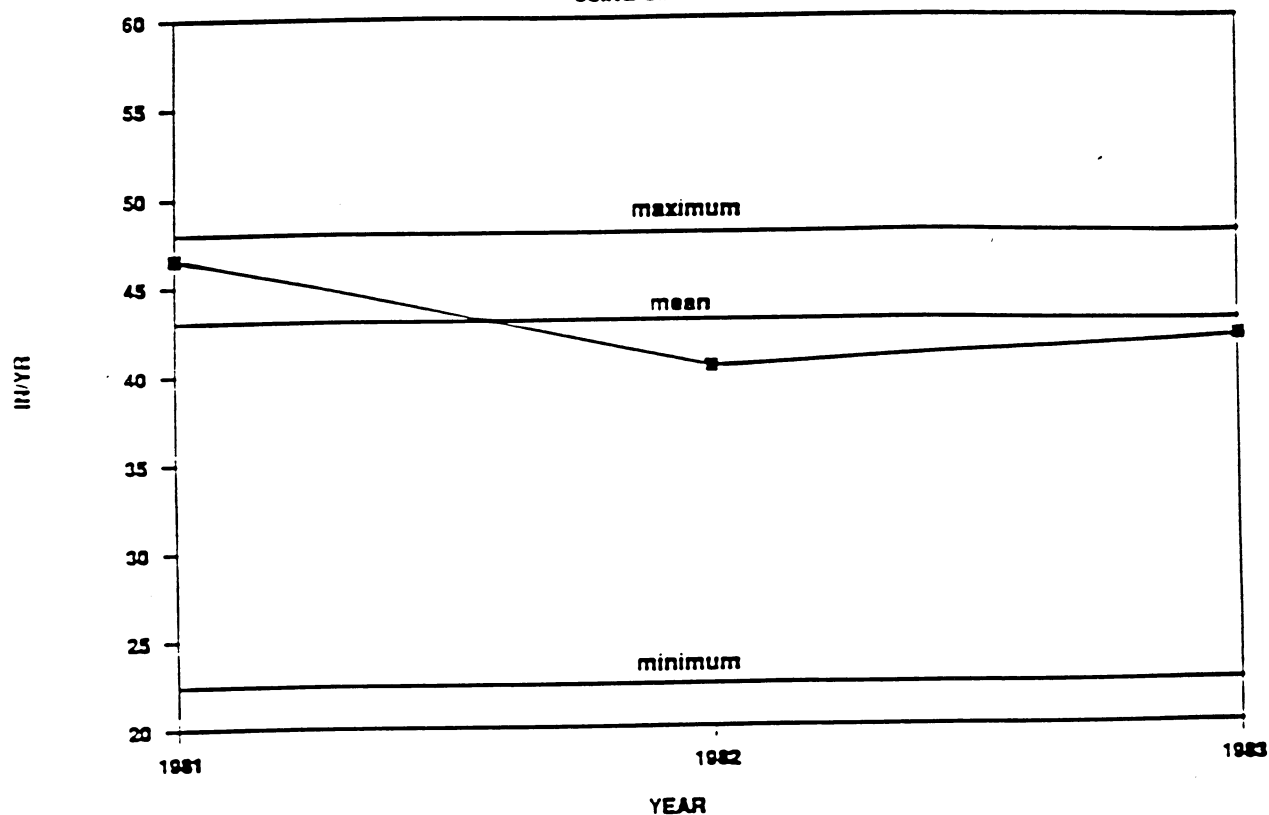


Figure 36. Long-Term Evaporation Rates from Mono Lake using a technique combining 1982 results from IEM with the Simis Station Evaporation Pan Data

EVAPORATION RATE FROM MONO LAKE USING GRANT LAKE DATA

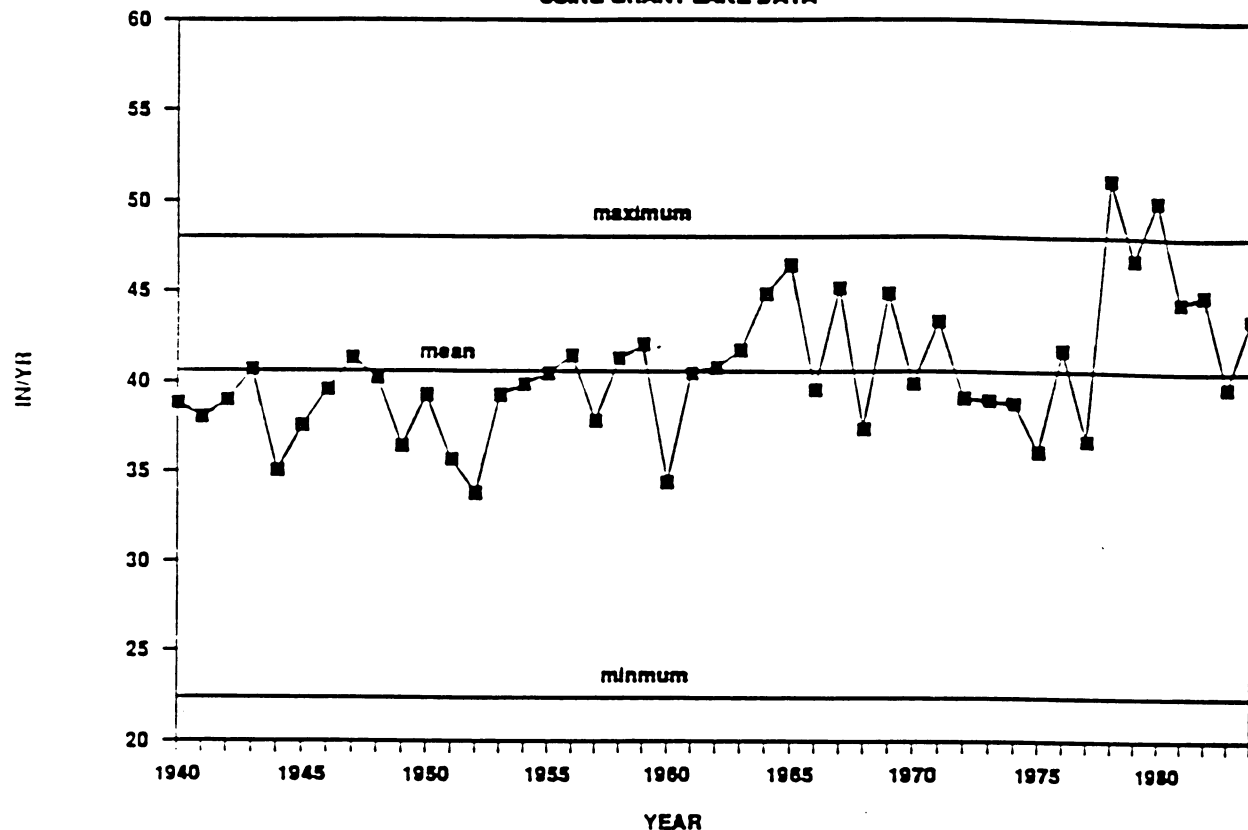


Figure 37. Long-Term Evaporation Rates from Mono Lake using a technique combining 1982 results from IEM with the Grant Lake Evaporation Pan Data. The maximum/minimum evaporation rates were used for checking evaporation rates from the evaporation pan method. The years 1978 and 1980 are when evaporation rates determined by the pan method exceeded the maximum evaporation benchmark. Therefore, the long-term evaporation results are considered questionable.

